EXPERIMENTAL STUDY OF ANTIPROTON - PROTON ANNIHILATION INTO AN ELECTRON - POSITRON PAIR AND ANTIPROTON - PROTON ANNIHILATION INTO TWO γ-RAYS FOR INCIDENT ANTIPROTON MOMENTA OF 1.50 GeV/c AND 2.50 GeV/c

Thesis by
Donald L. Hartill

In Partial Fulfillment of the Requirements
For the Degree of
Doctor of Philosophy

California Institute of Technology
Pasadena, California
1967

ACKNOWLEDGMENTS

Without the close cooperation of all the people in our group carrying out this experiment would not have been possible. Alvin Tollestrup, as head of our group, conceived the experiment jointly with Ted Zipf, provided the necessary motivation to all members of the group so that the experimental apparatus was ready when we were scheduled to run at the AGS, and was responsible for the design, construction, and operation of a large part of the electronic logic used in the experiment. Barry Barish, Douglas Fong, Ricardo Gomez, Al Maschke, Jerry Pine, and Ted Zipf have all shared equally in carrying out the experiment from its initial design to the final data analysis.

The AGS staff headed by Jim Sanford provided the antiprotons with great hospitality and without their conscientious help it would have been impossible to set up and run the experiment. The author wishes to personally thank Joe Lepicki and Jack Hennesy of the Cosmotron for providing one of their technicians for four months during the construction of the lead plate spark chambers. The design, construction, and conscientious operation of our hydrogen target by the Hydrogen Target Group at Brookhaven headed by Al Schlafke were also greatly appreciated.

The Electronics Shop, the crew at the Synchrotron Laboratory at Caltech, Hans Grau, and Bill Friedler assembled the logic circuits and much of the experimental apparatus. Members of our scanning group deserve special thanks for their consistent and conscientious scanning and measuring of the spark chamber film from the experiment. Ken

Young's assistance with the Monte Carlo programing was invaluable.

For financial support, the author is greatly indebted to the National Science Foundation, the Atomic Energy Commission, and to the California Institute of Technology.

ABSTRACT

Upper limits for the differential cross sections at 90° in the center of mass system for the reaction

$$\bar{p} + p \rightarrow e^{+} + e^{-}$$

have been measured for incident antiproton momenta of 1.50 GeV/c and 2.50 GeV/c. These limits to the 90% confidence level were 1.8×10^{-34} cm^2/st and 4.2×10^{-35} cm^2/st. respectively. Two thin foil spark chambers were used to measure the laboratory angles of the electron and positron and two lead plate spark chambers were used to identify the electron and positron by their characteristic electromagnetic showers produced in such chambers. Assuming a one photon exchange mechanism for the annihilation, upper limits equal to 0.2 if $|G_E| = |G_M|$ for the electric and magnetic form factors of the proton for time-like momentum transfers of $+ 5.1\ (GeV/c)^2$ and $+ 6.8\ (GeV/c)^2$ were obtained from the cross section limits.

The differential cross section at 90° in the center of mass system for the reaction

$$\bar{p} + p \rightarrow \gamma + \gamma$$

has been tentatively measured for an incident antiproton momentum of 1.50 GeV/c and an upper limit for this cross section has been measured for an incident antiproton momentum of 2.50 GeV/c. The differential cross section at 1.50 GeV/c is based on two events giving

$$\frac{d\sigma}{d\Omega}\Big|_{90^{\circ}} (\bar{p}p \rightarrow 2\gamma) = (1.6 \ {}^{+\ 1.9}_{-\ 0.8}) \times 10^{-31}\ cm^2/st.$$

The upper limit to a 90% confidence level at 2.50 GeV/c is

$$\frac{d\sigma}{d\Omega}\Big|_{90^\circ} (\bar{p}p \to 2\gamma) \leq 0.8 \times 10^{-31} \text{ cm}^2/\text{st}.$$

Upper limits for the cross sections of the process

$$\bar{p} + p \to 3\pi^\circ$$

for incident $\bar{p}$ momenta ranging from 1.00 GeV/c to 2.50 GeV/c have been measured. Differential cross sections for the process

$$\bar{p} + p \to 2\pi^\circ$$

have been tentatively measured for center of mass angles from 55° to 90° and for incident $\bar{p}$ momenta ranging from 1.00 GeV/c to 2.50 GeV/c. The results for the $2\pi^\circ$ final state could, however, contain up to 50% background from the $3\pi^\circ$ final states.

The relative rates between the $3\pi^\circ$ and the $\pi^+\pi^-\pi^\circ$ final states and between the $2\pi^\circ$ and the $\pi^+\pi^-$ final state appear to be at least a factor of two smaller than would be expected for a simple statistical model for the annihilation.

To Marian

TABLE OF CONTENTS

APPENDICES

APPENDICES (cont.)

LIST OF FIGURES

LIST OF FIGURES (cont.)

LIST OF FIGURES (cont.)

LIST OF FIGURES (cont.)

LIST OF FIGURES (cont.)

LIST OF FIGURES (cont.)

LIST OF FIGURES (cont.)

LIST OF TABLES

I. INTRODUCTION

The advent of the high energy proton synchrotrons, the AGS at Brookhaven and the Proton Synchrotron at CERN in Geneva, Switzerland, with primary beam energies of the order of 30 GeV and with correspondingly large yields of secondary particles from an internal target in the accelerator makes possible the experimental investigation of processes with small cross sections of the order of 10^{-33} cm^2. This thesis represents a study of the two such processes

$$\bar{p} + p \rightarrow e^+ + e^- \qquad (1)$$

$$\bar{p} + p \rightarrow \gamma + \gamma \qquad (2)$$

for incident antiproton momenta of 1.50 GeV/c and 2.50 GeV/c.

The principal interest in studying the first reaction comes from assuming a one photon exchange mechanism for the annihilation. Then, assuming no structure for the $\gamma e^- e^+$ vertex, analysis of the angular distribution of the electron from reaction (1) using the form of the Rosenbluth Formula[1,2] obtained from crossing symmetry yields directly the values of the electric and magnetic form factors for the proton for time-like momentum transfers. The extensive electron-proton elastic scattering experiments of Hofstadter[3] and co-workers, Wilson[4] and co-workers, Behrend[5] and co-workers, and Albrecht[6] and co-workers yield information on the electric and magnetic form factors for space-like momentum transfers. Figure 1 shows the pertinent Feynman diagrams and Figure 2 summarizes the known experimental results for the form factors. Figure 2 also includes the upper limit on the form

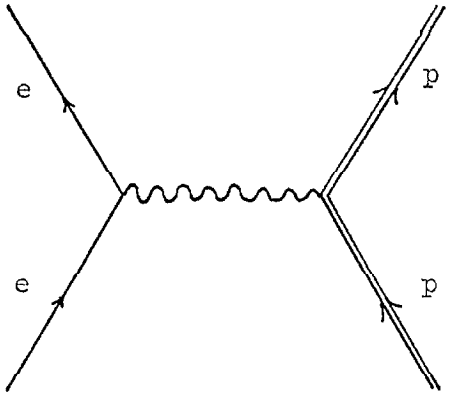

$e^- + p \rightarrow e^- + p$

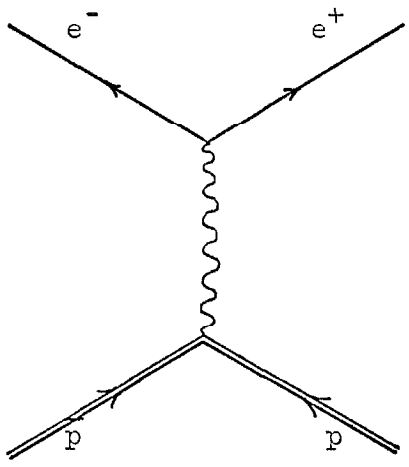

$\bar{p} + p \rightarrow e^+ + e^-$

Figure 1 Feynman Diagrams for $e^-p \rightarrow e^-p$ and $\bar{p}p \rightarrow e^+e^-$

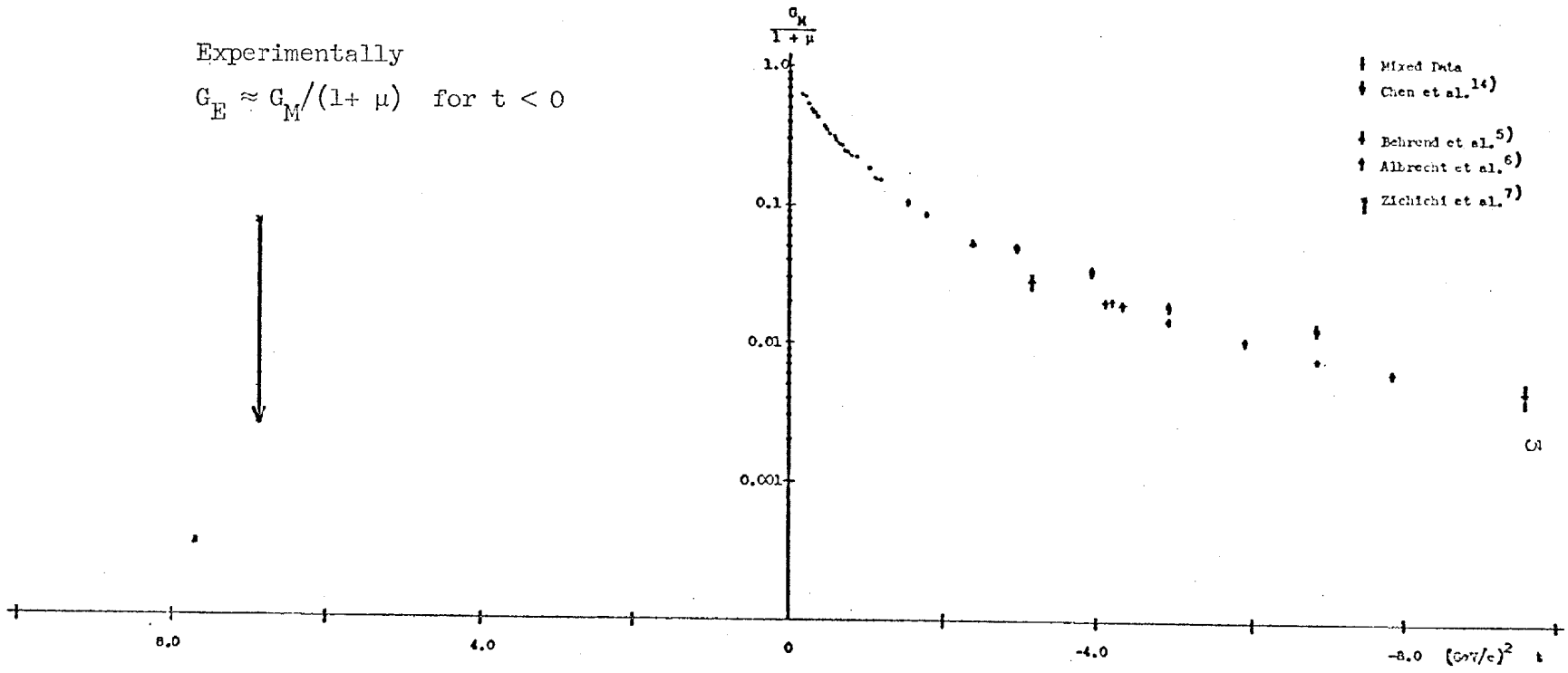

Figure 2 Summary of Experimental Information About the Proton Form Factors

factors for a time-like momentum transfer of + 6.8 $(GeV/c)^2$ measured by Zichichi[7] and co-workers who studied reaction (1) at CERN.

In terms of the electric form factor $G_E(q^2)$ and the magnetic form factor $G_M(q^2)$ the differential cross section for the first reaction is given by[2]

$$\frac{d\sigma}{d\Omega}(pp \to e^+e^-) = \frac{1}{16} \frac{\alpha^2}{E(E^2 - M_p^2)^{1/2}} \left[| G_M(q^2) |^2 (1 + \cos^2 \theta^*) + (\frac{M_p}{E})^2 | G_E(q^2) |^2 \sin^2 \theta^* \right]$$

with $\alpha = \frac{1}{137}$ = fine structure constant

M_p = proton mass

$q^2 = t = 4E^2$

E = total energy of the $\bar{p}$ in the center of mass system

θ^* = angle between $\bar{p}$ momentum vector and e^- momentum vector in center of mass system

and with $G_E(0) = 1$ and $G_M(0) = 1 + \mu = 2.79$

where μ = anomalous moment of the proton.

The convention used here for the Lorentz metric is $q^2 = q_o^2 - \vec{q} \cdot \vec{q}$. If the differential cross section has the dimensions cm^2/steradian and energies and masses are measured in GeV the coefficient $\frac{\alpha^2}{16}$ becomes numerically equal to 1.33×10^{-33}. The cross section can also be written in terms of the less convenient Dirac and Pauli form factors F_1 and F_2, related to G_E and G_M by

$$G_E(q^2) = F_1(q^2) + \frac{q^2}{4M_p^2}\,\mu\, F_2(q^2)$$

$$G_M(q^2) = F_1(q^2) + \mu\, F_2(q^2)$$

They are mentioned here because if $F_2(q^2)$ is to remain finite at $q^2 = 4M_p^2$ the condition

$$G_E(4M_p^2) = G_M(4M_p^2)$$

must be satisfied. In addition since the proton current operator is a Hermitian operator G_E and G_M must be real for space-like momentum transfers;however they can have imaginary parts for time-like momentum transfers.

Table 1 lists the known cross sections for several final states resulting from the antiproton-proton initial state. This list includes only final states which have two charged particles since these were thought to be the major source of background during the design of the experiment. At that time (Fall of 1963) the magnitude of G_E and G_M[4]) was thought to be ≈ 0.1 for space-like momentum transfers on the order of $-6.8\ (\mathrm{GeV/c})^2$. It was felt that this experiment should be designed to be sensitive to G_E and G_M also ≈ 0.1 for time-like momentum transfers of the order of $+6.8\ (\mathrm{GeV/c})^2$. Inserting these values into the cross section given above then implies $\left.\frac{d\sigma}{d\Omega}\right|_{90^o} \approx 10^{-35}$ cm^2/st. for antiprotons with 2.50 GeV/c incident momentum and $\left.\frac{d\sigma}{d\Omega}\right|_{90^o} \approx 3 \times 10^{-35}$ cm^2/st. for 1.50 GeV/c incident momentum or total cross sections of

$$\sigma \approx 1.2 \times 10^{-34}\ \mathrm{cm}^2 \text{ and } \sigma \approx 4 \times 10^{-34}\ \mathrm{cm}^2$$

respectively. Comparing these values to those in Table 1 then shows

TABLE 1

Average Differential Cross Sections for Several Final States in the Region of Angular Acceptance of the Detection Apparatus

	1.50 GeV/c	2.50 GeV/c
$\frac{d\sigma}{d\Omega}\Big\|_{90^\circ}$ $(\bar{p}p \rightarrow \bar{p}p)$	35×10^{-30} cm^2/st.	25×10^{-30} cm^2/st.
$\frac{d\sigma}{d\Omega}\Big\|_{90^\circ}$ $(\bar{p}p \rightarrow \pi^+\pi^-)$	15×10^{-30} cm^2/st.	3×10^{-30} cm^2/st.
$\frac{d\sigma}{d\Omega}\Big\|_{90^\circ}$ $(\bar{p}p \rightarrow K^+K^-)$	5×10^{-30} cm^2/st.	0.5×10^{-30} cm^2/st.
$\frac{d\sigma}{d\Omega}\Big\|_{90^\circ}$ $(\bar{p}p \rightarrow e^+e^-)_{est.}$	few $\times 10^{-35}$ cm^2/st.	few $\times 10^{-35}$ cm^2/st.

The differential cross sections given for the $\pi^+\pi^-$ and K^+K^- final states are from the preliminary analysis by Fong of the data collected during this experiment when the apparatus was modified to accept these final states. The elastic scattering cross sections are taken from the analysis of the data collected during this experiment with the PDP-5 computer interfaced to the hodoscope system. These cross sections are reported in the literature.[17)]

the requirements that the apparatus must satisfy.

The choice of 2.50 GeV/c for the upper value of the $\bar{p}$ momentum was a result of the desire to maximize the $\bar{p}$ yield while still obtaining a good separation of $\bar{p}$'s from the other secondary particles with the available electrostatic beam separators. Also a research group[7] at CERN was planning to do this experiment using 2.50 GeV/c antiprotons and a CH_2 target. The lower momentum, 1.50 GeV/c, was chosen because it was the lowest value where enough antiprotons could be obtained during the allotted running time to hope to reach the desired sensitivity to G_E and G_M.

Because any apparatus used in an experiment of this type has a finite amount of material between the point of annihilation and the part of the detector which distinguishes between neutral and charged particles a short experiment was carried out to look for the $\gamma + \gamma$ final state. If this process had an anomalously large cross section then because of pair production in the material in front of the charged particle detectors it could lead to a serious background to the experiment looking for the $e^+ + e^-$ final state.

II. EXPERIMENTAL METHOD AND APPARATUS

The reactions

$$\bar{p} + p \rightarrow e^+ + e^-$$

and

$$\bar{p} + p \rightarrow \gamma + \gamma$$

for incident antiproton momenta of 1.50 GeV/c and 2.50 GeV/c were studied at the AGS at the Brookhaven National Laboratory. A partially separated, momentum analyzed antiproton beam from the C-10 target in the AGS was focused on a two meter long liquid hydrogen target. Typically the $\pi^-/\bar{p}$ ratio was 1:1 at the hydrogen target and the momentum uncertainty was $\pm$ 3% of the mean beam momentum. The antiprotons were identified electronically by time of flight. A scintillation counter hodoscope, a thin foil spark chamber, a lead plate spark chamber, and a Čerenkov counter array were arranged on each side of the liquid hydrogen target to detect the $e^+ + e^-$ or the $\gamma + \gamma$ final state. To detect the $\gamma + \gamma$ final state the first tray of scintillation counters on each side of the target was used to veto events with charged particles passing through these trays. Behind these counters a 1/8" thick Al plate to which a 1/4" Pb plate was attached acted as a converter, which for the geometry of the experiment was $\approx$ 1.50 radiation lengths thick, for each γ-ray. The remainder of the apparatus was the same as used to detect the $e^+ + e^-$ final state. Since no magnet was used in the detection system it was impossible to distinguish the electron and positron.

In a two body reaction, the kinematical parameters are

overdetermined by one constraint if the laboratory angles of the final state particles are measured with respect to the incident beam direction and the momentum of the incident particle is known. In principle then the $e^+ + e^-$ final state could be detected just by measuring the laboratory angles of the two charged particles in the final state. However, in practice this is impossible because the difference in laboratory angles for the $\pi^+ + \pi^-$ final state and the $e^+ + e^-$ final state is only 0.2° for incident $\bar{p}$ momenta in the range 1.50 to 2.50 GeV/c. Current spark chamber techniques with lever arms of the order of ten inches, the beam divergence, and the finite target thickness do not permit measurements of angles to this accuracy.

The method used to separate out the $e^+ + e^-$ final state in this experiment was to measure the laboratory angles of the two particles with two thin foil spark chambers with eight gaps spanning a distance of 6.4". This permitted angle measurements with an accuracy of $\pm 1^\circ$ and insured that the final state was essentially either $\pi^+ + \pi^-$ or $e^+ + e^-$. The final identification was made by requiring that an electromagnetic shower be present in each of the lead plate spark chambers and that a large pulse come from the Čerenkov counters placed behind the lead chamber. The lead plate chambers were made from 0.11 radiation length thick plates and for typical angles were 4 radiation lengths thick. The plates in the chamber were arranged in a herring bone pattern so that particles from the annihilation traversed the plates as close to their normal as possible. For the operating parameters used in the experiment the Čerenkov counters were each 20% efficient for π's and

> 95% efficient for electrons and the lead chambers each had a final detection efficiency of 0.03% for π's and 91 $\pm$ 2% for electrons.

Since the spark chamber system used in this experiment could only be triggered (and photographed) once per AGS cycle it was necessary to electronically pre-select the trigger events as much as possible to limit the dead time losses due to the spark chamber system.

The scintillation counters on each side of the target were arranged in a forty-five counter hodoscope. These counters were connected to a fast digital computer which in approximately 150 nanoseconds performed the following operations:

1.) Checked that only two charged particles, one on each side of the target, were emitted from an annihilation.

2.) Measured the angle of coplanarity of the two particles with respect to the beam and required that they be coplanar to within $\approx 15^{\circ}$.

3.) Measured the polar angle of each of the particles with respect to the beam with a resolution of $\approx 5^{\circ}$, and accepted those events with angles appropriate for the reaction $\bar{p} + p \rightarrow e^+ + e^-$.

This system had sufficient angular resolution to eliminate elastic scattering events and nearly all of the $\pi^+\pi^- n\pi^o$ final state annihilations while having $\approx$ 100% efficiency for the $e^+ + e^-$, the $\pi^+ + \pi^-$, and the $K^+ + K^-$ final states. As much as was possible the angular regions not covered by the two hodoscopes were covered by lead (1/4" thick) faced scintillation counters which acted as veto counters for γ-rays and charged particles. Their detection efficiency for γ-rays

in the energy range from 50 MeV to 1 GeV was 65% ± 15% as determined from measurements using similar counters in the Caltech tagged γ-ray beam. The final spark chamber trigger was formed by requiring that the kinematics as determined by the hodoscope and computer corresponded to the $e^+ + e^-$ final state, that the pulse height in both Čerenkov counters be greater than a fixed level and that no veto counters had been hit by either a γ-ray or a charged particle.

Table 2 gives a typical set of numbers of triggers for 3×10^{11} protons on the G-10 target in the AGS. During the experiment the AGS beam dump had a 400 millisecond duration and there were typically 4×10^{11} protons striking the G-10 target.

Figures 3 and 4 show schematically the layout of the hydrogen target and the detection apparatus.

To detect the $\gamma + \gamma$ final state a 1/8" thick Al - 1/4" thick Pb plate was placed behind the first tray of counters in the hodoscope on each side of the target. To trigger the spark chambers the electronic logic was modified as follows. The fast computer was modified so that it required that no pulse come from the first tray of counters, that there was at least one charged particle in each of the other trays of counters, that the particles from the γ-ray conversion in the Pb plate be confined to an angular square approximately $20^\circ \times 30^\circ$, and that the particles on each side of the target be coplanar to within $\approx 20^\circ$. The minimum pulse height requirement for the Čerenkov counters was decreased by a factor of two. If both pulses from the Čerenkov counters were greater than this minimum, the requirements of the fast computer were

TABLE 2

Average Number of Triggers for 3×10^{11} Protons on the G-10 Target

	1.50 GeV/c	2.50 GeV/c
Total $\bar{p}$'s	31,000	21,000
Interacting $\bar{p}$'s	7,000	7,000
Kinematics OK in fast computer	5	2
Kinematics OK + Čerenkov OK	0.2	0.05

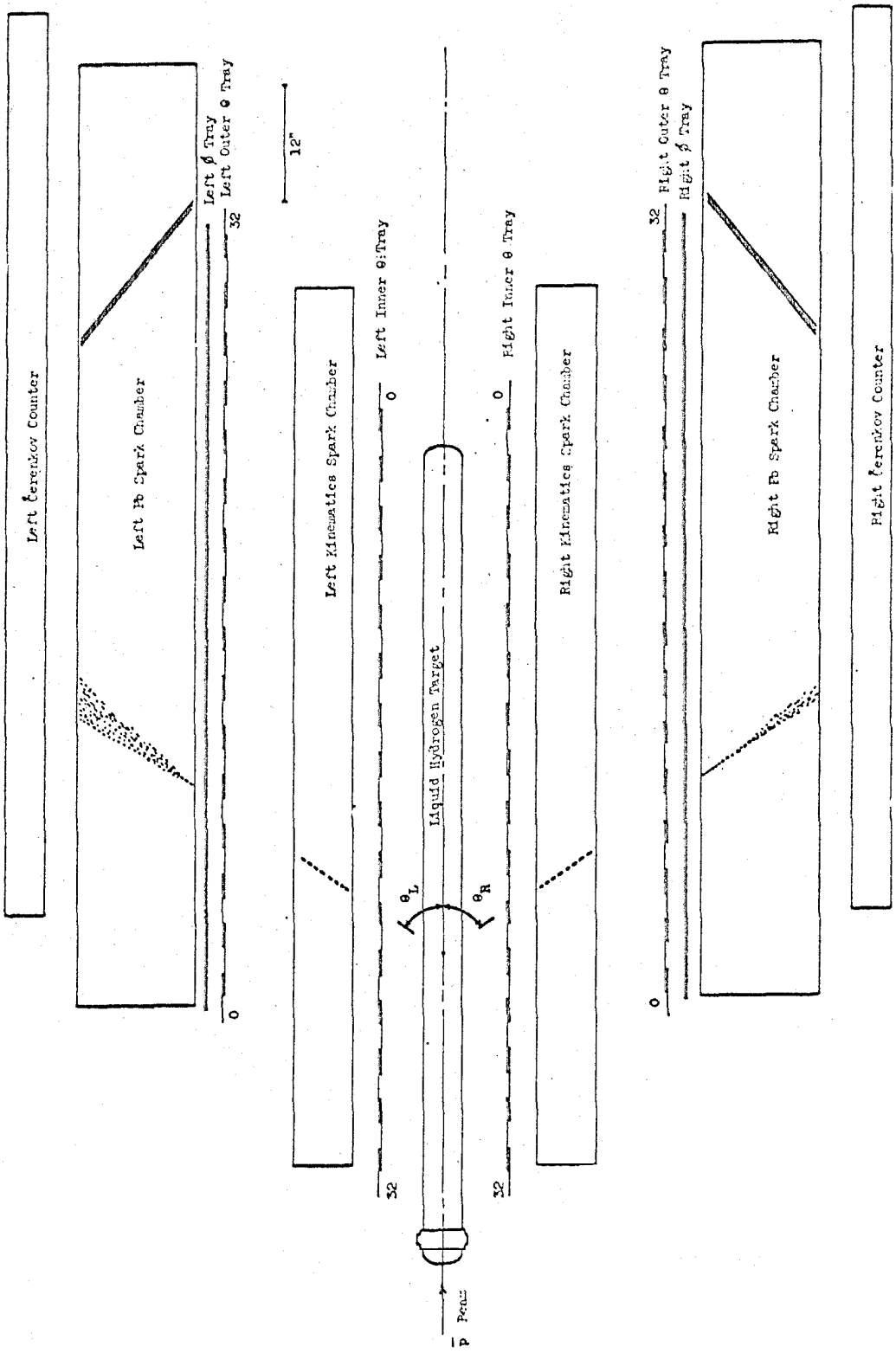

Figure 3 Top View of the Detection Apparatus

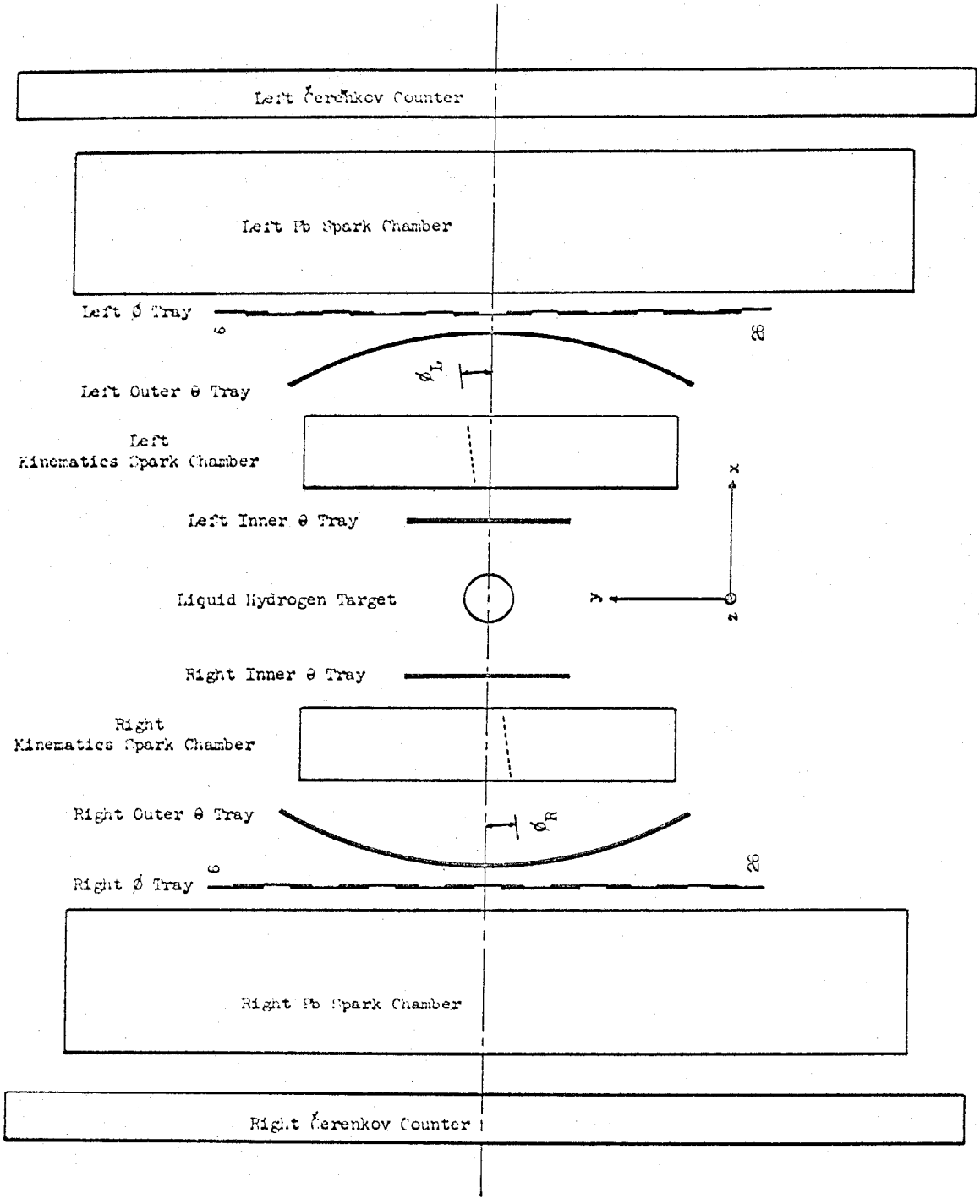

Figure 4 End View of the Detection Apparatus

satisfied, and no veto counters were struck the spark chambers were triggered.

In the final analysis only those events with either a pair of charged particles with opening angle $\leq 10^{o}$ or a single charged particle coming from the Pb plate on each side of the target were considered. The γ-ray conversion efficiency with this requirement was measured in the tagged γ-ray beam at the 1.50 GeV Caltech Electron Synchrotron. The mean angles of the pair or the angles of the single track were taken as the direction of motion of the γ-rays and were required to fit the angles appropriate to the $\gamma + \gamma$ final state to within $\pm 3^{o}$. The showers in the Pb chambers were required to correspond to the tracks in the thin foil chambers and the pulse heights in the Cerenkov counters were required to be the same as for electrons with the same energy and angles. These requirements lead to an overall detection efficiency of $(6.5 \pm 2.0) \times 10^{-3}$ for the $\gamma + \gamma$ final state.

As a consistency check for each event which triggered the spark chambers an IBM card was punched which recorded the event number, which counters in each tray of the hodoscope were triggered, the fast computer answers for θ_R, θ_L and $\Delta\phi$, and the pulse height as measured by a 15 channel fast multichannel analyzer of the pulse from each Cerenkov counter. This information was also recorded on the spark chamber film to aid in scanning by means of lighted numbers along the edges of the spark chambers and on a master data panel which was photographed in the end view of the thin foil chambers.

The spark chambers were photographed by four cameras. One camera photographed the top view of both lead plate spark chambers while the top view of each thin foil chamber was photographed by separate cameras and the end view of both thin foil chambers was photographed by one camera. For details of the spark chambers and the camera system see Appendices XI and XII.

In the following sections the detailed properties of each part of the detection apparatus will be left to the Appendices. Only the properties necessary to the discussion will be included.

III. CONSISTENCY CHECKS AND DATA ANALYSIS

a. Consistency Checks

In addition to continuously monitoring thirty-two counting rates by means of conventional scalers attached at various stages of the electronic logic a PDP-5 digital computer interfaced to the fast computer was used to monitor all counters in the hodoscopes and the operation of the fast computer. For details of the PDP-5, the interface and the fast computer see Appendices XIII and XV.

During the experiment after each 1.50×10^8 antiprotons had entered the liquid hydrogen target the scalers were printed out and a short run was taken. During this short run which took approximately five minutes the PDP-5 accepted 5000 events which had only two charged particles which came from the target and which satisfied the coplanarity requirement. The computer printout was then compared to a standard run as were the numbers from the scalers. If any of the numbers disagreed by more than the expected statistical fluctuations the trouble was remedied before continuing the experiment. It was very easy to spot counters whose gains had changed or electronic difficulties in the fast computer with these short runs. Also at this time the spark chambers were triggered off the same requirement as was used for the PDP-5 and their operation was checked visually. Serious troubles with the chambers could be easily detected in this manner. The film was developed the same day that it was exposed and spot scans of the developed film were made to detect more subtle difficulties with the

chambers, the fiducial system, or the cameras.

The singles rates from the Čerenkov counters were a sensitive monitor of the gains of the 5" photomultipliers and the bias levels of the discriminators used to determine the Čerenkov pulse height requirements. A 1% change in these rates was easily detected which corresponded to less than a 1% change in the electron detection efficiency. In addition the gains of each of the forty 5" photomultiplier tubes were checked weekly by means of Sr^{90} sources irradiating a 1/16" thick x 1" x 1" scintillator glued to the light pipes of each of the Čerenkov counters and looking at the resulting pulse height distributions. The maximum variation in gains was less than 4% during the course of the experiment.

Figure 5 shows the consistency of the various rates over a two week portion of the experiment looking for the $e^+ + e^-$ final state.

b. Data Analysis

1. Scanning and Measuring

The data from the $e^+ + e^-$ experiment which consisted of an IBM Card and four photographs of the spark chambers for each event were first analyzed by scanning the lead plate spark chambers for events which had a shower-like track in each chamber agreeing with the hodoscope lights arranged along the edges of the chamber. A shower-like track was any track which started within 3 gaps of the front of the chambers and whose number of sparks was greater than the number for a straight track plus ten sparks. This first scan was carried out twice on all the data and three times on part of the data. One of these scans was made by a

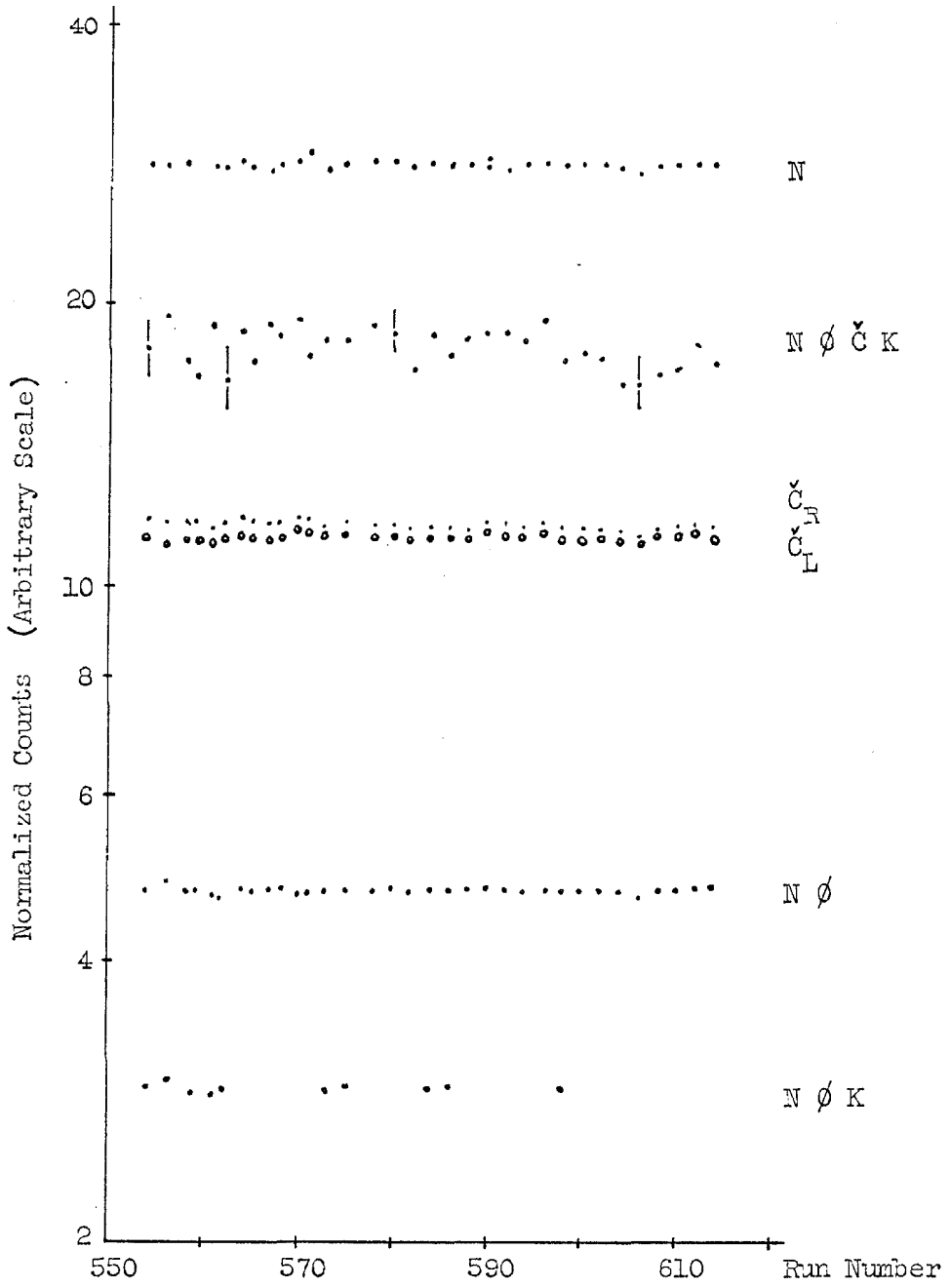

An explanation of the labels used in this figure is given on the following page.

Figure 5 Normalized Counting Rates for a Series of Runs

Explanation of Labels Used in Figure 5

N: An antiproton disappearing in the target with one charged particle passing through each tray of the hodoscope on each side of the hydrogen target and with no signal from any of the veto counters.

$\emptyset$: The two charged particles from the hydrogen target satisfied the coplanarity requirement set by the fast computer.

$\check{C}$: The pulses from each of the Čerenkov counters were each greater in amplitude than the minimum pulse height expected for > 95% of a sample of electrons with energies and angles corresponding to those for the $e^+ + e^-$ final state.

K: The fast computer answers for cot θ_L and cot θ_R for the two charged particles from the hydrogen target were consistent with those expected for $\bar{p}p \rightarrow e^+e^-$, $\pi^+\pi^-$, or K^+K^-.

$\check{C}_R$: The number of pulses greater than the above mentioned minimum pulse height from the right Čerenkov counter in coincidence with an antiproton entering the hydrogen target.

$\check{C}_L$: The number of pulses greater than the above mentioned minimum pulse height from the left Čerenkov counter in coincidence with an antiproton entering the hydrogen target.

N$\emptyset\check{C}$K: Final trigger for the spark chambers for the e^+e^- final state.

N$\emptyset$K: Final trigger for the spark chambers for the $\pi^+\pi^-$ and K^+K^- final states.

physicist. All surviving events were then rescanned using the lead film and only those events were kept which satisfied the following criteria:

1.) There were no straight tracks or tracks with a single scatter coming from the same vertex in the target.

2.) There was at most one γ-ray in addition to the "shower" in each chamber to allow for γ-rays due to radiative corrections.

3.) The "shower" in either chamber had no definite single vertex which was characteristic of a π-interaction in the lead plates.

4.) The "shower" in either chamber had no breaks in the track with no sparks for $\geq$ four consecutive gaps.

This rescan was carried out twice, once by a scanner and once by a physicist.

The film from the thin foil chambers for each of the events that survived the second rescan was then measured on a digitized drafting machine measuring table which was interfaced to an IBM 526 Summary Card Punch. This machine measured an x, y position on the scanning table to $\pm$ 0.030" and an angle to $\pm$ 0.4 milliradians. The four punched cards characterizing the event were then analyzed by a spatial reconstruction and two body kinematics computer program.

This program instructed the computer to compute the position of the annihilation vertex, the polar angles, θ, of both tracks, the azimuthal angles, ϕ, of both tracks, $\Delta\phi$ the coplanarity error, and checked to see if the proper fiducials had been measured and that the second sparks in the tracks had been used as references to measure the positions and angles of the tracks. The laboratory reference frame used for the

analysis had its origin at the center of the liquid hydrogen target with the z-axis along the direction of motion of the $\bar{p}$'s in the beam. $\phi = 0$ was taken to be the horizontal plane to the left of the beam line as seen by an observer traveling with the beam. Using the calculated position of the vertex in the target the energy loss of the antiproton in the liquid hydrogen was corrected for and then assuming that the two final state particles had equal mass this mass was calculated from the known antiproton momentum and the θ angles of the two final particles.

Figures 6, 7, and 8 show the $\Delta\phi$ histogram, $(\text{mass})^2$ histogram, and $(\text{mass})^2$ histogram for events with $\Delta\phi \leq 2.5^{\circ}$ for a sample of events for which the electronic logic had been modified to accept the $\pi^+ + \pi^-$ and $K^+ + K^-$ final states by omitting the Čerenkov counter pulse height requirements. The shifts of the peaks corresponding to the π mass and the K mass are due to a 3% systematic decrease in the mean beam momentum due to a combination of a 1% error in the first bending magnet in the beam and the choice of the point in the target at which the mean beam momentum is defined. Figure 9 shows a histogram of the distance of nearest approach for the two reconstructed tracks for this sample of events. The incident antiproton momentum for these events is 1.50 GeV/c. Figures 10, 11, and 12 show the same histograms for 2.50 GeV/c antiprotons.

The data from the spatial reconstruction program were used as the input to another program which using this information would predict which counters in the hodoscope should have been struck by the final state particles. This information was then compared with the

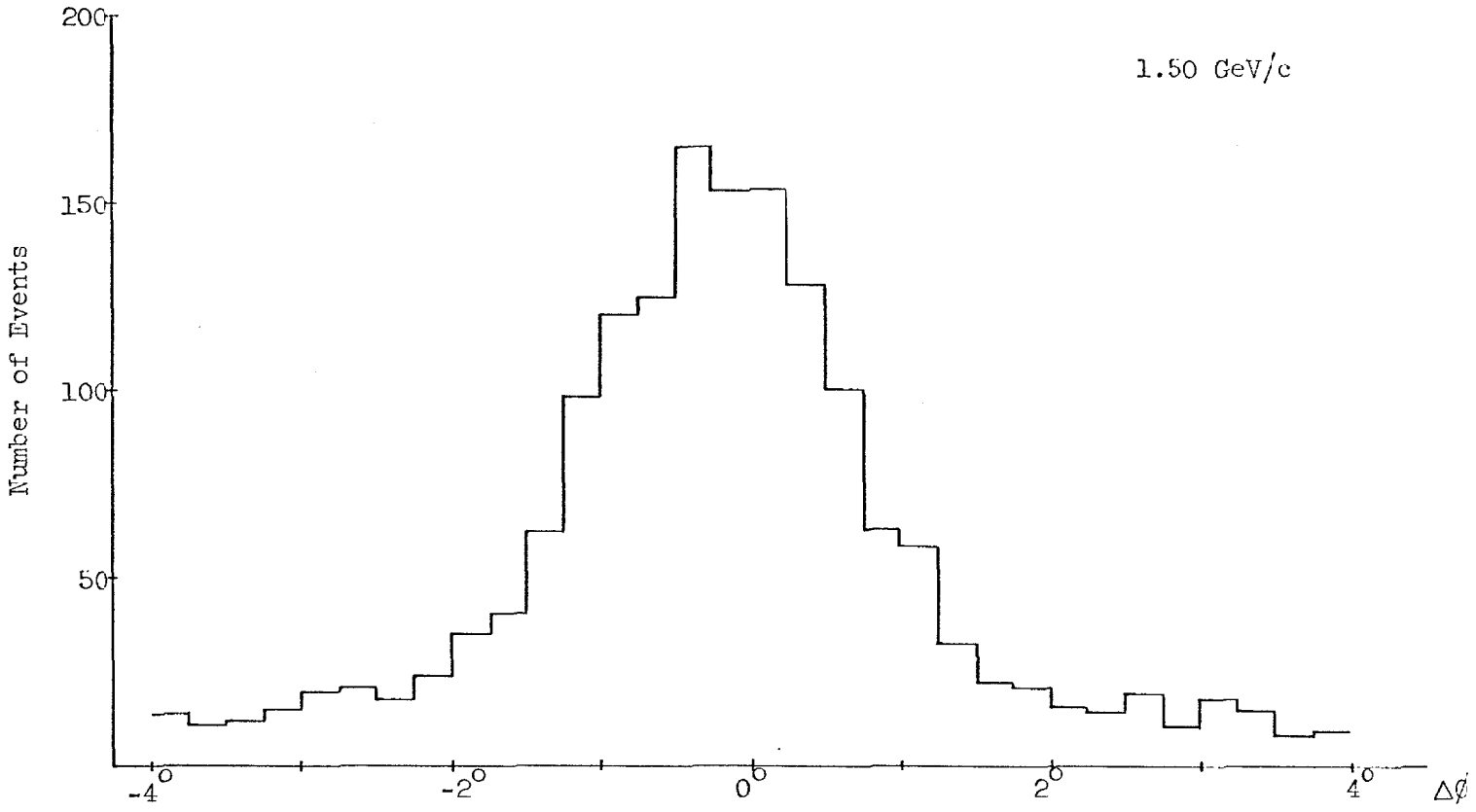

Figure 6 $\Delta\phi$ Histogram for Events Satisfying the $\pi^+\pi^-$ and K^+K^- Trigger Requirements

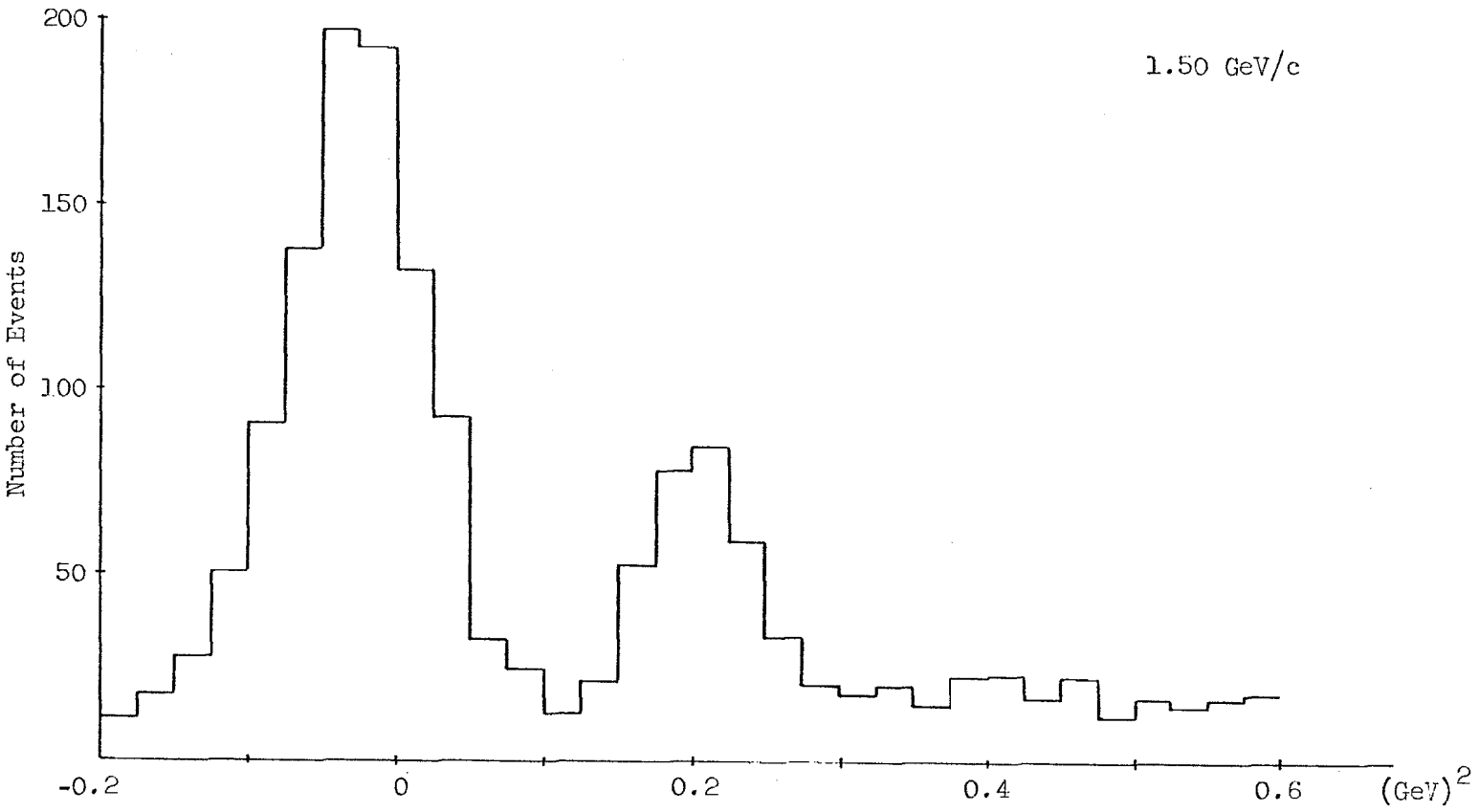

Figure 7 $(\text{mass})^2$ Histogram for Events Satisfying the $\pi^+\pi^-$ and K^+K^- Trigger Requirements

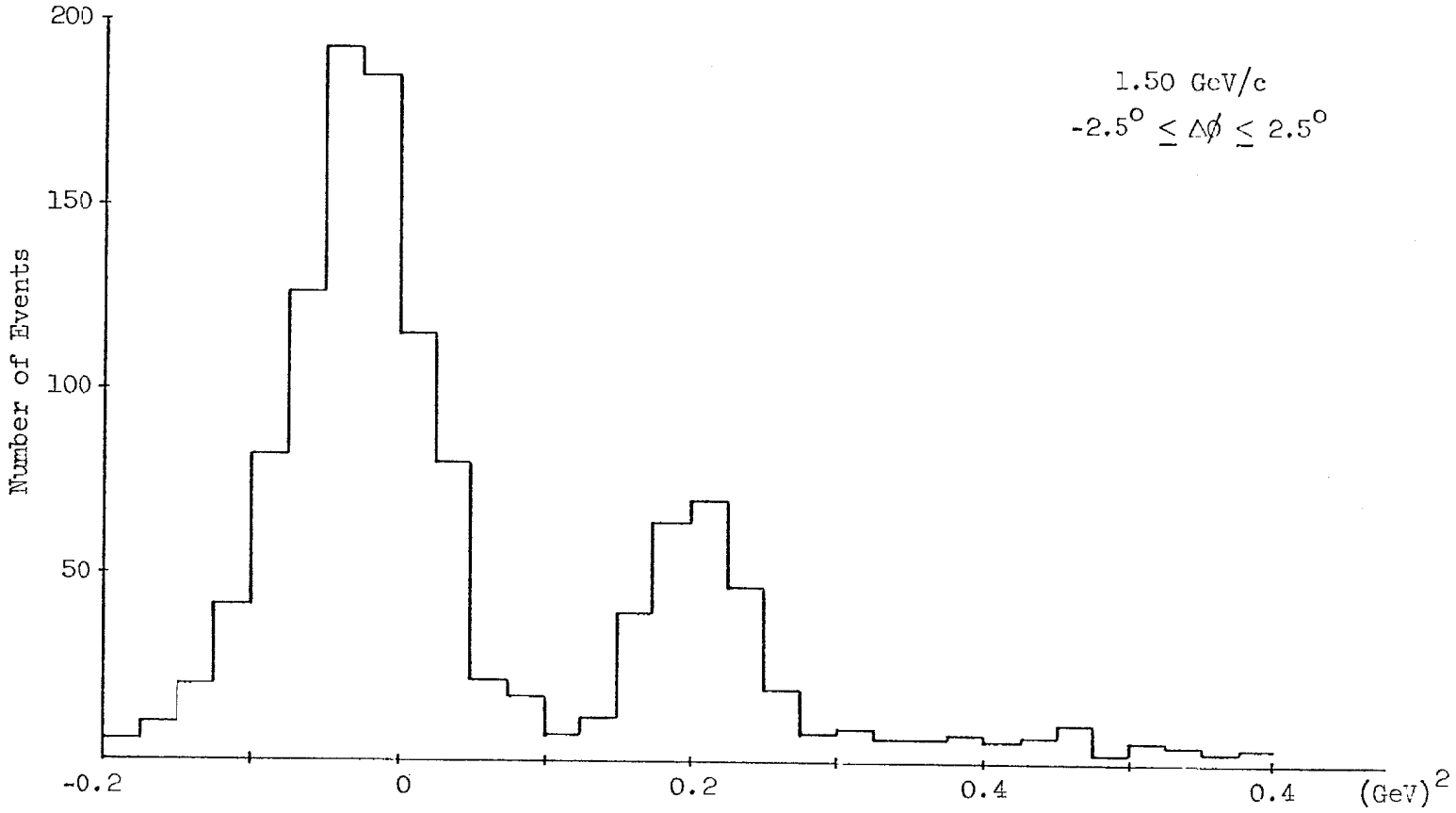

Figure 8 $(mass)^2$ Histogram for Events Satisfying the $\pi^+\pi^-$ and K^+K^- Trigger Requirements and with $|\Delta\phi| \leq 2.5^{o}$

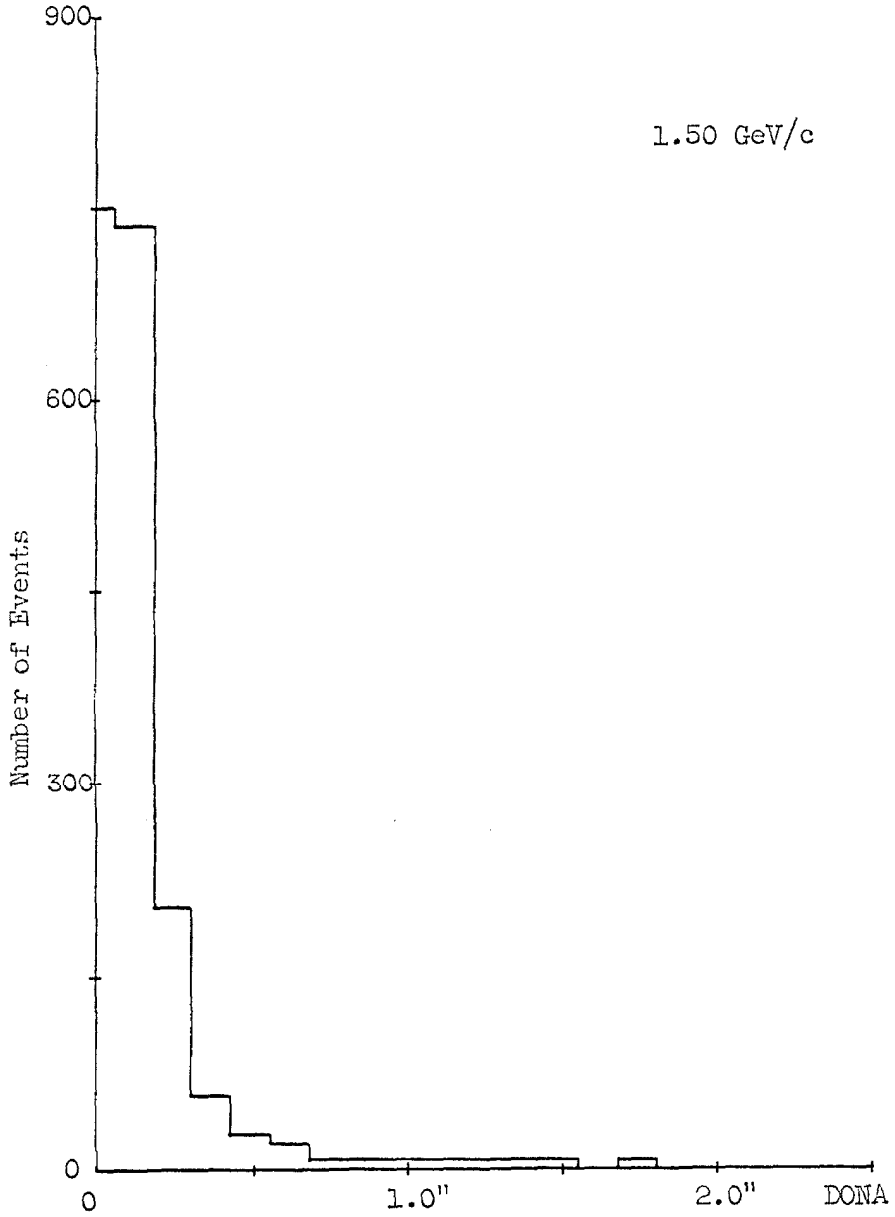

Figure 9 Distance of Nearest Approach for Events Satisfying the $\pi^+\pi^-$ and K^+K^- Trigger Requirements

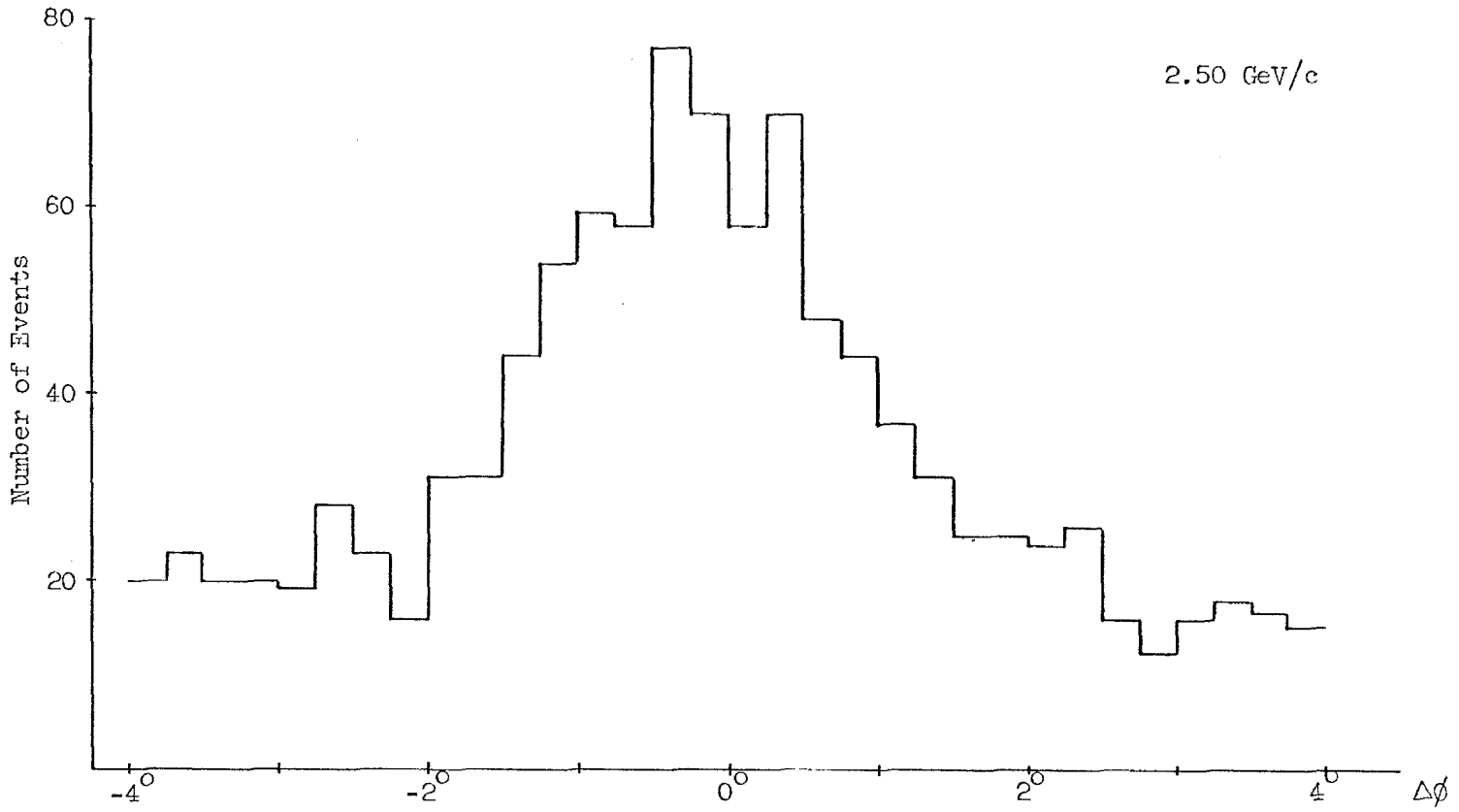

Figure 10 $\Delta\phi$ Histogram for Events Satisfying the $\pi^+\pi^-$ and K^+K^- Trigger Requirements

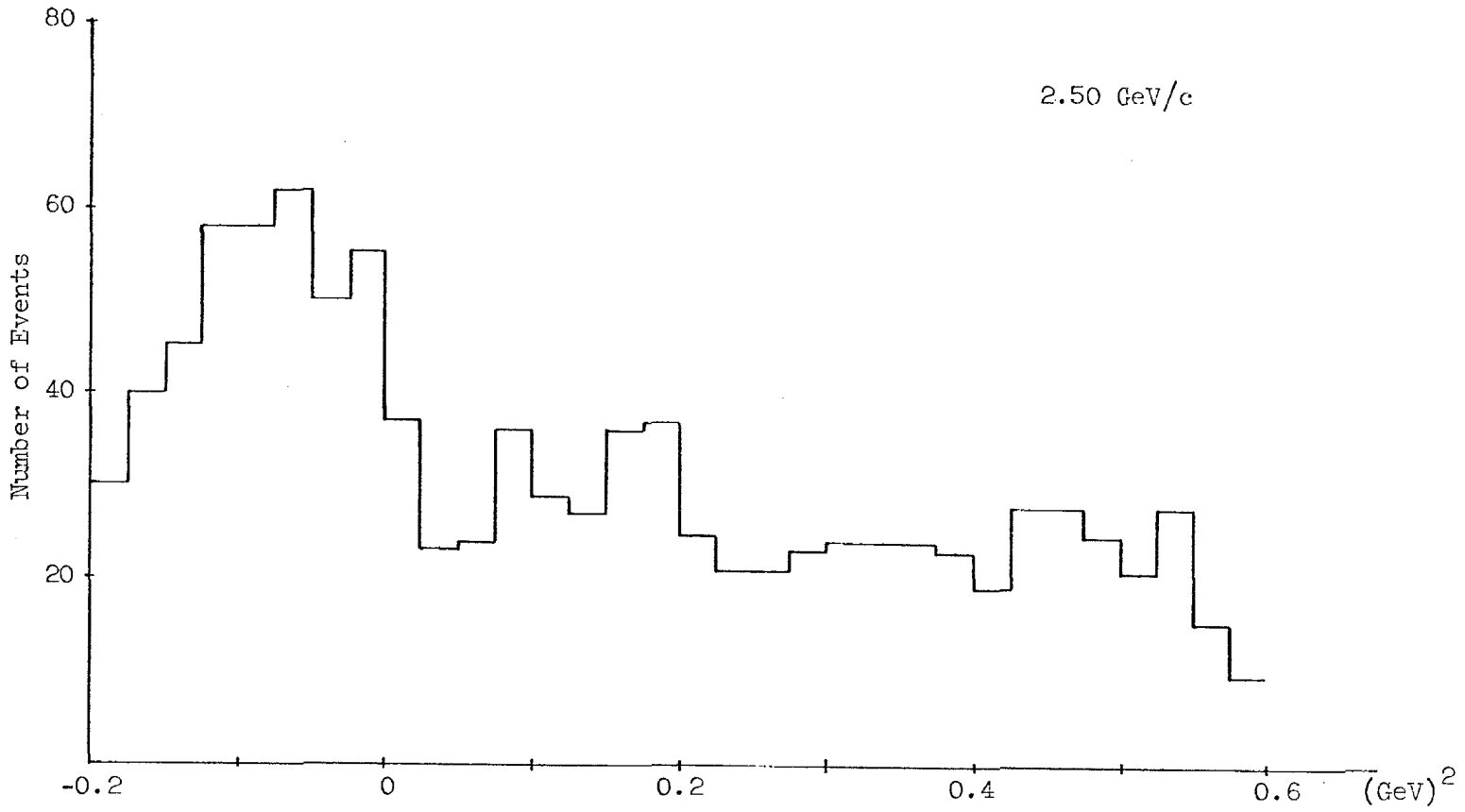

Figure 11. (mass)^2 Histogram for Events Satisfying the $\pi^+\pi^-$ and K^+K^- Trigger Requirements

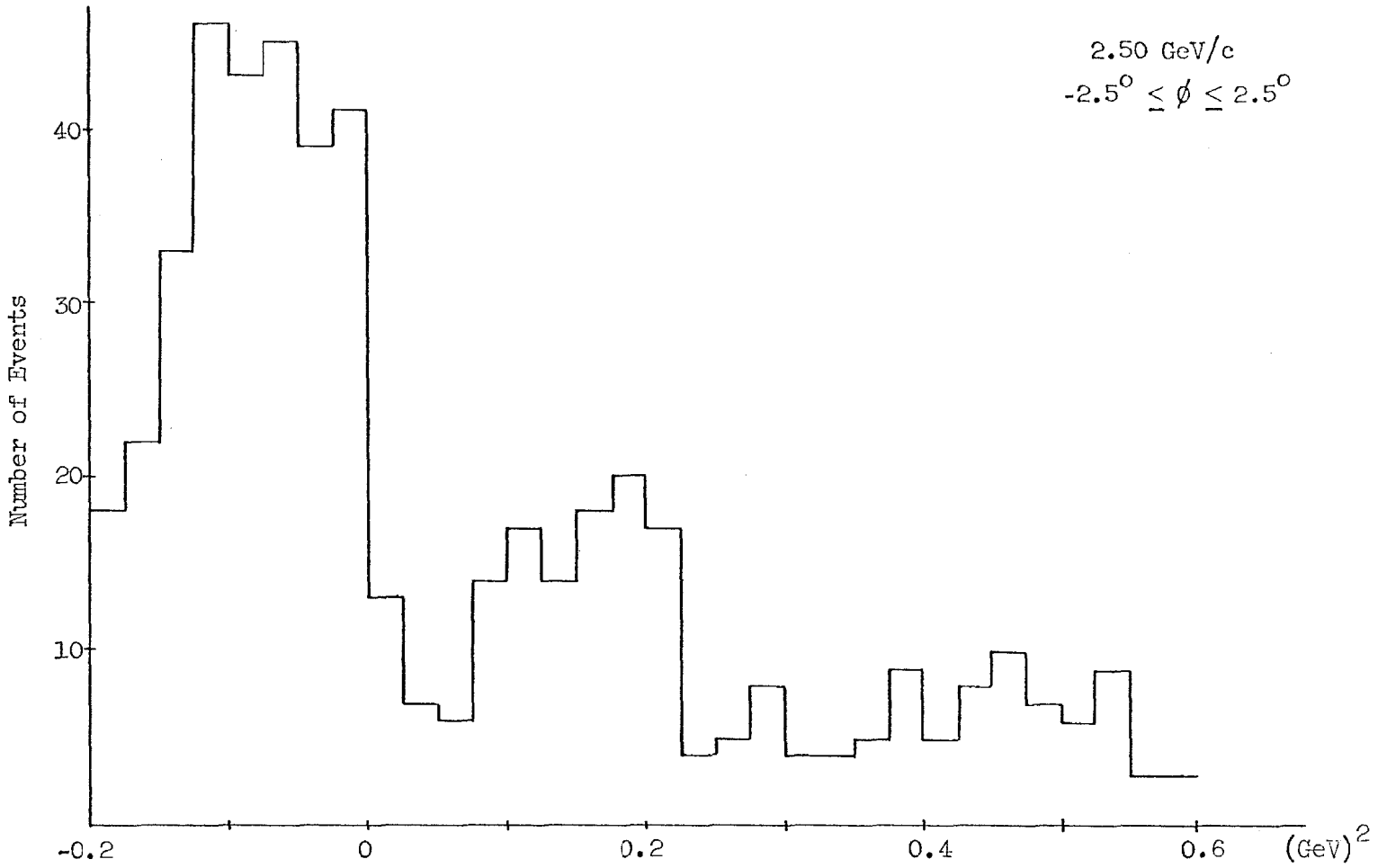

Figure 12 $(mass)^2$ Histogram for Events Satisfying the $\pi^+\pi^-$ and K^+K^- Trigger Requirements and with $|\Delta\phi| \leq 2.5^{\circ}$

information on the card that was punched when the event was photographed. If this information disagreed the event was remeasured.

If a measured event had $\Delta\phi$ within the range -1.90° to $+1.4^{\circ}$, the distance of nearest approach of the reconstructed tracks less than 1.0", its vertex inside the hydrogen target, and its $(\text{mass})^2$ of the final particles within the range $-0.13\ (\text{GeV})^2$ to $+0.03\ (\text{GeV})^2$ for 1.50 GeV/c or $-0.18\ (\text{GeV})^2$ to $+0.02\ (\text{GeV})^2$ for 2.50 GeV/c the showers in the lead chambers were analyzed in detail. These ranges corresponded to the 95% efficiency cuts as determined by fitting a Gaussian to the experimental distributions for $(\text{mass})^2$ and for $\Delta\phi$ for the $\pi^+\pi^-$ final state and shifting the mean of Gaussian for the $(\text{mass})^2$ to the value corresponding to the electron mass.

In the detailed analysis of the showers in the final candidates if either of the showers was asymmetric, i.e. no sparks on one side of the incident particle direction, or had a straight track as the core of the "shower" (typical of a γ-ray superimposed on a straight track), or on close analysis was found to have a single definite vertex, or a track from the shower which made an angle of greater than 45° with the shower axis the event was disregarded. Both showers were required to have single sparks in the first or second gap of the chamber. This eliminated narrow angle pairs which appeared as single tracks in the thin foil chambers and most of the γ-rays which converted early in the lead chambers. The projected θ angles of both showers measured in the lead chambers were required to be within $\pm 4^{\circ}$ of the projected angles of the measured tracks. In addition only events with one extra γ-ray were

accepted as final candidates.

In a sample of 198 known 1.50 GeV/c electrons passing through one of the lead chambers at an angle corresponding to $\theta = 50^{\circ}$, $\phi = 0^{\circ}$, 20 of the resulting showers failed to pass the above criteria for rejecting showers in the data. Results for known electrons for different angles and energies encountered in the experiment were similar. For details see Appendix XII.

In Table 3 the numbers of surviving events at the various stages of scanning for the $e^+ + e^-$ final state are listed for both the 1.50 GeV/c and 2.50 GeV/c incident antiproton momenta.

The film for the $\gamma + \gamma$ final state was scanned first by looking for either one or two electron showers in each lead chamber. The separation between the two showers was required to be less than four inches on the scanning table. This corresponded to the $\leq 10^{\circ}$ opening angle cutoff used in the thin foil chambers. The end view of the thin foil chambers for these events was then scanned and those events having one or two tracks in each chamber with their vertex in the lead sheet and having an opening angle $\leq 10^{\circ}$ were retained. If only one or two tracks with an opening angle of $\leq 10^{\circ}$ appeared in both top views of the thin foil chambers the event was measured. The γ-ray direction was assumed to be the direction of the single track or the bisector of the angle of two tracks for the two track case. The measured events were then analyzed using the same program as for the $e^+ + e^-$ final state. Since the initial scan criteria were very similar to the $e^+ + e^-$ case and all events were scanned twice the scanning efficiency has been taken to be

TABLE 3

Summary of Scanning and Measuring Results for $e^+ + e^-$ Final State

	1.50	2.50
Total Pictures	58,000	26,000
First Scan of Pb Chambers	1,600	500
Second Scan of Pb Chambers	144	49
Kinematics OK	26	7
Final Analysis of Showers	2	0
No Extra γ-ray	2	0

TABLE 4

Summary of Scanning and Measuring Results for $\gamma + \gamma$ Final State

	1.50	2.50
Total Pictures	1990	932
First Scan Pb Chambers	85	30
Thin Foil	12	3
Kinematics $\pm 3^{o}$	2	0

the same as for the $e^+ + e^-$ case namely > 98%.

The scanning and measuring results are listed in Table 4. The numbers in the table represent the number of events satisfying all criteria up to and including the heading of the row containing the number.

2. Scanning Efficiency

About one third of the 1.50 GeV/c data was scanned initially by three different scanners. In this sample there were thirty-two events which survived the second scan. Two of the scanners each missed one of these events while the third missed six of these events in their initial scans. Comparison of the events surviving the initial scans of two scanners showed that one scanner missed on the order of 20-30% of the events surviving in the combined initial scans. This disagreement arose because of the very fuzzy cut-off for good and bad events in the first scan. The results of the comparison using events surviving the second scan represented the scanning efficiency much more realistically and gave a scanning efficiency of > 98% for the combined scans of two scanners.

3. Solid Angle

The solid angle acceptance of the detection apparatus was calculated for the $e^+ + e^-$ final state with a Monte Carlo computer program. As a check, the solid angle for a flat center of mass angular distribution was calculated using scale drawings of the apparatus by measuring the actual target length from which the final state could be detected.

Figures 13 and 14 illustrate these measurements. The graphical results and the results from the Monte Carlo program agree to within

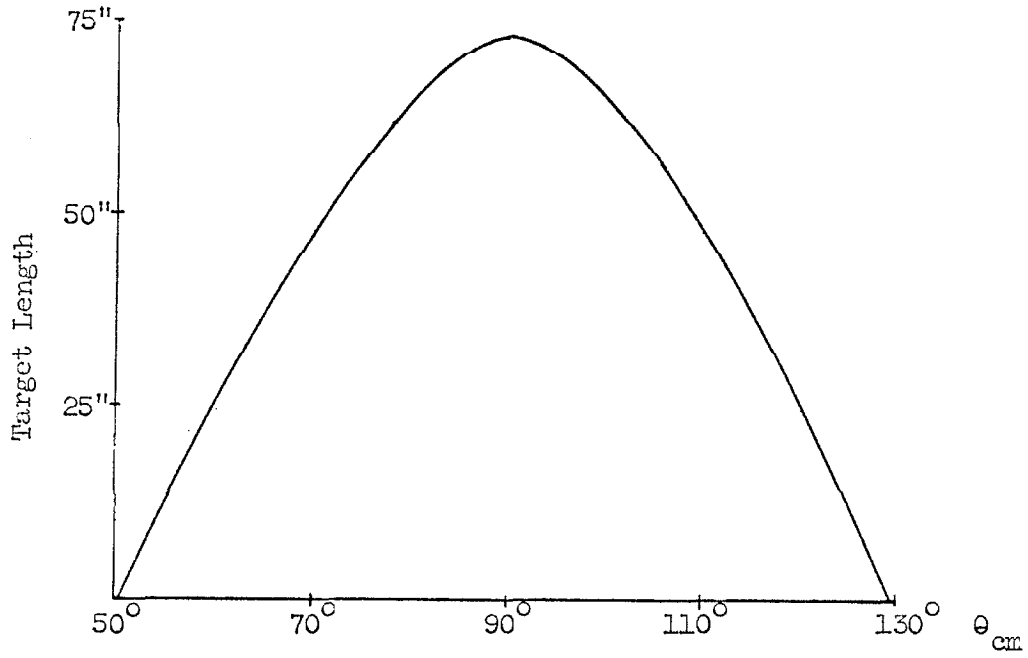

Figure 13 Target Length as a Function of θ_{cm} for 1.50 GeV/c

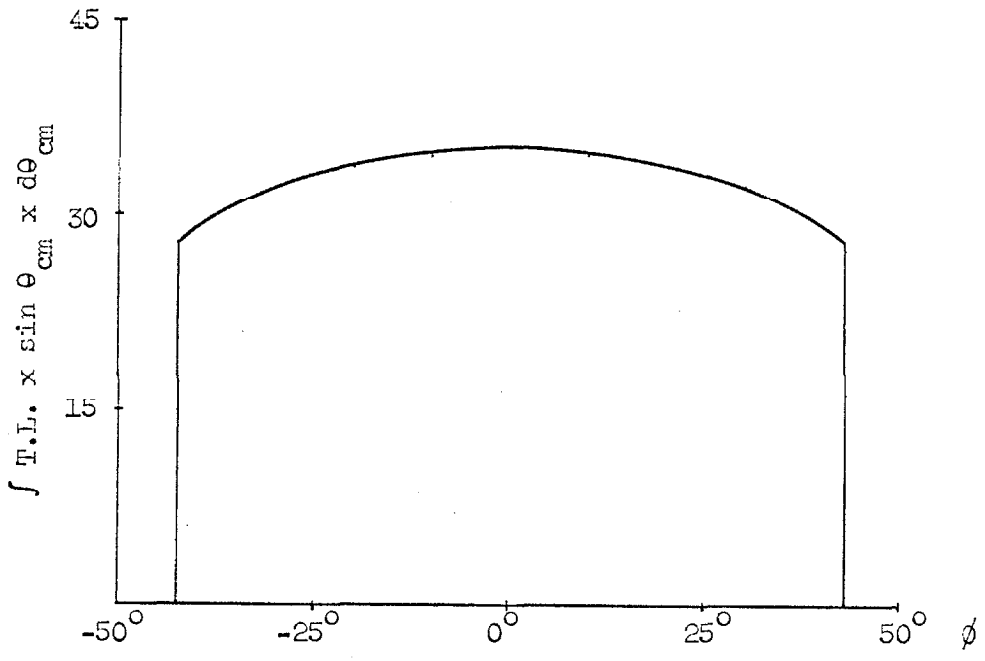

Figure 14 Integrated Target Length as a Function of ϕ

$\pm$ 5%.

The Monte Carlo program includes the beam attenuation in the target (assuming an attenuation length $\lambda = \frac{1}{\rho N_o \sigma_{tot.}}$ where $\sigma_{tot.}$ = total $\bar{p}p$ cross section, N_o = Avogadro's number, and ρ = density of liquid hydrogen), the expected center of mass angular distribution, and the Čerenkov counter detection efficiency. The program is described in detail in Appendix III. A summary of the results is given in Table 5.

The average Čerenkov counter efficiency for detecting both particles in the $e^+ + e^-$ final state with the bias used during the experiment was 94% $\pm$ 1%. In addition effects due to spreading of the electron showers and the choice of the "edge" of the Čerenkov counters can lead to systematic uncertainties of the order of 10%. Thus the quoted errors on the above acceptances which are statistical due to the finite number of trails used in the Monte Carlo program were increased to 10% in the cross section calculations.

The acceptance for the $\gamma + \gamma$ final state would be the same as for the $e^+ + e^-$ if the pairs from the converted γ-rays had zero opening angles. Using the experimental opening angle distribution for pairs from lead as described in Appendix II, the overall acceptance is decreased by 0.95 $\pm$ 0.03 giving for a flat angular distribution

$$\Delta\Omega \times \mathcal{A} = (0.73 \pm 0.05) \times \pi \text{ for 1.50 GeV/c}$$

and $$\Delta\Omega \times \mathcal{A} = (0.91 \pm 0.05) \times \pi \text{ for 2.50 GeV/c.}$$

These are subject to the same systematic uncertainties as those for the $e^+ + e^-$ final state.

TABLE 5

Summary of Monte Carlo Calculations of the Solid Angle Acceptance

	1.50	2.50
Flat Angular Distribution	$(0.772 \pm 0.030) \times \pi$	$(0.957 \pm 0.034) \times \pi$
$G_E = \frac{G_M}{1 + \mu} = \frac{G_M}{2.79}$	$(0.640 \pm 0.026) \times \pi$	$(0.765 \pm 0.030) \times \pi$
$G_E = G_M$	$(0.664 \pm 0.030) \times \pi$	$(0.794 \pm 0.030) \times \pi$
$G_E = 0$	$(0.616 \pm 0.025) \times \pi$	$(0.736 \pm 0.030) \times \pi$

The units are steradian-meters (i.e. target length x $\Delta\Omega$).

4. Overall Detection Efficiencies

Besides the efficiencies already mentioned the hodoscope efficiency, the multiples veto efficiency, dead time losses due to only one picture per machine pulse, and the efficiency due to the cuts made for the allowed angles for the measured events must also be included in the cross section calculation. These amounted to

hodoscope efficiency	$\epsilon_h = .95 \pm 0.01$,
multiples veto efficiency	$\epsilon_m = .97 \pm 0.005$,
dead time efficiency	$\epsilon_d = .92 \pm 0.03$, and
kinematic cuts	$\epsilon_k = .90 \pm 0.02$.

The detailed calculations of these efficiencies are given in Appendices IV and XV.

For the $\gamma + \gamma$ final state there was an additional inefficiency due to the stringent requirements placed on the conversion of the γ-rays in the lead plate in front of the thin foil chambers. These requirements lead to a detection efficiency of $\epsilon_\gamma = (8 \pm 2) \times 10^{-2}$ for each γ-ray. Including all corrections except dead time losses and solid angle the overall detection efficiency for the $\gamma + \gamma$ final state was

$$\epsilon_{det} = (6.5 \pm 2.0) \times 10^{-3}.$$

The detailed calculation of this efficiency is given in Appendix I.

IV. BACKGROUNDS

In any experiment which ends up as this one does with only two final candidates for each of two different final states the background analysis is important. It becomes especially important when one of these final states (2γ) represents a serious background to the other (e^+e^-). In the present case there is the added difficulty that the available data on the final states of the $\bar{p}p$ system which are the major contributors to the backgrounds of both the 2γ and the e^+e^- final states are not very good.

The background to the 2γ final state comes about primarily from the inability of the apparatus to detect or resolve the extra γ-rays from the $\pi^o\gamma$, $2\pi^o$,... final states. Estimates of the contribution of final states of the type $\pi^+\pi^- n\pi^o$, n = 1, 2... and $\pi^+\pi^-\pi^+\pi^- n\pi^o$, n = 1, 2... indicate that it is much smaller than that due to the neutral final states. This smallness is due to the high detection efficiencies of the veto counters and the spark chambers (>98%), the $\pm 3^o$ kinematics resolution, and the decrease in the γ-ray energies due to the sharing of the total cm energy among the many final state particles.

For the e^+e^- final state the background divides naturally into two parts. The first part is due to the final states $\pi^+\pi^- n\pi^o$, n = 0, 1, 2, ... in which the π^+ and π^- have the e^+e^- kinematics and the overlappings of the converted γ-ray (s) from π^o decay (s) and the $\pi^\pm$ in the Pb chambers give "showers" which satisfy the electron shower selection criteria. For n = 0 it is the interactions of the π^+ and π^- in the Pb

chambers which satisfy the electron shower criteria. These criteria are listed in Part III, Section b. As in the 2γ case estimates of the contribution to the background from final states of the type $\pi^+\pi^-\pi^+\pi^- n\pi^o$ indicate that it is small compared to the major sources discussed below.

The second part of the background to the e^+e^- final state comes from the conversion of γ-rays from final states of the type 2γ, $\pi^o\gamma$, $2\pi^o$,... in the material between the point of annihilation and the charged particle detectors (the inner trays of counters in the hodoscopes). Because of the small amount of material between the average conversion point and the front of the Pb chambers and the relatively short path length between them the average separation of the narrow angle pair due to multiple scattering is $< 0.1''$ at the front of the Pb chambers. For this reason, it is impossible to differentiate between a narrow angle pair from a converted γ-ray and a single electron in a small sample of events.

Since previous to this experiment there were no data on the neutral final states 2γ, $\pi^o\gamma$, $2\pi^o$, and $3\pi^o$ for the $\bar{p}p$ annihilation short runs were made at the end of the e^+e^- running to look for these processes.

The data for the $\pi^o\gamma$, $2\pi^o$, and $3\pi^o$ final states consisted of photographs of the top view of the Pb chambers. The chambers were triggered if there were no charged particles coming from the target and the pulse from both Cerenkov counters were greater than one half the minimum value accepted for the e^+e^- final state. Because only the top view of the Pb chambers was photographed exact reconstruction of the event was

impossible. Instead, distributions of the differences between the expected and the measured opening angles of the particles were used to isolate the various final states. The π^o direction was taken to be the mean of the two γ-ray angles in this comparison. The $2\pi^o$ and $3\pi^o$ final states were studied by scanning the film for events with two converting γ-rays in each Pb chamber. Events with two converting γ-rays in one chamber and one in the other chamber were used to study the $\pi^o\gamma$ final state.

The details of the scanning, measuring, and analysis of the data for the $2\pi^o$ and $3\pi^o$ final states are the subject of Appendix V. The $\pi^o\gamma$ final state is treated in Appendix VI.

Because of this data analysis scheme the $3\pi^o$ final state is a background to the $2\pi^o$ final state which in turn is a background to the $\pi^o\gamma$ final state. The $\pi^o\gamma$ final state is one of the main contributors to the background of the data for the 2γ final state which in turn provides the most serious background in the data for the e^+e^- final state. The whole procedure can be compared to an onion where the outer layers (sources of background) must be removed one at a time to reach the inner core here represented by the upper limits on the cross section for the e^+e^- final state. Figure 15 is a flow diagram illustrating the interconnections in the background analysis.

In Table 6 the results of the background analysis are presented. In all cases the differential cross section is defined by

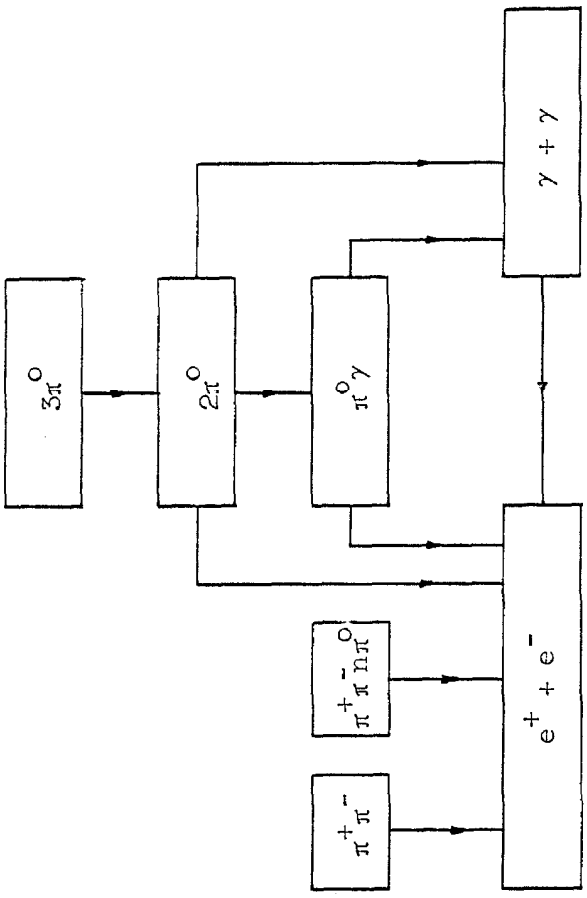

Figure 15 Flow Diagram of the 1.50 GeV/c Background Analysis

Table 6 Summary of the Background Analysis for the 1.50 GeV/c Data

Annihilation	Cross Section ($\frac{d\sigma}{d\Omega}_{90^o}$ $cm^2/st.$) (No Background Subtraction)	Background $\frac{d\sigma}{d\Omega}_{90^o}$ (90% confidence level) $cm^2/st.$	
$\bar{p}p \to 2\pi^o$	$(1.9 \pm 0.2) \times 10^{-30}$	$3\pi^o$	$\leq 1.0 \times 10^{-30}$
$\bar{p}p \to 2\gamma$	$(1.6 \,^{+\,1.9}_{-\,0.8}) \times 10^{-31}$	$2\pi^o$	$\leq 0.1 \times 10^{-31}$
		$\pi^o\gamma$	$\leq 0.3 \times 10^{-31}$
		Total	$\leq 0.4 \times 10^{-31}$
$\bar{p}p \to e^+e^-$	$(1.2 \,^{+\,1.1}_{-\,0.6}) \times 10^{-34}$	$\pi^+\pi^-$	$\leq 1.5 \times 10^{-35}$
		$\pi^+\pi^- n\pi^o$	$\leq 1.4 \times 10^{-36}$
		$2\pi^o$	$\leq 3.1 \times 10^{-35}$
		$\pi^o\gamma$	$\leq 0.8 \times 10^{-35}$
		2γ	$= (1.3 \,^{+\,1.5}_{-\,.65}) \times 10^{-34}$

$$\frac{d\sigma}{d\Omega} = \frac{\text{no. of events}}{\text{solid angle of detector x no. of target particles/cm}^2 \text{ x no. of beam particles.}}$$

This definition differs from the more conventional one where the no. of events is replaced by the no. of particles. For distinguishable particles the two definitions are equivalent. However, for two identical particles ($2\pi^0$ or 2γ) the cross sections given here are equal to <u>one half</u> the conventional differential cross sections. The reason for using this particular definition is that it greatly simplifies the bookkeeping problem for factors of two when comparing various final states as is necessary in the background analysis.

To avoid confusion about the meaning of the statement to a "90% confidence level upper limit" or "90% conf." these statements are defined to be the number equal to the mean expected value + 1.8 standard deviations. For Poisson statistics which are used in all calculations presented here the standard deviation = $(\text{mean value})^{\frac{1}{2}}$. It will be further assumed that the number of observed events is the mean of Poisson distribution governing these events. The errors quoted for the cross sections will always be the standard errors which are defined by the minimum and maximum values for the cross section that have a probability ≥ 0.16 of being found if the cross section is remeasured. For means ≥ 20 the standard errors become very nearly equal to the standard deviation. The standard errors are determined from the integrals of the Poisson distribution given in Reference 25.

The remainder of this chapter is devoted to a more detailed discussion of the background analysis. Section a deals with the

background analysis for the 2γ final state while Section b treats the analysis of the background for the e^+e^- final state. Since no final candidates for either the 2γ or the e^+e^- final state were found in the 2.50 GeV/c data only the detailed analysis for the 1.50 GeV/c case will be presented below.

For the 2.50 GeV/c the maximum expected background cross sections considering the same sources as for the 1.50 GeV/c case are estimated to be

$$\frac{d\sigma}{d\Omega}\Big|_{90^\circ} (\text{Fake } e^+e^-) \approx 1.3 \times 10^{-35} \text{ cm}^2/\text{st.} \qquad (2.50 \text{ GeV/c})$$

and $$\frac{d\sigma}{d\Omega}\Big|_{90^\circ} (\text{Fake } 2\gamma) \approx 3 \times 10^{-33} \text{ cm}^2/\text{st.} \qquad (2.50 \text{ GeV/c})$$

In obtaining these rough limits the cross sections of the major contributing final states at 1.50 GeV/c have been scaled by a factor of 1/10 determined from the dependence of the $\pi^+\pi^-$ and $2\pi^\circ$ cross sections on the incident $\bar{p}$ momentum.

a. 2γ Final State Background

From the arguments given above the $\pi^\circ\gamma$ and the $2\pi^\circ$ final states have been taken as the major contributors to the background in the data for the 2γ final state. Only these two final states have been analyzed in detail. The basic tools in these analyses have been Monte Carlo calculations using slightly modified versions of the basic computer program described in Section b of Appendix III. In these calculations the center of mass angular distribution of the final state particles was always assumed to be flat.

The following effects were taken into account in these calculations.

The two detected γ-rays were required to have kinematics within $\pm 3^{\circ}$ of the expected 2γ kinematics. The 65% detection efficiency of the veto counters and the 75% conversion efficiency of the Pb plate in front of the thin foil chambers for the extra γ-rays were included. Since there was only a top view of the Pb chambers it was possible for the extra γ-rays converting in the Pb chambers to overlap the electron showers and escape detection. This possibility was taken into account by only accepting events in which the extra γ-rays converted within a minimum projected angular region ($= \pm 1^{\circ}$) about one of the electron directions. The spreading of the electron shower was taken into account in this acceptance.

In the cases where only two γ-rays were detected the ϕ distribution of the successful Monte Carlo events shown in Figures 16 and 17 was taken into account in calculating the background for the two final candidates. Since both of these candidates has $|\phi| < 10^{\circ}$ the correction factor used for the $\pi^{o}\gamma$ case was 0.50 and was 0.05 for the $2\pi^{o}$ case. This last factor represents the probability that zero events are observed when three are expected (for a flat distribution) and is clearly an upper limit for the correct factor.

The results of these calculations can be summarized in the form of relative detection efficiencies for fake 2γ events from these final states. The labels used for these efficiencies indicate the final state and the number of γ-rays from this final state that are detected in the Pb chambers. The results for the $2\pi^{o}$ final state are

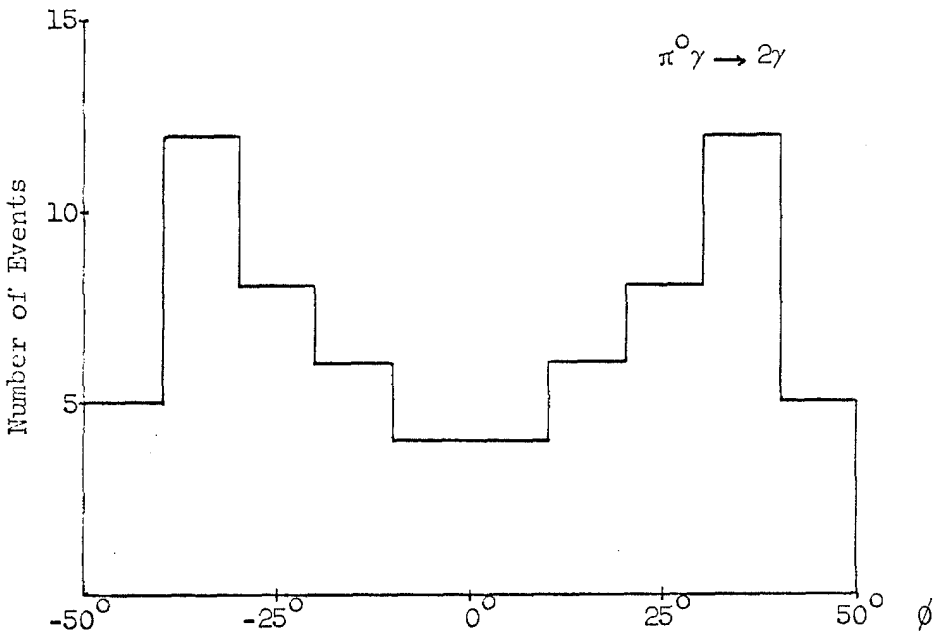

Figure 16 ϕ Distribution for Successful Monte Carlo Events for $\pi^o\gamma \rightarrow 2\gamma$

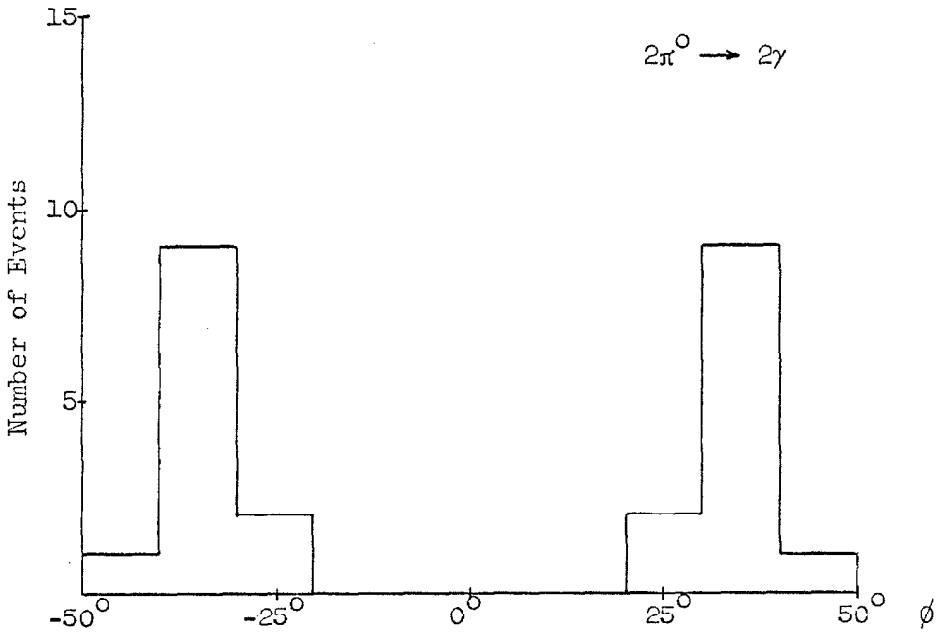

Figure 17 ϕ Distribution for Successful Monte Carlo Events for $2\pi^o \rightarrow 2\gamma$

$$\epsilon_{2\pi^0 \rightarrow 4\gamma} = (1.7 \pm 0.4) \times 10^{-3}$$

$$\epsilon_{2\pi^0 \rightarrow 3\gamma} = (2.5 \pm 1.3) \times 10^{-3}$$

$$\epsilon_{2\pi^0 \rightarrow 2\gamma} = (0.6 \pm 0.2) \times 10^{-3}$$

or combining these

$$\epsilon_{2\pi^0}\ (2\gamma \text{ Fake}) = (4.8 \pm 1.3) \times 10^{-3}.$$

The results for the $\pi^0\gamma$ final state are

$$\epsilon_{\pi^0\gamma \rightarrow 3\gamma} = (0.68 \pm .15) \times 10^{-2}$$

$$\epsilon_{\pi^0\gamma \rightarrow 2\gamma} = (3.6 \pm 0.5) \times 10^{-2}$$

or combining these gives

$$\epsilon_{\pi^0\gamma}\ (2\gamma \text{ Fake}) = (4.3 \pm 0.5) \times 10^{-2}.$$

As in indicated in Table 6 the data used to determine the $2\pi^0$ cross sections could contain a 50% background due to the $3\pi^0$ final state. In addition the cross section for the $\pi^0\gamma$ final state with the $2\pi^0$ background subtracted is really an upper limit for the reasons mentioned in Appendix VI. However, to carry out the background analysis these cross sections are assumed to be the correct ones for the $2\pi^0$ and $\pi^0\gamma$ final states. They are

$$\frac{d\sigma}{d\Omega}\Big|_{90^0}(\bar{p}p \rightarrow 2\pi^0) = (1.9 \pm 0.2) \times 10^{-20}\ \text{cm}^2/\text{st.} \quad (1.50\ \text{GeV/c})$$

$$\frac{d\sigma}{d\Omega}\Big|_{90^0}(\bar{p}p \rightarrow \pi^0\gamma) = (0.41 \pm 0.05) \times 10^{-30}\ \text{cm}^2/\text{st.} \quad (1.50\ \text{GeV/c})$$

where the differential cross section for the $\pi^0\gamma$ final state is assumed to be flat in the $\bar{p}p$ cm system.

Combining these cross sections with the relative detection efficiencies gives

$$\frac{d\sigma}{d\Omega}\Big|_{90^0}(\bar{p}p \rightarrow 2\pi^0)_{\text{Fake } 2\gamma} = (0.9 \pm 0.2) \times 10^{-32}\ \text{cm}^2/\text{st.}\ (1.50\ \text{GeV/c})$$

γ-ray was constrained as in the 2γ case.

According to Tsai [26] one half of the radiative correction γ-rays make an angle with respect to the electron of $< \overline{\theta} = \frac{1}{\sqrt{\gamma_{el.}}}$ where $\gamma_{el.} = \frac{E_{cm}(\text{electron})}{m_e} \approx 2200$. The choice of 4° for the allowed projected opening angle includes $\approx 75\%$ of the radiative correction γ-rays that could be detected in the Pb spark chamber.

The results of the Monte Carlo calculations can be summarized in the form of relative detection efficiencies which are

$$\epsilon_{\pi^{o}\gamma \rightarrow 3\gamma} = (1.0 \pm 0.3) \times 10^{-2}$$

$$\epsilon_{2\pi^{o} \rightarrow 3\gamma} = (2.5 \pm 1.0) \times 10^{-3}$$

$$\epsilon_{2\pi^{o} \rightarrow 4\gamma} = (8.5 \pm 2.0) \times 10^{-3}.$$

The notation is the same as for the 2γ case.

The average amount of material available for the conversion of the γ-rays in order to be detected as electrons was $X_o = 0.037$ radiation lengths. Combining the conversion probability $= \frac{7}{9} \times 0.037 = 0.029$ with the Dalitz decay probability $= \frac{1}{160}$ in the present case the conversion efficiency for both γ-rays which have the $e^{+}e^{-}$ kinematics is

$$\epsilon_{2\pi^{o}} = 1.3 \times 10^{-3}$$

and $\epsilon_{\pi^{o}\gamma} = 1.0 \times 10^{-3}$.

Multiplying these conversion efficiencies by the appropriate detection efficiencies gives the overall detection efficiencies which are

$$\bar{\epsilon}_{2\pi^{o}} = (1.4 \pm 0.4) \times 10^{-5}$$

and $\bar{\epsilon}_{\pi^{o}\gamma} = (1.0 \pm 0.3) \times 10^{-5}$.

Taking the cross sections for $\bar{p}p \rightarrow 2\pi^{o}$ and $\bar{p}p \rightarrow \pi^{o}\gamma$ given above in Section a gives using these detection efficiencies

and

$$\frac{d\sigma}{d\Omega}\Big|_{90^o}(\bar{p}p \rightarrow \pi^o\gamma)_{\text{Fake } 2\gamma} = (1.8 \pm 0.5) \times 10^{-32} \text{ cm}^2/\text{st. (1.50 GeV/c)}$$

The overall background cross section is then given by

$$\frac{d\sigma}{d\Omega}\Big|_{90^o}(\bar{p}p \rightarrow 2\gamma)_{\text{Fake}} = (2.7 \pm 0.6) \times 10^{-32} \text{ cm}^2/\text{st.}$$

Provided that no major contributions to the background in the data for the 2γ final state have somehow been omitted this represents an upper limit to the background to the 2γ final state. This is due to the assumptions about the $2\pi^o$ and $\pi^o\gamma$ cross sections.

b. e^+e^- Final State Background

The analysis of the first part of the e^+e^- background is carried out in Appendices XII and XVII. The results are

$$\frac{d\sigma}{d\Omega}\Big|_{90^o}(\bar{p}p \rightarrow \pi^+\pi^-)_{\text{Fake } e^+e^-} = (2.3 \,^{+\,12.0}_{-\,1.2}) \times 10^{-36} \text{ cm}^2/\text{st.(1.50 GeV/c)}$$

and

$$\frac{d\sigma}{d\Omega}\Big|_{90^o}(\bar{p}p \rightarrow \pi^+\pi^- n\pi^o)_{\text{Fake } e^+e^-} = (8.8 \,^{+\,4.7}_{-\,3.0}) \times 10^{-37} \text{ cm}^2/\text{st. (1.50 GeV/c)}$$

The results of Fong's preliminary analysis of the data for $\bar{p}p \rightarrow \pi^+\pi^-$ are used to obtain the first background contribution.

In analyzing the second part of the e^+e^- background the contributions from the $2\pi^o$ and $\pi^o\gamma$ final states were determined from calculations made using essentially the same Monte Carlo programs as used in the 2γ background analysis. The kinematics requirement was changed to $\pm 1.8^o$ corresponding to the 95% kinematics cuts used for the e^+e^- final state. In addition one of the extra γ-rays was allowed to make up to a 4^o projected opening angle with respect to the electron direction. This allowed for $\approx 75\%$ of the real γ-rays associated with the e^+e^- final state due to radiative corrections. The opening angle of the other

$\frac{d\sigma}{d\Omega}|_{90^\circ}\ (\bar{p}p \rightarrow 2\pi^\circ)_{\text{Fake } e^+e^-} = (2.5 \pm 0.4) \times 10^{-35}\ \text{cm}^2/\text{st.}\ (1.50\ \text{GeV/c})$

and

$\frac{d\sigma}{d\Omega}|_{90^\circ}\ (\bar{p}p \rightarrow \pi^\circ\gamma)_{\text{Fake } e^+e^-} = (0.4 \pm 0.2) \times 10^{-35}\ \text{cm}^2/\text{st.}\ (1.50\ \text{GeV/c})$

The contribution of the 2γ final state to the background in the data for the e^+e^- final state is given simply by

$\frac{d\sigma}{d\Omega}|_{90^\circ}\ (\bar{p}p \rightarrow 2\gamma)_{\text{Fake } e^+e^-} = (0.029)^2 \times \frac{d\sigma}{d\Omega}|_{90^\circ}\ (\bar{p}p \rightarrow 2\gamma).$

If the cross section given in Part V for the 2γ final state is correct then the expected background cross section is

$\frac{d\sigma}{d\Omega}|_{90^\circ}\ (\bar{p}p \rightarrow 2\gamma)_{\text{Fake } e^+e^-} = (1.3\ ^{+\ 1.5}_{-\ .65}) \times 10^{-34}\ \text{cm}^2/\text{st.}\ (1.50\ \text{GeV/c})$

The if in the last sentence is important because the 2γ cross section is based on only two events. In addition there is a 30% uncertainty in the detection efficiency for the 2γ final state and the background contribution could be as large as one quarter of the cross section. Any cross section with this heritage must be used with caution.

If the above results are combined the total background for the e^+e^- final state is

$\frac{d\sigma}{d\Omega}|_{90^\circ}\ (\text{Fake } e^+e^-) = (1.6\ ^{+\ 1.5}_{-\ .7}) \times 10^{-34}\ \text{cm}^2/\text{st.}\qquad (1.50\ \text{GeV/c})$

V. RESULTS AND CONCLUSIONS

The results of the analysis of the data from the experiment can be broken down into three categories. The analyses of the data from the runs looking for the $2\pi^o$, $\pi^o\gamma$, and $3\pi^o$ final states provide interesting upper limits on the cross sections for these final states. Although the runs were originally made to check for possible backgrounds to the e^+e^- final state the results are sufficiently interesting so that they should not become lost in the Appendices. These results will be discussed in Section a below. Perhaps the most surprising result from the experiment comes from the analysis of the data for the 2γ final state for 1.50 GeV/c antiprotons. In this case two events survive all of the requirements that can be reasonably placed on their spark chamber photographs and their Čerenkov counter pulse heights. A detailed background analysis indicates that the probability that these two events are due to background is small. This of course assumes that all of the possible backgrounds have been thought of and have been included in the background analysis. These two events imply a cross section that is approximately twenty times larger than that predicted by two possible models for the annihilation. This result along with the models and the upper limit on the cross section for 2.50 GeV/c antiprotons obtained from this data is discussed in Section b below. In Section c the final results for the e^+e^- final state for 1.50 GeV/c and 2.50 GeV/c antiprotons are discussed.

To avoid confusion the definition used for the differential cross

sections reported here is that

$$\frac{d\sigma}{d\Omega} = \frac{\text{no. of events}}{\Delta\Omega \times \text{no. of target particles} \times \text{no. of beam particles}}.$$

For identical particles this definition gives a value equal to 1/2 the value given by the more conventional definition where the number of events is replaced by the number of detected particles. For distinguishable particles the two definitions are equivalent.

a. $3\pi^o$, $2\pi^o$, and $\pi^o\gamma$ Final States

The most striking feature of the results from the analysis of the data for the $3\pi^o$ and $2\pi^o$ final states is the small size of their cross sections compared to the known values for the $\pi^+\pi^-\pi^o$ and $\pi^+\pi^-$ final states. Figure 18 summarizes these results and includes the known results for the $\pi^+\pi^-\pi^o$ and $\pi^+\pi^-$ final states from various hydrogen bubble chamber experiments.[11, 18, 19, 20, 21] Fong's preliminary results from the analysis of the data for the $\pi^+\pi^-$ final state taken during this experiment agree in magnitude with Lynch's results at 1.61 GeV/c;however they do not agree with the dependence on the incident momentum indicated by combining Lynch's result and the CERN[19] result which is based on one event. Fong's results agree with the dependence on the incident momentum shown by the 90^o cm differential cross section for the $2\pi^o$ final state.

A simple statistical model which assumes that the antiproton-proton initial state has equal amplitudes with total isotopic spin = 1 and total isotopic spin = 0 predicts that

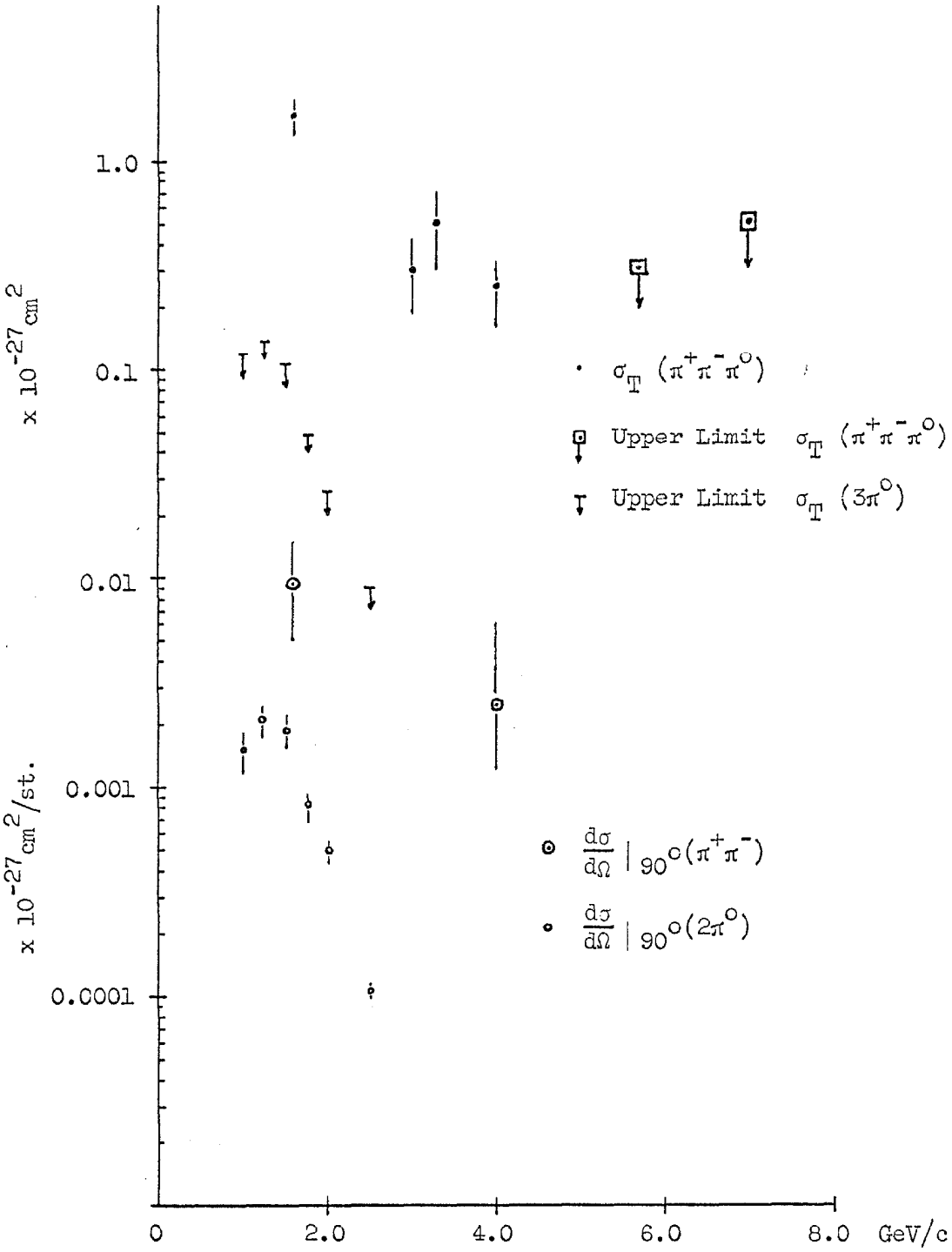

Figure 18 Summary of $\bar{p}p \rightarrow 2\pi$ and 3π Data

$$\frac{\frac{d\sigma}{d\Omega}\Big|_{90^\circ}(\pi^\circ\pi^\circ)}{\frac{d\sigma}{d\Omega}\Big|_{90^\circ}(\pi^+\pi^-)} = 1/5 = 0.20$$

whereas the experimental result from this data is that this ratio is 0.08 ± 0.01. Fong's preliminary results for the $\pi^+\pi^-$ final state have been used in this comparison. Since the $2\pi^\circ$ final state can only come from the $\bar{p}p$ initial state with total isotopic spin = 0 the smallness of the experimental ratio indicates that this state is somehow suppressed.

A similar model for the $\pi^+\pi^-\pi^\circ$ and the $3\pi^\circ$ final states predicts

$$\frac{\sigma_{\text{Total}}(3\pi^\circ)}{\sigma_{\text{Total}}(\pi^+\pi^-\pi^\circ)} = 1/17.$$

For the details of this prediction see Reference 22. Experimentally this ratio at 1.61 GeV/c is $\leq 1/27$ to a 90% confidence level. In this case the $3\pi^\circ$ final state can only come from the $\bar{p}p$ initial state with total isotopic spin = 1 and thus the experimental upper limit indicates that for $3\pi^\circ$ final state the isotopic spin = 1 $\bar{p}p$ initial state is somehow suppressed.

The additional information about the $2\pi^\circ$ final state from the data analysis also indicates that a simple statistical model for the annihilation is not sufficient. The differential cross sections for $\bar{p}p \rightarrow 2\pi^\circ$ for a fixed $\bar{p}$ momentum are not flat even though the data could contain up to a 50% background from the $3\pi^\circ$ final state. In addition the shape of $\frac{d\sigma}{d\Omega}(\bar{p}p \rightarrow 2\pi^\circ)$ changes for different $\bar{p}$ momenta. The detailed analyses of the data for the $3\pi^\circ$ and $2\pi^\circ$ final states along with the

detailed angular distributions for the $2\pi^o$ final state are given in Appendix V. The descriptions of the computer programs used in these analyses are given in Appendix III, Sections b and c, and in Appendix IV, Section b.

The result from the analysis of the $\pi^o\gamma$ final state for the $\bar{p}p$ system can be stated as an upper limit (to a 90% confidence level) on the cross section for this process. This limit for 1.50 GeV/c, the only incident momentum for which this final state was studied, is

$$\frac{d\sigma}{d\Omega}\Big|_{90^o}(\bar{p}p \to \pi^o\gamma) \leq 0.5 \times 10^{-30} \text{ cm}^2/\text{st.} \qquad (1.50 \text{ GeV/c}).$$

This should be compared with the result for $\bar{p}p \to 2\gamma$ given below which is

$$\frac{d\sigma}{d\Omega}\Big|_{90^o}(\bar{p}p \to 2\gamma) = (.16 \pm {}^{.19}_{.08}) \times 10^{-30} \text{ cm}^2/\text{st.} \quad (1.50 \text{ GeV/c}).$$

An order of magnitude estimate would predict that

$$\frac{\frac{d\sigma}{d\Omega}\Big|_{90^o}(\bar{p}p \to 2\gamma)}{\frac{d\sigma}{d\Omega}\Big|_{90^o}(\bar{p}p \to \pi^o\gamma)} = \alpha = 1/137 = \text{fine structure constant.}$$

The detailed analysis of the data for the $\pi^o\gamma$ final state is the subject of Appendix VI.

b. 2γ Final State

In the 2.50 GeV/c data obtained from 4.0×10^8 antiprotons on the target there were no events which satisfied simultaneously all the final selection criteria for the 2γ final state. These selection criteria were listed in Part II on Page 15.

Using the overall 2γ detection efficiency of the apparatus which is calculated in Appendix I the 90% confidence level upper limit on the 2γ

differential cross section implied by no events is

$$\frac{d\sigma}{d\Omega}\Big|_{90^o}(\bar{p}p \to 2\gamma) \leq 0.8 \times 10^{-31} \text{ cm}^2/\text{st.} \qquad (2.50 \text{ GeV/c}).$$

In this case the 90% confidence level upper limit is given by 2.3 times the expected cross section for one event. The expected background is estimated to be $\frac{d\sigma}{d\Omega}\Big|_{90^o}(\text{Fake } 2\gamma) \approx 3.0 \times 10^{-33} \text{ cm}^2/\text{st.}$ (2.50 GeV/c).

There were two events in the 1.50 GeV/c data which satisfied all of the final selection criteria for the 2γ final state. These data were obtained from 1.8×10^8 antiprotons incident on the target.

Using the 2γ detection efficiency calculated in Appendix I these two events lead to the differential cross section

$$\frac{d\sigma}{d\Omega}\Big|_{90^o}(pp \to 2\gamma) = (1.6 \,^{+\,1.9}_{-\,0.8}) \times 10^{-31} \text{ cm}^2/\text{st.} \qquad (1.50 \text{ GeV/c}).$$

Because of the difference in the calculated γ-ray conversion efficiency of the lead plate based on the Monte Carlo shower calculations of Messel[10] and the experimental result from the measurements made at Caltech (used in the cross section calculation) there could be a systematic decrease in the 2γ differential cross section by a factor of ≈ 4. However, it is felt that the experimental measurements which are discussed in Appendix II of this conversion efficiency are more reliable than the theoritical Monte Carlo shower calculations.

An attempt was made to confirm this surprisingly large result by scanning the Pb chamber film used to study the $2\pi^o$ final state for events with only one converting γ-ray in each Pb chamber. If the above cross section were correct there would be approximately fifteen real 2γ events in the 1.50 GeV/c sample of data. The events were analyzed with the same analysis program as used for the $2\pi^o$ events. Unfortunately

based on the cross sections for the $2\pi^o$ and the $\pi^o\gamma$ final states given in Appendices V and VI the expected background in this 2γ data was approximately forty events.

If this large and uncertain (because of the large uncertainties in the $2\pi^o$ and $\pi^o\gamma$ cross sections) background subtraction is carried out the result is a possible upper limit to the 2γ cross section. It is equal to one half the value given above. The details of this analysis are given in Appendix VII. The most reasonable conclusion to be drawn from this check is that it doesn't rule out the above result.

The background analysis from Section a of Part IV yields for the expected background to the 2γ final state

$$\frac{d\sigma}{d\Omega}\Big|_{90^o}(\bar{p}p \to 2\gamma)_{Fake} = (0.31 \pm 0.06) \times 10^{-31} \text{ cm}^2/\text{st. (1.50 GeV/c)}.$$

This result includes only the $2\pi^o$ and $\pi^o\gamma$ final states which are thought to be the major contributors to the background. The cross sections for the $2\pi^o$ and the $\pi^o\gamma$ final states used in this calculation are based on data which could also contain backgrounds as large as 50%. Because of this, this value for the expected background to the 2γ final state is really an upper limit. Thus, unless there is a major source of background other than the $2\pi^o$ and the $\pi^o\gamma$ final states the above cross section for the 2γ final state for 1.50 GeV/c $\bar{p}$'s looks real.

A simple calculation of the theoretically expected differential cross section for $\bar{p}p \to 2\gamma$ assuming that the interaction obeys QED (i.e., the proton is taken to be a positron with mass = M_p and the antiproton an electron with mass = M_p) yields the result

$$\frac{d\sigma}{d\Omega}\Big|_{90^\circ}(\bar{p}p \to 2\gamma)_{\text{QED Theory}} = 5.2 \times 10^{-33}\ \text{cm}^2/\text{st.} \quad (1.50\ \text{GeV/c}).$$

A perhaps more realistic model of the annihilation is provided by assuming that the annihilation is dominated by $\rho^o\rho^o$, $\rho^o\omega^o$, and $\omega^o\omega^o$ intermediate states. Since the coupling constants for $\rho^o \to \gamma$ and $\omega^o \to \gamma$ are roughly equal to $\alpha = 1/137$ a rough estimate of the expected 2γ cross section is provided by multiplying the sum of the experimental cross sections for $\bar{p}p \to \rho^o\rho^o$, $\rho^o\omega^o$, and $\omega^o\omega^o$ by α^2. There are no experimental data on these cross sections at 1.50 (GeV/c) so estimates are obtained by assuming the ratios of the measured rates for $\bar{p}p \to \rho^o\rho^o$ and $\rho^o\omega^o$ compared to $\bar{p}p \to \pi^+\pi^-$ at rest[16] are the same at 1.50 GeV/c. In addition it is assumed that $\bar{p}p \to \rho^o\rho^o$ and $\bar{p}p \to \omega^o\omega^o$ have equal cross sections as is predicted by a simple statistical model. The result for $\bar{p}p \to 2\gamma$ using these crude approximations and assuming a flat cm angular distribution is

$$\frac{d\sigma}{d\Omega}\Big|_{90^\circ}(\bar{p}p \to 2\gamma)_{\substack{\text{Resonance}\\ \text{Theory}}} = 3 \times 10^{-33}\ \text{cm}^2/\text{st.} \qquad (1.50\ \text{GeV/c})$$

Thus, both models lead to values for $\frac{d\sigma}{d\Omega}\Big|_{90^\circ}(\bar{p}p \to 2\gamma)$ which are less than or equal to one twentieth of the experimental value given above.

c. $e^+ + e^-$ Final State

There were no events in the data for the $e^+ + e^-$ final state from 2.50 GeV/c antiprotons incident on the liquid hydrogen target which satisfied simultaneously all the selection criteria for the $e^+ + e^-$ final state. These criteria which involve conditions which the electromagnetic showers in the Pb chambers must satisfy and the

requirement that the kinematics measurements of the tracks in the thin foil chambers lie within the experimentally determined 95% acceptance regions for the kinematics of the $e^+ + e^-$ final state were discussed in Part III, Section b.

Since there were no events the result of the analysis of the data is an upper limit for the cross section for $\bar{p}p \rightarrow e^+e^-$ for 2.50 GeV/c antiprotons. Assuming a one photon exchange mechanism for the annihilation then gives upper limits on the proton form factors for a momentum transfer of +6.8 $(GeV/c)^2$. These upper limits to a 90% confidence level are

$$\frac{d\sigma}{d\Omega}\Big|_{90^\circ} (\bar{p}p \rightarrow e^+e^-) \leq 4.2 \times 10^{-35} \text{ cm}^2/\text{st.} \qquad (2.50 \text{ GeV/c})$$

and

$$|G_M(t)| \leq 0.16 \text{ for } t = +6.8 \text{ (GeV/c)}^2 \text{ if } |G_M| = |G_E| .$$

The expected background is estimated to be

$$\frac{d\sigma}{d\Omega}\Big|_{90^\circ} (\text{Fake } e^+e^-) \simeq 1.3 \times 10^{-35} \text{ cm}^2/\text{st.} \qquad (2.50 \text{ GeV/c}).$$

Table 7 lists the limits for $|G_M|$ and $|G_E|$ for the assumption $\frac{G_M}{1+\mu} = G_E$ which seems to be true for measurements of the form factors for space-like momentum transfers ($e^-p \rightarrow e^-p$) along with the expected values if the proton was a point particle. The values for the proton form factors predicted by the DESY[6] dipole fit to the form factors are also included. The table also includes the latest published upper limit on the form factors at this momentum transfer determined by Zichichi and his co-workers[7] at CERN.

During part of Zichichi's experiment the detection apparatus was

TABLE 7

Summary of Results for $e^+ + e^-$ Final State for 2.50 GeV/c Antiprotons

$t = 6.8\ (GeV/c)^2$ $\quad E_{Total\ cm} = 2.602\ GeV$ $\quad$ Total $\bar{p}$'s $= 8.5 \times 10^9$

Assumption	$\lvert G_E \rvert$	$\lvert G_M \rvert$	$\frac{d\sigma}{d\Omega}\Big\rvert_{90^\circ} (\bar{p} + p \rightarrow e^+ + e^-)$
point proton	4.35	2.79	2.0×10^{-32} cm^2/st.
$\lvert G_M \rvert = \lvert G_E \rvert$	≤ 0.16	≤ 0.16	$\leq 4.2 \times 10^{-35}$ cm^2/st.
$\lvert G_M \rvert = \lvert G_E \rvert$[7]	≤ 0.15*	≤ 0.15*	$\leq 3.9 \times 10^{-35}$ cm^2/st.*
$\lvert G_E \rvert = \lvert \frac{G_M}{1+\mu} \rvert$	≤ 0.06	≤ 0.16	$\leq 4.5 \times 10^{-35}$ cm^2/st.
DESY fits[6]	$= 0.0$	$= 0.03$	$= 1.1 \times 10^{-36}$ cm^2/st.

* This limit is the combined limits for $\bar{p} + p \rightarrow e^+ + e^-$ and $\bar{p} + p \rightarrow \mu^+ + \mu^-$.

modified to detect $\bar{p} + p \rightarrow \mu^+ + \mu^-$ which has the same cross section as $\bar{p} + p \rightarrow e^+ + e^-$ in the one photon approximation to terms of the order of $(\frac{m_e}{m_\mu})^2 \approx 10^{-4}$. The limit in Table 7 combines the results for the two final states. Their experiment differs from the one reported in this thesis principally because they used a CH_2 target instead of liquid hydrogen. The main disadvantage in using CH_2 is the loss of the strict two body kinematics. The angles are smeared out $\approx 5^\circ$ by the Fermi momentum of the protons in the carbon nucleus. In addition the increased amount of material between the annihilation vertex and the charged particle detectors increases the background to the $e^+ + e^-$ final state due to the conversion of γ-rays from the $\pi^\circ\gamma$ and $2\pi^\circ$ final states in this part of the apparatus.

The result from the data analysis of the 1.50 GeV/c data for the e^+e^- final state is not as clearcut as in the 2.50 GeV/c case discussed above. In the 1.50 GeV/c data there are two events which satisfy simultaneously all of the selection criteria for the e^+e^- final state listed in Section b of Part III. The Čerenkov counter pulse heights for each of these events are those expected for the θ and ϕ angles of the respective tracks. If these two events are real e^+e^- events they lead to a cross section

$$\frac{d\sigma}{d\Omega}\Big|_{90^\circ} (\bar{p}p \rightarrow e^+e^-)_{\text{No Background}} = (1.2 \,^{+\,1.1}_{-\,0.6}) \times 10^{-34} \text{ cm}^2/\text{st.}$$

for the e^+e^- final state at 1.50 GeV/c. This cross section then implies that the form factors would be, assuming $G_E = G_M$,

$$|G_E(t)| = |G_M(t)| = 0.2 \text{ for } t = +5.1 \text{ (GeV/c)}^2.$$

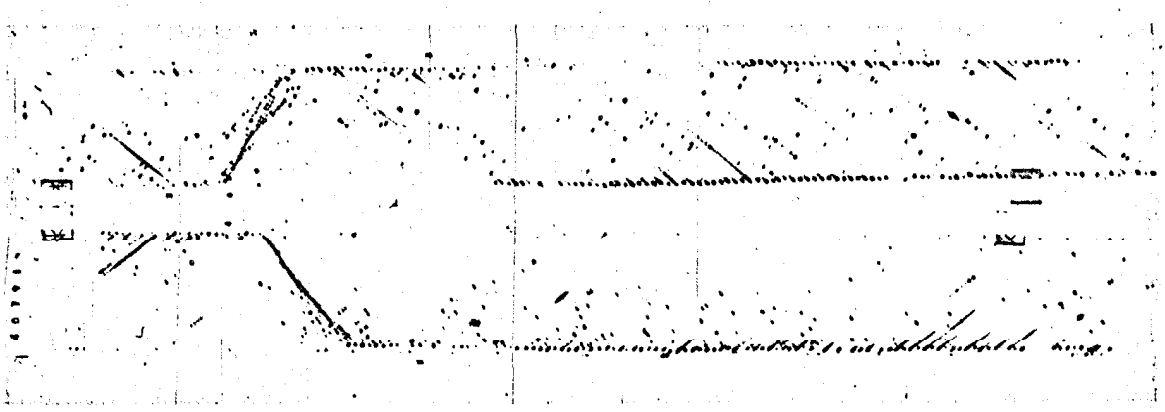

(a)

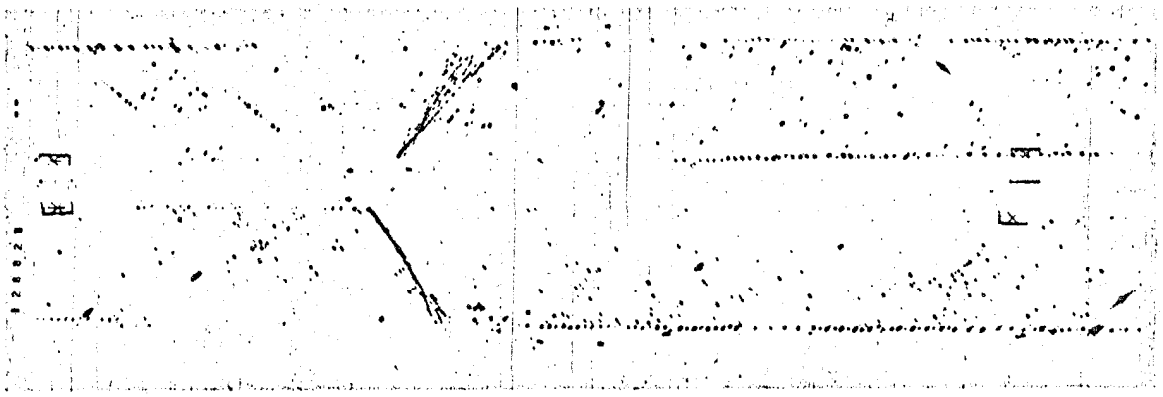

(b)

Figure 19 The Two Final Candidates for $pp \rightarrow e^+e^-$ (1.50 GeV/c)

However, from Section b of Part IV the expected background to the e^+e^- final state data is

$$\frac{d\sigma}{d\Omega}\Big|_{90^\circ} (\bar{p}p \rightarrow e^+e^-)_{Fake} = (1.6 \begin{smallmatrix} + 1.5 \\ - 0.65 \end{smallmatrix}) \times 10^{-34} \text{ cm}^2/\text{st.} \quad (1.50 \text{ GeV/c})$$

Eighty precent of the background is due to conversion in front of the charged particle detectors of the two γ-rays from the 2γ final state. Most of the remaining twenty percent comes from the conversion of two γ-rays from the $2\pi^0$ final state. An additional fact which adds credibility to the interpretation that both final e^+e^- candidates are background events is that one of the electron showers in each event has two sparks in the second gap of the Pb chamber. From the results of the study of the starting points of the showers of known electrons in the Pb chambers described in Appendix XII, the starting points (first gap with two sparks) of these showers are greater than two standard deviations from the expected starting points. These early starting points would be expected for the showers of a narrow angle pair from the conversion of a γ-ray in front of the charged particle detectors.

Even though the cross section for the 2γ final state for 1.50 GeV/c antiprotons given in Section b is obtained from poor data it can not be ignored as a major source of background in the data for the e^+e^- final state. Taking the above background cross section to be correct then gives (since a cross section cannot be negative)

$$\frac{d\sigma}{d\Omega}\Big|_{90^\circ} (\bar{p}p \rightarrow e^+e^-)_{Real} = (0 \begin{smallmatrix} + 1.3 \\ - 0 \end{smallmatrix}) \times 10^{-34} \text{ cm}^2/\text{st.} \quad (1.50 \text{ GeV/c})$$

or to a 90% confidence level

$$\frac{d\sigma}{d\Omega}\Big|_{90^\circ} (\bar{p}p \rightarrow e^+e^-)_{Real} \leq 1.8 \times 10^{-34} \text{ cm}^2/\text{st.} \quad (1.50 \text{ GeV/c}).$$

This 90% confidence level upper limit is the result of subtracting the 90% confidence level lower limit for the background from the 90% confidence level upper limit for the cross section based on the two events. This upper limit then implies, if $G_E = G_M$,

$$|G_M(t)| = |G_E(t)| \leq 0.2 \text{ at } t = +5.1 \text{ (GeV/c)}^2.$$

Table 8 includes this result and lists the expected values for possible models for the form factors for time-like momentum transfers.

Finally, the question of radiative corrections to the cross section limits for the e^+e^- final state must be considered. In the final results there has been no attempt to make these corrections because the statistical uncertainties are much larger than the estimates of the corrections.

The real photon emission part of the radiative corrections affect the results in two ways. The first effect is to cause the kinematics of the electron and positron to be outside the kinematics acceptance ranges. A rough estimate of this part of the correction has been made using the results of a theoretical calculation by Tsai[23] for the corrections to the process $e^+e^- \rightarrow \bar{p}p$. Using the angular and energy resolutions of the present experiment ($= \pm 1.8^\circ$ and $\approx 50\%$ respectively) gives the result that the true cross section is $\approx 15\%$ larger than the experimentally measured cross section.

The second effect is due to the conversion of the γ-rays from this process in the Pb chambers. Ideally to avoid this correction events with an extra γ-ray should not be thrown out because of the extra γ-ray. Unfortunately it is necessary to only accept events with an

TABLE 8

Summary of Results for $e^+ + e^-$ Final State for 1.50 GeV/c Antiprotons

$t = 5.1\ (GeV/c)^2$ $\quad E_{Total\ cm} = 2.254\ GeV$ $\quad$ Total $\bar{p}$'s $= 3.1 \times 10^9$

Assumption	$\lvert G_E \rvert$	$\lvert G_M \rvert$	$\frac{d\sigma}{d\Omega}\Big\rvert_{90^\circ}\ (\bar{p} + p \rightarrow e^+ + e^-)$
point proton	3.58	2.79	$3.0 \times 10^{-32}\ cm^2/st.$
$\lvert G_M \rvert = \lvert G_E \rvert$	≤ 0.2	≤ 0.2	$\leq 1.8 \times 10^{-34}\ cm^2/st.$
$\lvert G_E \rvert = \lvert \frac{G_M}{1+\mu} \rvert$	≤ 0.07	≤ 0.2	$\leq 1.8 \times 10^{-34}\ cm^2/st.$
DESY fits[6]	0.024	0.067	$5.0 \times 10^{-36}\ cm^2/st.$

extra γ-ray if that γ-ray makes a projected angle $\leq 4^{\circ}$ in the Pb chamber with the electron. If this is not done the background due to the $2\pi^{\circ}$ final state becomes large. This choice of angle is such that $\approx 75\%$ of the γ-rays from the real photon emission part of the correction are included. From Tsai[26] one half of these γ-rays are contained within 1° of the electron direction. If in addition the minimum detectable γ-ray energy in the Pb chambers (20-50 MeV) and the energy spectrum $\left(= \frac{1}{E_{\gamma}} \right)$ of these γ-rays are taken into account this second effect probably leads to less than a 10% correction.

Thus, the overall correction is probably on the order of 20% which is much less than the statistical uncertainties and so it has been neglected in the final results.

The theoretical implications of the upper limits to the proton form factors for the two time-like momentum transfers measured in the present experiment can be stated simply as follows. The proton does not behave as a point particle for time-like momentum transfers. A model for the form factors proposed by Wu and Yang[24] predicts that

$$G_M(t) \approx (1 + \mu) \exp\left[- (-t)^{\frac{1}{2}}/0.6 \right]$$

for space-like momentum transfers ($t \leq 0$). Analytically continuing this function to time-like momentum transfers ($t > 0$) gives

$$\left| G_M(t) \right| = 1 + \mu = 2.79 = \text{constant for all } t > 0.$$

The upper limits on the form factors from this experiment are in contradiction with a form factor this large. These limits also rule out large imaginary parts to the form factors. Any of the multiple resonance fits to the form factors, e.g. the Harvard four pole fits[14]

and the DESY[6] dipole fits, for space-like momentum transfers are compatible with the upper limits set by this experiment when they are continued to the values of t measured in this experiment. These upper limits do rule out, however, strong contributions to the form factors from high mass (2.3 - 2.6 GeV) resonances.

At this point a summary of what has been learned from all this is in order. The numerical values for the cross sections of the various final states of the $\bar{p}p$ annihilation investigated in this experiment are summarized in Table 9.

Perhaps the most interesting results of this experiment come from the analysis of the data from the background runs for the e^+e^- final states. Both the $2\pi^o$ final state and the $3\pi^o$ final state compared to the $\pi^+\pi^-$ and $\pi^+\pi^-\pi^o$ final states occur less than one half as frequently as would be expected from a simple statistical model. The curiosity in this result is that the $2\pi^o$ and the $3\pi^o$ final states come from different isotopic spin states of the $\bar{p}p$ system. Perhaps the most surprising result if it is true comes from the analysis of the 2γ final state data. Two events were found in the 1.50 GeV/c data which lead to a tentative cross section twenty times larger than the value predicted by two simple theoretical models. Analysis of the background in this data indicates that the background is small provided of course that all the contributions have been included in the analysis.

The upper limits for the proton form factors set by this experiment unfortunately are not small enough to provide very interesting tests of possible fits to the form factors. They do indicate, however, that

Table 9 Summary of Experimental Results

Cross Section	Incident Antiproton Momentum (GeV/c)					
	1.00	1.25	1.50	1.75	2.00	2.50
$\sigma_T(\bar{p}p \to 3\pi^o)_{90\%}$* x 10^{-27} cm^2	$\leq$ 124	$\leq$ 138	$\leq$ 107	$\leq$ 48	$\leq$ 26	$\leq$ 9
$\frac{d\sigma}{d\Omega}\|_{90^o}(\bar{p}p \to 2\pi^o)$** x 10^{-30} cm^2/st.	1.5$\pm$0.2	2.1$\pm$0.3	1.9$\pm$0.2	0.8$\pm$0.1	0.49$\pm$.06	0.11$\pm$.02
$\frac{d\sigma}{d\Omega}\|_{90^o}(\bar{p}p \to \pi^o\gamma)_{90\%}$* x 10^{-30} cm^2/st.			$\leq$ 0.5			
$\frac{d\sigma}{d\Omega}\|_{90^o}(\bar{p}p \to 2\gamma)$*** x 10^{-31} cm^2/st.			$1.6^{+1.9}_{-0.8}$			< 0.8(90%*)
$\frac{d\sigma}{d\Omega}\|_{90^o}(\bar{p}p \to e^+e^-)_{90\%}$* x 10^{-34} cm^2/st.			$\leq$ 1.8****			$\leq$ 0.42

* 90% implies "to a 90% confidence level".

** Cross sections could include up to a 50% background from the $3\pi^o$ final state.

*** Cross section is correct if no large backgrounds have been omitted from the analysis. See Section b of the text for details.

**** The result is based on a large background subtraction due to the 2γ final state.

nothing "funny" (i.e. large imaginary parts, high mass resonance contributions, etc.) is happening in the time-like region ($t = +5.1$ $(GeV/c)^2$ and $t = +6.8$ $(GeV/c)^2$) covered by this experiment.

APPENDIX I

2γ Detection Efficiency

a. Hodoscope Efficiency for $\gamma + \gamma$ Final State

The fast computer was modified so that it had the following properties during the experiment looking for the $\gamma + \gamma$ final state.

1. The inner hodoscope trays were placed in anticoincidence.
2. In the outer θ hodoscope trays and in the ϕ trays (coplananity determining trays) a multiples veto was generated only if two non-adjacent counters in a tray were struck by charged particles. However, if every counter in a tray had a charged particle passing through it there was no multiples veto generated. The encoder answers used to calculate the ϕ answer were determined by the lowest numbered counter which was struck by a charged particle since counter N-1 vetoed counter N in the GMC for a particular tray.

Since in the final analysis only events which have either one charged particle (presumably a very narrow angle e^+e^- pair) or a e^+e^- pair with projected opening angles $\leq 10^\circ$ coming from the lead plates on each side of the target were accepted only these two cases have been considered. The above properties then required that both members of the pair pass through either the same counter or adjacent counters in both the outer θ trays and the ϕ trays. Because of the overlapping counters there were two possible maximum separations for the two charged particles in the trays.

Figure I.1 illustrates these two maximum separations.

From the experimental layout the following table can be formed for the angular acceptance, Ψ, for the pair for each tray which satisfy the above trigger requirements. These are given in Table I.1.

Table I.1

	Case A	Case B
$\phi_\gamma = 0^\circ$	$\psi_\phi = 21^\circ$	$\psi_\phi = 33^\circ$
$\phi_\gamma = 30^\circ$	$\psi_\phi = 16^\circ$	$\psi_\phi = 26^\circ$
$\theta_\gamma = 30^\circ$	$\psi_\theta = 7^\circ$	$\psi_\theta = 12^\circ$
$\theta_\gamma = 40^\circ$	$\psi_\theta = 12^\circ$	$\psi_\theta = 19^\circ$
$\theta_\gamma = 56^\circ$	$\psi_\theta = 19^\circ$	$\psi_\theta = 30^\circ$
$\theta_\gamma = 75^\circ$	$\psi_\theta = 25^\circ$	$\psi_\theta = 38^\circ$
$\theta_\gamma = 90^\circ$	$\psi_\theta = 27^\circ$	$\psi_\theta = 40^\circ$

The angles ϕ_γ, and θ_γ are the laboratory angles of the γ-ray.

Using the experimentally determined opening angle distribution given in Appendix II for a pair resulting from the conversion of a 1200 MeV γ-ray in the lead plate and including the 10° cutoff for the projected opening angles the efficiency calculation proceeds as follows. The angular acceptance rectangle is divided up into 2.5° squares and the probability that the pair would be detected if the γ-ray direction intersected the center of that square is calculated by counting the number of pairs that would be successful including the one

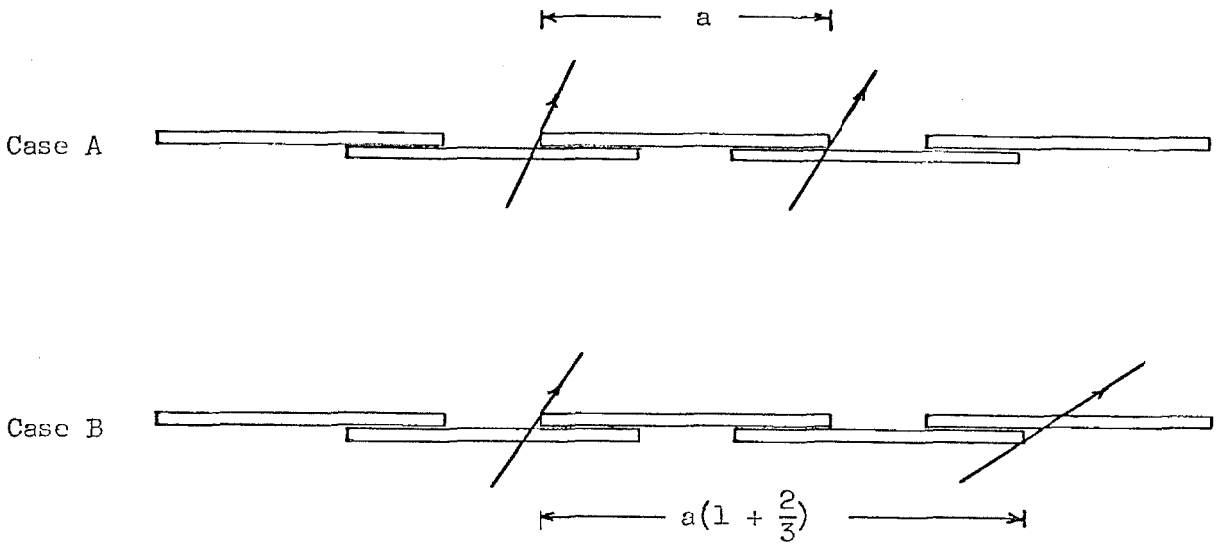

Figure I.1 Maximum Allowable Separation of the Pair in the Outer θ Trays and the ∅ Trays

track events and dividing by the total number of pairs plus one track events. The efficiency for the angular acceptance is then obtained by assuming each small square is equally probable and averaging over the whole angular acceptance. To obtain the overall efficiency the four cases due to the appropriate combinations of Case A and Case B for each tray are averaged. The results are given in Table I.2.

Table I.2

	Efficiency
$\theta_\gamma = 30^\circ$, $\phi_\gamma = 0$	$.57 \pm 0.15$
$\theta_\gamma = 30^\circ$, $\phi_\gamma = 30^\circ$	$.52 \pm 0.15$
$\theta_\gamma = 56^\circ$, $\phi_\gamma = 0$	$.71 \pm 0.15$
$\theta_\gamma = 56^\circ$, $\phi_\gamma = 30^\circ$	$.68 \pm 0.15$
$\theta_\gamma = 90^\circ$, $\phi_\gamma = 0^\circ$	$.74 \pm 0.15$
$\theta_\gamma = 90^\circ$, $\phi_\gamma = 30^\circ$	$.71 \pm 0.15$
$\theta_\gamma = 40^\circ$, $\phi_\gamma = 0^\circ$	$.66 \pm 0.15$
$\theta_\gamma = 75^\circ$, $\phi_\gamma = 0^\circ$	$.73 \pm 0.15$

Weighting each of the above efficiencies with its corresponding solid angle or available target length the average efficiency for both γ-rays in the $\gamma + \gamma$ final state can be calculated. This gives

$$\epsilon\,(2\gamma) = \epsilon_\gamma \times \epsilon_\gamma = 0.48 \pm 0.21.$$

Additional effects due to requirements on the ϕ - answer, counter inefficiencies, and accidentals in the trays are all much smaller than the uncertainty in $\epsilon\,(2\gamma)$ and hence have been neglected.

b. Čerenkov Counter Efficiency

The Čerenkov counters sample the electron showers past shower maximum and in this region the number of charged particles in the shower depends to a good approximation linearly on the energy of the incident electron.[9] Since the sum of the energies of the positron and electron forming the pair is equal to the incident γ-ray energy the response of the Čerenkov counters to the pair will be the same as for an electron with incident energy equal to the γ-ray energy. The Čerenkov counter efficiency is thus taken to be equal to the Čerenkov counter efficiency for the $e^+ + e^-$ final state with 1/2 the bias level used for that final state. Averaging over the solid angle acceptance of the apparatus the efficiencies are

$$(\epsilon_C^{\check{}})^2 = .96 \pm .04$$

for both the 1.50 GeV/c case and the 2.50 GeV/c case.

c. γ-ray Conversion Efficiency

From the results of a check run made at the Caltech 1.50 GeV Electron Synchrotron with a similar spark chamber array which is described in detail in Appendix II there were 32 $e^+ + e^-$ pairs which had two tracks in the thin foil chambers and only two electron showers in the lead plate chamber. There were two single tracks in the thin foil chamber whose directions were within 3^o of the γ-ray beam direction with single showers in the lead plate chambers. These resulted from 278 incident 1200 MeV γ-rays. The conversion efficiency was then

$$\epsilon_{conv.} = \frac{34 \pm 6}{278} = 0.12 \pm 0.02$$

for each γ-ray.

d. Scanning and Measuring Efficiency

Since the scanning in the lead chambers was very similar to the scanning for the $e^+ + e^-$ final state the efficiency was taken to be equal to that case. In the final analysis the requirements that the mean direction of each pair correspond to within 3^o of the theoretical directions of the 2γ's in the $\gamma + \gamma$ final state introduced an additional efficiency correction which was calculated in the following way. If the projected opening angle of the pair was less than or equal to 6^o the efficiency was 1.0. If it was 7^o, $\epsilon_m = .86$, if it was 9^o, $\epsilon_m = .66$ etc. Using these efficiencies and averaging according to their respective probabilities determined by the experimental opening angle distribution this became $\bar{\epsilon}_m = .96 \pm .03$ for each angle so that $\epsilon_m = \epsilon_\theta \times \epsilon_\phi = (.96)^2 = .92 \pm .06$.
Since one γ-ray must be used as a standard this efficiency only appeared once in the final detection efficiency.

e. Overall Efficiency

Combining all these factors then gives for the overall detection efficiency

$$\epsilon_{det.} = (\epsilon_m)(\epsilon_{conv.})^2 (\epsilon_{\chi_C})^2 (\epsilon_{hodo.})$$

$$= (.92)(.12)^2 (.96)(.48)$$

$$= (6.5 \pm 2.0) \times 10^{-3}.$$

APPENDIX II

γ-ray Studies at Caltech

a. Apparatus

The apparatus used in the γ-ray studies is shown schematically in Figure II. 1.

The two four gap thin foil chambers were arranged so that the two outer gaps had the same spatial separation as the two outer gaps of the chambers used at Brookhaven. The Pb chamber was made up of four of the ten gap modules used in the Pb chambers at Brookhaven. The condenser banks, spark gaps and trigger circuit were identical to those used at Brookhaven and geometry of the driving circuits was made as close as possible to copy those used at Brookhaven. The gas mixture used in the chambers was the same as used at Brookhaven as were the sweep field and the trigger delay ($\approx$ 400 nsec.). The spark chambers were photographed with the camera used for the Pb chambers at Brookhaven from an apparent 50 feet above the chambers by means of a mirror suspended from the crane carriage in the Synchrotron hall. No field lens was used.

b. γ-ray Beam

The tagged γ-ray beam at the Caltech 1.5 GeV Electron Synchrotron was used as the source of the γ-rays. Momentum analysed ($\frac{\Delta p}{p} \approx 6\%$, $\Delta\theta \approx 1^{\circ}$) positrons from a Cu radiator in the Southwest Bremstrahlung beam were passed through 1/20 radiation length of Cu and the scattered positrons were detected in a 200 MeV/c magnetic

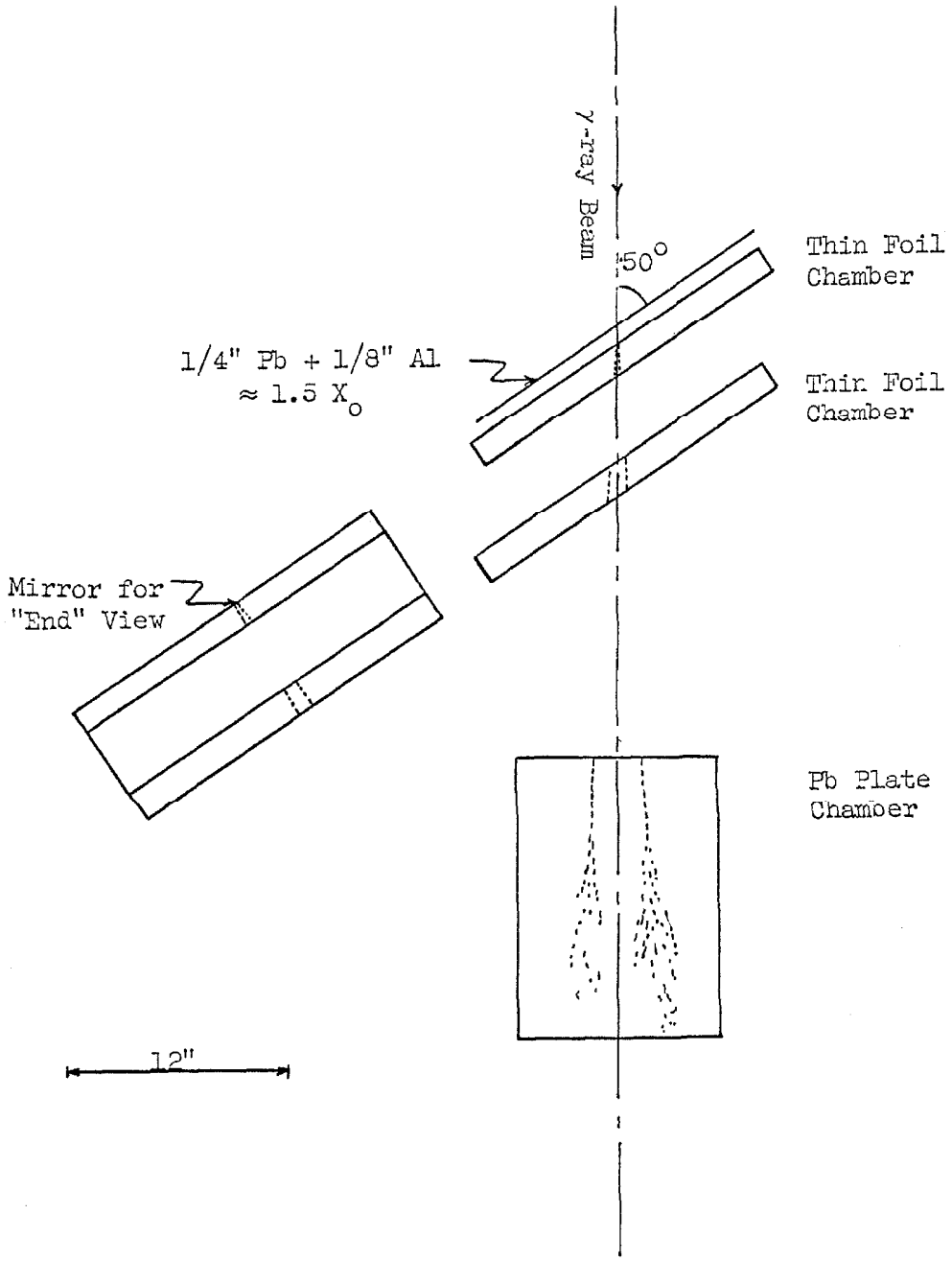

Figure II.1 Top View of Detection Apparatus for γ-ray Studies at Caltech

spectrometer with a 15% momentum acceptance. Typically for 1300 MeV positrons and with the spectrometer set at 100 MeV/c 700 positrons were required for one γ-ray trigger. This corresponded to about one γ-ray trigger per accelerator pulse. To determine the efficiency of the γ-ray trigger short runs with the positron momentum and the spectrometer adjusted for various γ-ray energies were taken without the Al + Pb plate in front of the thin foil chambers. The film was then scanned for converting γ-rays ($\geq$ 10 correlated sparks) in the Pb chamber. For the three lowest γ-ray energies spark counts were made on events with $\geq$ 3 correlated sparks.

Table II.1 lists these experimentally determined efficiencies which have been corrected for the detection efficiency of the Pb chamber ($\approx$ .94) due to its finite thickness (= 4.8 radiation lengths).

Table II.1

E_γ(MeV)	Real γ-rays / γ-ray Trigger
50	0.58 $\pm$ 0.04
100	0.62 $\pm$ 0.07
200	0.64 $\pm$ 0.06
400	0.82 $\pm$ 0.07
500	0.84 $\pm$ 0.07
600	0.86 $\pm$ 0.07
800	0.87 $\pm$ 0.07
1200	0.84 $\pm$ 0.07

c. Results

The film taken with the 1/8" Al + 1/4" Pb plate in place was scanned in the following manner. For events with one track in each thin foil chamber and only one electron shower in the lead chamber the angle θ that the track made with the beam line was measured in the top view and the angle ϕ was measured in the side view. For events with two tracks the opening angles ψ_θ and ψ_ϕ were measured in the top and side views respectively. In addition it was noted whether or not the beam direction was included within the opening angles of the pair and whether or not the Pb chamber contained just two electron showers with no extra converting γ-rays. In the other events which had ≥ 10 correlated sparks in the Pb chamber the number of tracks (a track = 2 or more correlated sparks in adjacent gaps in the thin foil chambers) in the the thin foil chambers was recorded.

Figures II.2 thru II.11 are a summary of the data.

In both the 1200 MeV data and the 500 MeV data on the number of charged particles coming from the Pb plate there is sharp disagreement with the Monte Carlo calculations of Messel,[10] etal. There seems to be an excess in the experimental curves of events with n charged particles by nearly a factor of two for n = 3, 4, 5, ... while the numbers of events with zero or two charged particles seem to be down by a factor of two. A partial explanation of this discrepancy may lie in the fact that the cutoff energy for the detection of charged particles in the thin foil chambers was approximately 2 MeV (estimated from the observed multiple scattering in the Ne gas in the thin foil

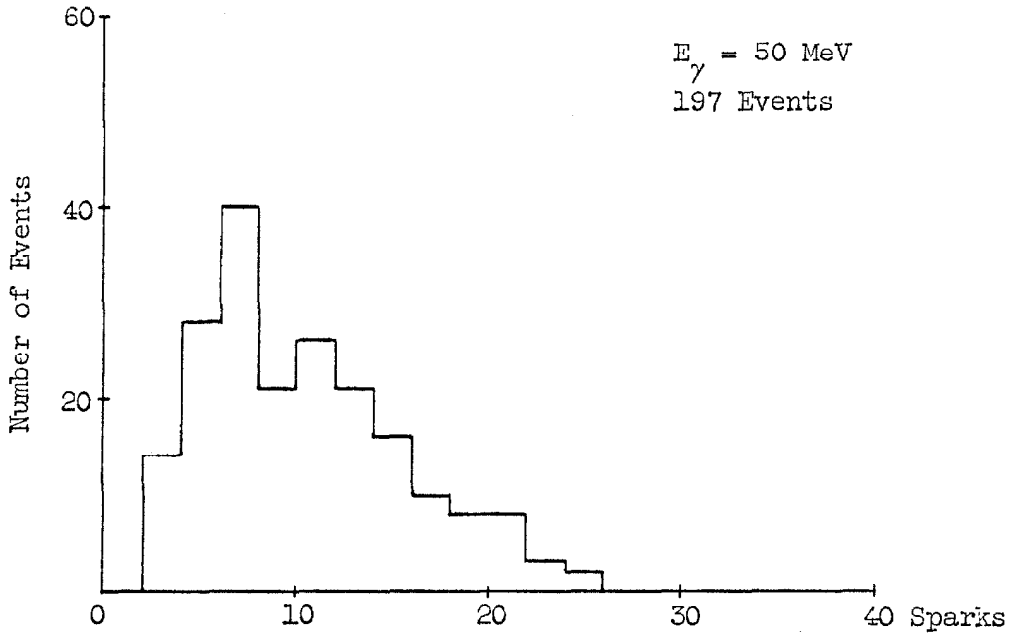

Figure II.2 Distribution of the Number of Sparks in the Shower for γ-rays in Pb Chamber with Pb + Al Plate Removed

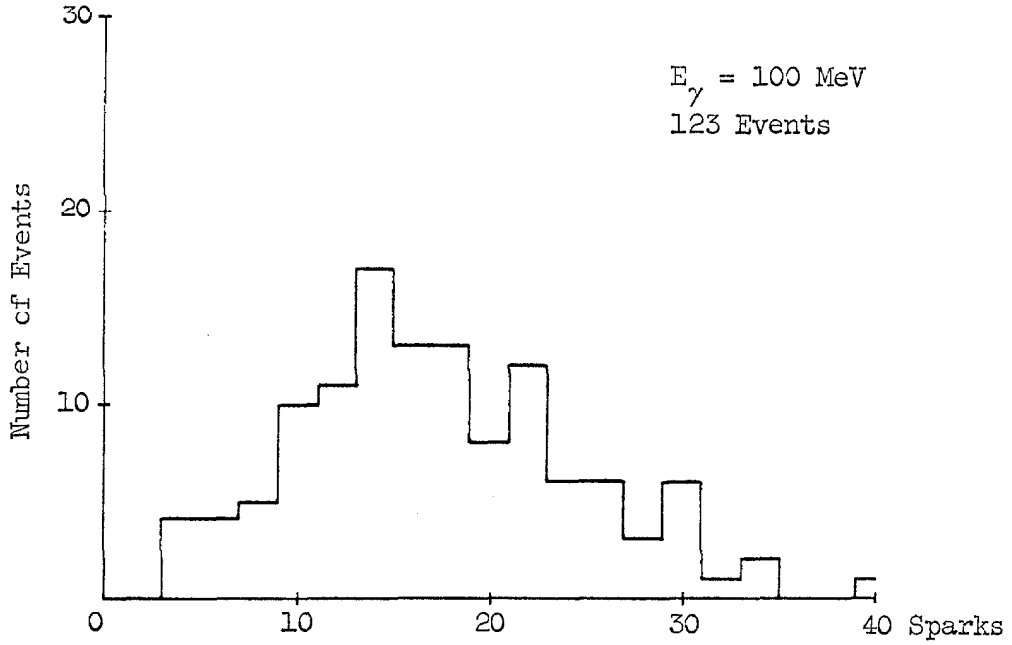

Figure II.3 Distribution of the Number of Sparks in the Shower for γ-rays in Pb Chambers with Pb + Al Plate Removed

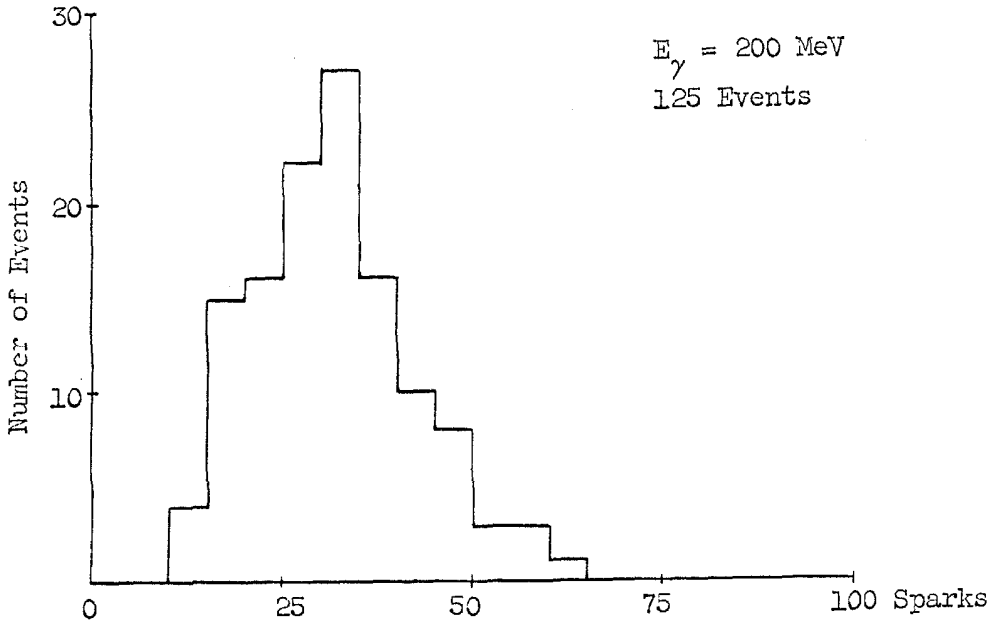

Figure II.4 Distribution of the Number of Sparks in the Shower for γ-rays in Pb Chamber with Pb + Al Plate Removed

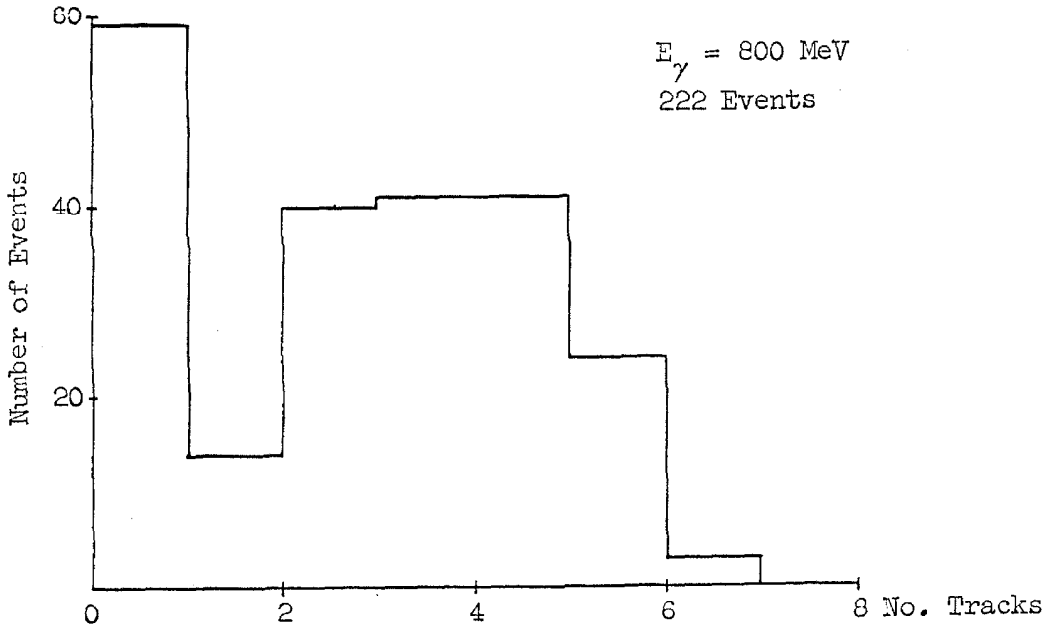

Figure II.5 Distribution of the Number of Tracks in the Thin Foil Chambers

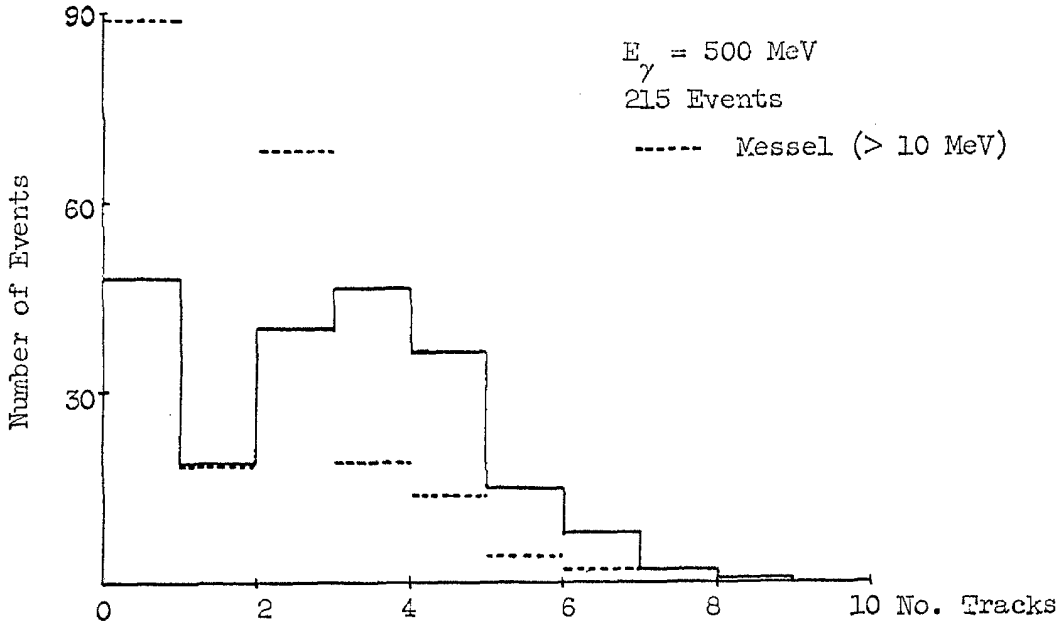

Figure II.6 Distribution of the Number of Tracks in the Thin Foil Chambers

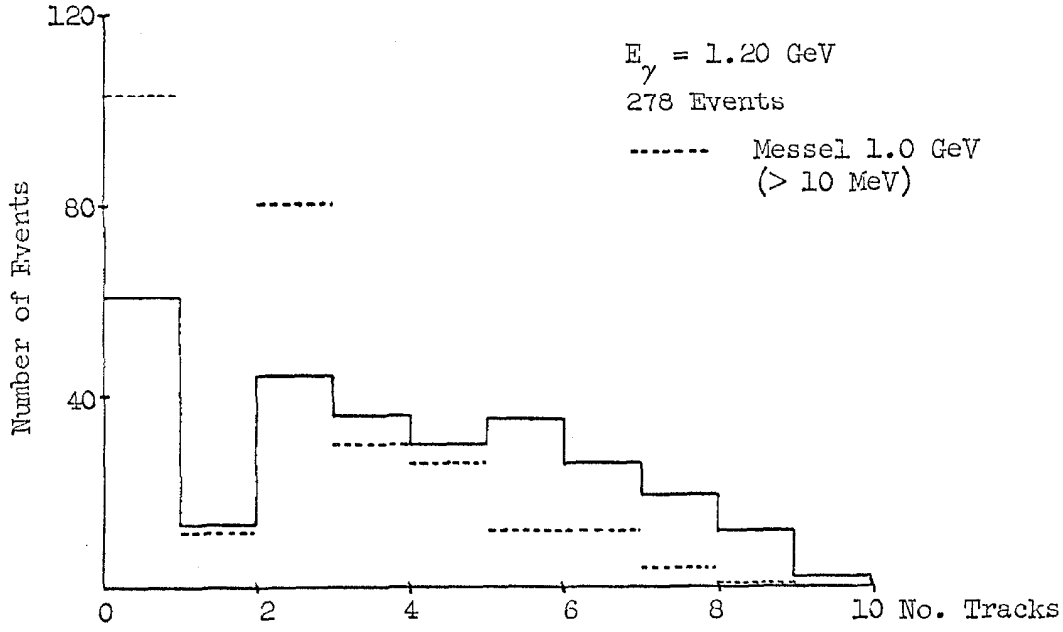

Figure II.7 Distribution of the Number of Tracks in the Thin Foil Chambers

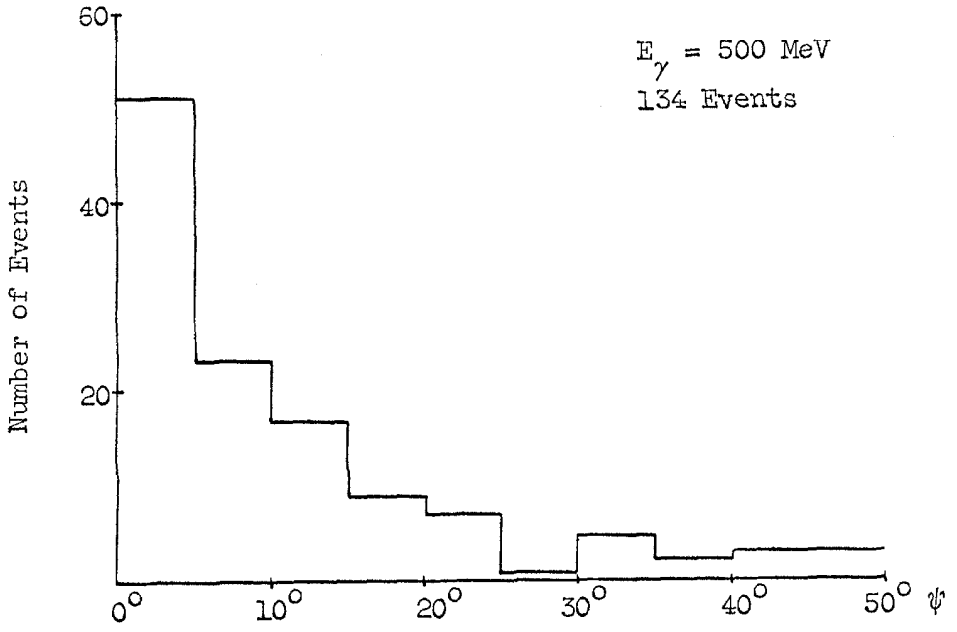

Figure II.8 Projected Opening Angle Distribution for Pairs

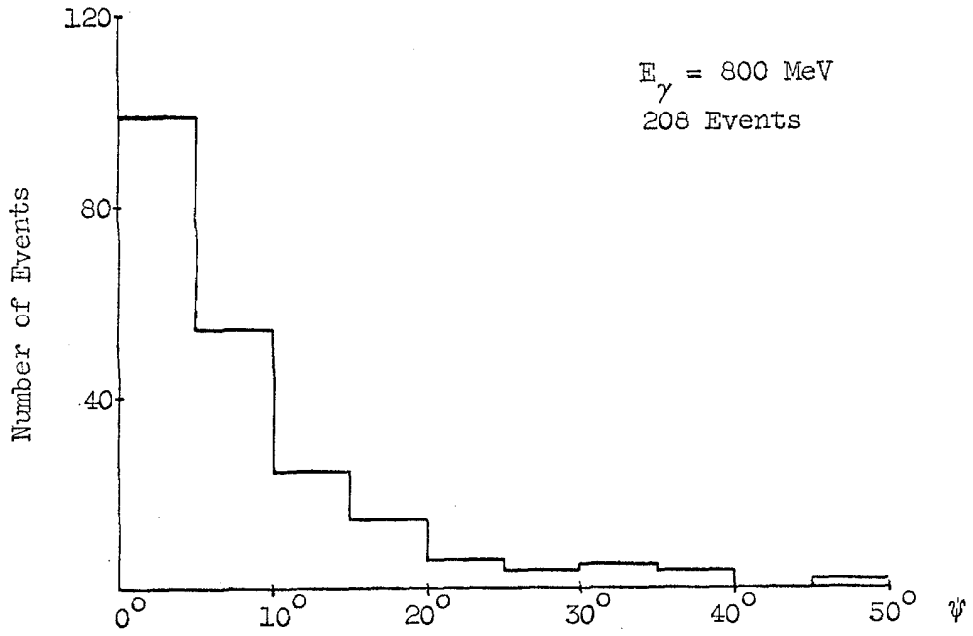

Figure II.9 Projected Opening Angle Distribution for Pairs

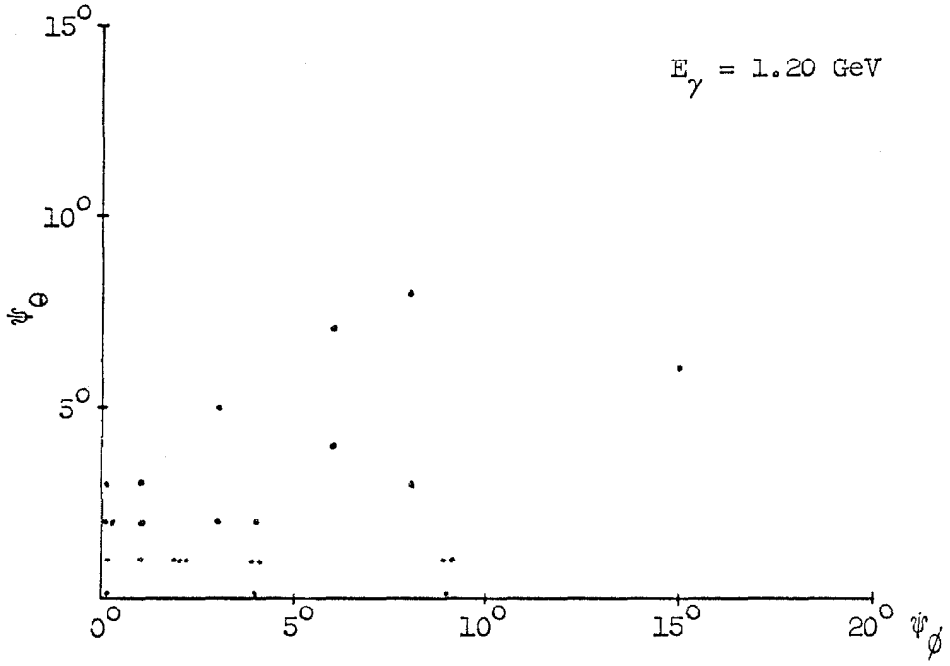

Figure II.10 Correlation of Projected Opening Angles for Pairs

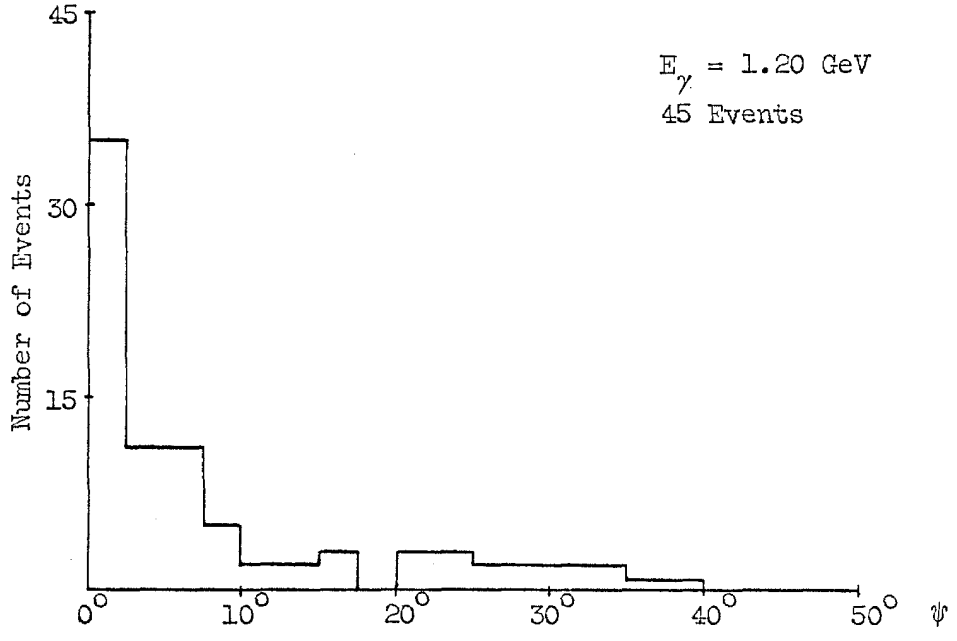

Figure II.11 Projected Opening Angle Distribution for Pairs

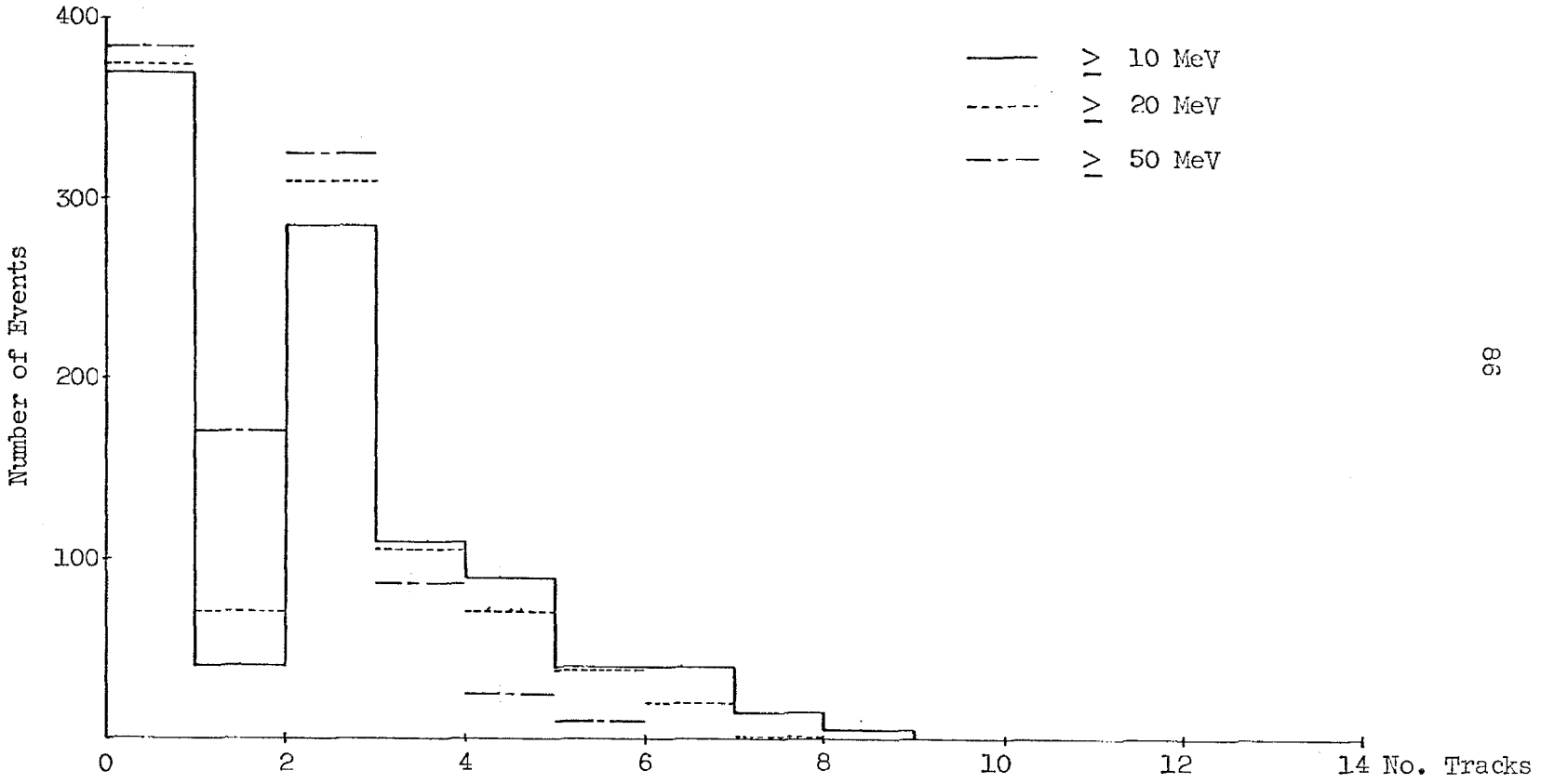

Figure II.12 Distribution of the Number of Electrons at $t = 1.5\ X_o$ in Pb with $E > E_{min}$ from Messel's Monte Carlo Calculations for 1.0 GeV γ-rays

chambers) which is five times smaller than the 10 MeV cutoff used by Messel. Figure II.12 is a plot of Messel's results for 1.0 GeV γ-rays for cutoff energies of 10, 20, and 50 MeV which seems to show such a trend however it seems too small to explain the experimental data.

APPENDIX III

Monte Carlo Computer Programs

a. Solid Angle for $e^+ + e^-$ Final State

In this program an annihilation vertex was chosen at random in the target subject to the beam attenuation arising from the total $\bar{p}p$ cross section. The beam was confined to the center line of the target. A $\cos \theta_{cm}$ for one of the particles subject to a center of mass angular distribution of the form $A + B \cos \theta_{cm} + C \cos^2 \theta_{cm}$ and a ϕ were then chosen at random.

The trajectories of the e^+ and e^- in the laboratory system were calculated and tests made to see if they passed through all the hodoscope trays and the Čerenkov counters. In these tests it was also determined which counter(s) in each tray the particles passed through and from this information the fast computer answers were calculated and used to generate $\cot \theta_R$ vs. $\cot \theta_L$ matrices which could be compared to the ones obtained during the experiment.

Using the experimental Čerenkov counter response as a function of $\cot \theta$ and ϕ two random numbers for the Čerenkov counter pulse heights were chosen subject to this response for the corresponding $\cot \theta$'s and ϕ's for the two trajectories and were tested to see if they satisfied the pulse height requirement used during the experiment.

Comparing the number of successes satisfying various combinations of the requirements to the total number of trials then gave directly the detection efficiency for those combinations of requirements.

For 10,000 trials which usually gave ≈ 700 successes satisfying all the requirements for the $e^+ + e^-$ final state the program required approximately four minutes of computing time on the IBM 7094.

b. $2\pi^o$, $\pi^o\gamma$, and 2γ Final States

A second Monte Carlo program was written which in addition to choosing the z-coordinate of the annihilation subject to the total $\bar{p}p$ cross section also chose at random an x- and y- coordinate subject to the experimentally determined beam distributions in x and y given in Appendix VIII. A $\cos \theta_{cm}$ and a ϕ for one of the π^o's were then chosen at random. In addition $\cos \theta_{cm\ \pi^o}(1)$, $\cos \theta_{cm\ \pi^o}(2)$, $\phi_{cm\ \pi^o}(1)$, and $\phi_{cm\ \pi^o}(2)$ were chosen at random for the two π^o decays in their respective center of mass systems. The four γ-ray trajectories were then transformed back to the laboratory system. Each of the trajectories was tested to see if it passed through any of the lead faced veto counters and/or if it passed through one of the Čerenkov counters and that all the γ-rays had energies $\geq$ 20 MeV.

If all four γ-rays passed through the Čerenkov counters with the two γ-rays from one π^o lying on one side and the other two on the other side and if they satisfied the energy cutoff all the kinematical parameters of the "event" were printed out and an event number was assigned to the success. An IBM card was also punched with the event number and the four γ-ray angles projected on the $\phi = 0$ plane in a format identical to the data cards from the $2\pi^o$ scanning and measuring of the film from the Po chambers.

To check the contribution of the $2\pi^o$ final state to the background

of the $\pi^{o}\gamma$ final state the program was modified to require that only three of the four γ-rays strike the Čerenkov counters. The success was then assigned an event number and all the kinematical parameters were printed out with one variable telling whether or not the extra γ-ray had struck one of the veto counters. A card was also punched in the same format as for the $2\pi^{o}$ case with the third and fourth projected angles equal to the projected angle of single γ-ray detected on one side.

For the contribution to the 2γ final state only one γ-ray was required to strike the Čerenkov counter on each side. Each of these successes was assigned an event number and all kinematic parameters of each of the four γ-rays were printed out. Two variables defined for each γ-ray were also printed out which indicated whether or not that γ-ray had struck one of the veto counters or had passed through the lead plate in front of the thin foil chambers. A card was also punched for each success in the same format as for the $2\pi^{o}$ case with the first and second projected angles set equal to the projected angle of the γ-ray detected on one side and the third and fourth set equal to the projected angle of the γ-ray detected on the other side.

For the $\pi^{o}\gamma$ final state the program was modified so that one of the π^{o} directions was taken as the γ-ray direction. The other π^{o} was allowed to decay as in the program for the $2\pi^{o}$ final state. The three γ-rays were then transferred back to the laboratory system. The maximum error made in taking the laboratory angle of the γ-ray to be one of the π^{o} directions was 0.3^{o} for 1.50 GeV/c incident antiprotons.

Each of the γ-rays was then tested to see if it had struck one of the Čerenkov counters or one of the veto counters and whether or not it had passed through one of the lead plates in front of the thin foil chambers and if it had an energy $E_\gamma \geq E_{min} = 20$ MeV. If all three γ-rays had struck the Čerenkov counters and had energies $\geq E_{min}$ the success was assigned an event number and all the kinematic parameters including whether or not the γ-ray had passed through one of the lead plates were printed out for each γ-ray and a card was punched. The format was the same as for the $2\pi^o$ final state with the first two projected angles being set equal to the projected angles of the two γ-rays from the π^o decay and the third and fourth being set equal to the projected angle of the other γ-ray (i.e. the projected angle of the other π^o).

To find the contribution of the $\pi^o\gamma$ final state to the 2γ final state the trial was considered a success if only one of the γ-rays from the π^o decay struck the Čerenkov counter on one side and the other γ-ray (not from the π^o decay) struck the Čerenkov counter on the other side. The undetected π^o-decay γ-ray was tested to see if it had struck one of the veto counters or had passed through the lead plate on either side of the target. The success was then assigned an event number and all the kinematic parameters were printed out for each γ-ray along with the information concerning the veto counters and the lead plates for the γ-ray which didn't strike one of the Čerenkov counters. A card was also punched in the same format as for the 2γ background from the $2\pi^o$ final state.

A third Monte Carlo program was written to study the 2γ final state. This program used the same vertex selection scheme as described for the $2\pi^o$ case. A $\cos\theta_{cm}$ and a ϕ were chosen at random for one of the γ-ray directions in the center of mass. The direction of the other γ-ray was then determined by energy and momentum conservation. The two γ-ray trajectories were transformed back to the lab system and tested to see whether or not they both passed through the Čerenkov counters. If they did the success was assigned an event number, its kinematical parameters were printed out, and a data card was punched in the same format as for the 2γ background from the $2\pi^o$ and $\pi^o\gamma$ final states described above.

These various froms of the general program all required approximately three minutes of computing time for 2000 trials which typically lead to 300 successes.

c. $3\pi^o$ Final State

To investigate the possible contribution to the experiment looking for events with two γ-rays in each lead chamber from the $3\pi^o$ final state a different Monte Carlo program was written. The selection of the vertex for the annihilation was the same as before, however, since there were three particles in the first state their energies were not uniquely determined.

Since there is experimentally no appreciable contribution from the ρ-meson to the $\pi^+\pi^-\pi^o$ final state for antiproton proton annihilation at 1.61 GeV/c[11] the energy distribution chosen for the $3\pi^o$'s was that

dictated by three-body phase space namely

$$\frac{dP(E_1,E_2)}{dE_1\,dE_2} = (\text{const.})$$

where $P(E_1,E_2)$ is the probability one π^o has energy, E_1, and a second has energy, E_2, with the energy of the third being fixed by energy conservation.

The program selected two energies at random and the direction of one of the π^o's in the center of mass system at random. The plane of annihilation was specified by taking the cross product of the chosen π^o direction and the z-axis (the beam direction). The problem was then determined and the three π^o's were allowed to decay as in the $2\pi^c$ program and the decay γ-ray directions and energies were transformed back to the laboratory system.

If two γ-rays with energies $\geq E_{min}$ passed through the Čerenkov counters on each side of the target the trial was called a success and was given an event number. The kinematic parameters of all six γ-rays were then printed out along with a variable for each γ-ray indicating whether or not it had passed through one of the veto counters. A card was also punched with the four detected γ-rays being treated as in the program for $2\pi^o$ final state.

The program typically required seven minutes of computing time for 3000 trials with approximately 200 successes.

APPENDIX IV

Data Analysis Programs

a. Kinematics Reconstruction

For each measured event there were four data cards (one card for each view of each thin foil chamber) from the measuring machine. Each card contained the event number, a view number and four sets of readings of the three angle encoders. The first set represented the position of a standard fiducial line, the second set was the position and angle of the fiducial line to the left of the beginning of the track, the third set was the position of the second spark in the track and the angle of the track, and the fourth was the position of the end of the first fiducial line to the right of the beginning of the track.

The computer program instructed the computer to carry out the following operations on the information from these four data cards.

1.) Check that all four cards have the same event number and that each view number only appears once. Check that the scanner measured the second spark in each view.

2.) In each view calculate the apparent position of the second spark with respect to the two adjacent top fiducial lines which were measured and by means of the known relationship between the top and bottom fiducial lines calculate its apparent position with respect to the two adjacent bottom fiducial lines.

3.) From the measured angle of the track and the known separation

of the second and eighth gaps calculate the theoretical position of the eighth spark with respect to the top and bottom fiducial lines.

4.) Transform the positions of the second and the eighth sparks to points in real laboratory space. These two points on each side of the target then define two lines.

5.) Find the position of nearest approach of the two lines and calculate their minimum separation at that point. This position is taken as the vertex of the annihilation.

6.) Calculate the angles θ and ϕ for each track with the z-axis taken to be the direction of the beam and (+z is in the direction that the beam particles move) with the x-axis horizontal and the y-axis vertical.

7.) Calculate $\Delta\phi = \phi_L - \phi_R - 180^\circ$.

8.) Calculate the mean expected antiproton momentum at the position of the vertex using the known energy loss relationships. Using this expected momentum and the measured θ_R and θ_L calculate, assuming that the two particles have equal mass, the invariant $(\text{mass})^2$ of one of the particles.

9.) Calculate the derivatives $\frac{\partial(\text{mass})^2}{\partial \text{momentum}}$, $\frac{\partial(\text{mass})^2}{\partial\ \theta_R}$, and $\frac{\partial(\text{mass})^2}{\partial\ \theta_L}$. Calculate $\theta_{R\ cm}$ and $\theta_{L\ cm}$.

10.) Print out the event number along with all the calculated values listed above. Punch a card characterizing the vertex and the two lines in space for this event.

11.) Increase by one the number in the appropriate bin in the

$(\text{mass})^2$, $\Delta\phi$, z, x, and y histograms. Increase by one the number in the appropriate position in the two dimensional matrices of x vs. y, $(\text{mass})^2$ vs. $\theta_{R\ cm}$ and $(\text{mass})^2$ vs. $\theta_{L\ cm}$.

12.) Read in the next event.

13.) When all of the events have been read in print out all of the histograms and matrices.

A separate program predicted which counters in each hodoscope tray should have been hit by the particles using the cards punched by the above program. These predictions were then compared to the card punched at the time the event was photographed as a second scanning check.

b. Analysis Program for the Events Measured in the Pb Chambers

The data for each event measured in the Pb chambers for the $2\pi^o$, $\pi^o\gamma$, and the 2γ final states were punched on a card from scan sheets made up by the scanners. The card contained the event number and the four angles, γ_i, which were the projected angles (since there was no end view of the Pb chambers) on the $\phi = 0^o$ plane of the two γ-rays in each Pb chamber for the $2\pi^o$ final state. For the $\pi^o\gamma$ final state (two γ's on one side and one on the other) the projected angle of the single γ-ray was punched twice. The other two were punched as in the $2\pi^o$ case. For the 2γ case (one γ-ray on each side) the projected angle of each γ-ray was punched twice.

The analysis program instructed the computer to carry out the following operations for all three types of data.

1.) Check that the projected angles γ_i satisfy the conditions

$$\gamma_1 \geq \gamma_2 - 2.0^\circ$$

and

$$\gamma_3 \geq \gamma_4 - 2.0^\circ$$

where γ_1 and γ_3 are the γ-rays farthest upstream with respect to the beam in the left and right Pb chambers respectively. If this was not satisfied the event number was listed followed by an appropriate statement and a new event was read in.

2.) Calculate the opening angles $\alpha_1 = \gamma_1 - \gamma_2$ and $\alpha_2 = \gamma_3 - \gamma_4$.

3.) Calculate the angles γ_i^* of the γ-rays in the antiproton-proton center of mass system assuming that they all lie in the $\phi = 0$ plane.

4.) Check that the center of mass angles satisfy the conditions

$$\gamma_1^* + \gamma_3^* \geq 170^\circ$$

and

$$\gamma_2^* + \gamma_4^* \leq 180^\circ.$$

If they do set A = 0 and if not list the event number with the statement that the projected cm angles are inconsistent with $2\pi^\circ$ final state and set A = 1.

5.) Calculate

$$\theta_\pi{}^\circ(1) = \frac{\gamma_1 + \gamma_2}{2}, \quad \theta_\pi{}^\circ(2) = \frac{\gamma_3 + \gamma_4}{2}$$

and

$$\theta_{op} = \theta_\pi{}^\circ(1) + \theta_\pi{}^\circ(2)$$

6.) Calculate $\theta_{\pi^o cm}$ (1) and $\theta_{\pi^o cm}$ (2) from θ_{π^o} (1) and θ_{π^o} (2) respectively.

7.) Calculate the expected $\overline{\theta_{\pi^o}(2)}$ and $\overline{\theta_{\pi^o}(1)}$ assuming θ_{π^o} (1) and θ_{π^o} (2) to be the correct π^o directions respectively.

8.) Calculate

$$\Delta\theta_{op}(1) = \theta_{op} - (\theta_{\pi^o}(1) + \overline{\theta_{\pi^o}(2)})$$

and

$$\Delta\theta_{op}(2) = \theta_{op} - \overline{(\theta_{\pi^o}(1) + \theta_{\pi^o}(2))}.$$

9.) Check that both α_1 and α_2 are $\leq \Omega$ = maximum allowed opening angle for the γ-rays. If they are, set B = 0, if not set B=1.

10.) Increase by one the number in the appropriate bin in the $\Delta\theta_{op}$, $\theta_{\pi^o cm}$ (1), $\theta_{\pi^o cm}$ (2), α_1 and α_2 histograms. The $\Delta\theta_{op}$ histogram is the sum of the $\Delta\theta_{op}$ (1) and $\Delta\theta_{op}$ (2) histograms, i.e. each event is counted twice in the $\Delta\theta_{op}$ histogram. There are seven sets of these histograms containing separately events which satisfy set of combinations (B = 0, A = 0), (B = 0, A = 1), and (B = 0, A = 0, or 1) and the same set with B = 1 and a final set with A = 0 or 1 and B = 0 or 1.

11.) After the last event is calculated print out all the histograms.

The complete analysis of three hundred events required approximately thirty seconds of computing time.

APPENDIX V

$\bar{p} + p \rightarrow 2\pi^o$ and $\bar{p} + p \rightarrow 3\pi^o$

The data for the neutral final states involving γ-rays were obtained during several short runs during which the spark chambers were triggered if an antiproton disappeared in the liquid hydrogen target, if there were no charged particles striking the hodosocpe counters, if there were no signals from the veto counters which were > 98% efficient for charged particles and 65 $\pm$ 15% efficient for γ-rays, and if the pulse from both of the Čerenkov counters was $\geq$ 1/2 the minimum pulse accepted for the $e^+ + e^-$ final state. The incident antiproton momentum ranged from 1.00 to 2.50 GeV/c for these runs.

The Pb spark chamber film from these runs was scanned for events with (1) two γ-rays converting in each lead chamber, (2) two γ-rays converting in one and one γ-ray converting in the other lead chamber, and (3) one γ-ray converting in each chamber. These classes of events represented the $2\pi^o$ and $3\pi^o$ final states, the $\pi^o\gamma$ final state, and the 2γ final state. If an event was in one of these three classes the angles of the γ-rays in the Pb chambers were measured with respect to the beam direction. Since there was no end view of the Pb chambers these measured angles were the angles of the γ-ray trajectories projected onto the $\phi = 0$ (horizontal) plane. The event number and the measured angles for these events were punched on an IBM card.

Since the detection apparatus plus the lead faced veto counters didn't cover the complete sphere around the liquid hydrogen target the

$3\pi^o$ final state could give rise to only four γ-rays in the Pb spark chambers. Similarly the $2\pi^o$ state could fake the $\pi^o\gamma$ and 2γ final state and the $\pi^o\gamma$ could fake the 2γ final state. With these possibilities in mind the following analysis scheme was developed for these data.

Because the measured angles were projected angles there was no possibility of exact kinematic reconstruction. The energies of the π^o's for these final states were $\approx$ 1-2 GeV in the lab system so that the opening angles of the two decay γ-rays was $\leq 20^o$. With this small opening angle the maximum error that could be made in taking the π^o direction as the mean of the 2γ-ray angles on one side was then $\approx 10^o$ which was roughly equal to the error in taking the projected angles of the γ-rays as their polar angles (θ). In view of these uncertainties a convenient way of analyzing these events was to take the π^o direction to be the bisector of the two γ-ray angles on each side and to assume that the π^o trajectories lay in the $\phi = 0$ plane. Under these assumptions the two π^o "angles" in the lab were added to give an opening angle θ_{op}. This experimentally measured opening angle was then compared to the two expected opening angles determined by two body kinematics taking each π^o angle to be the correct π^o angle.

Since the opening angle of the π^o decay γ-rays was only $\approx 20^o$ requiring that the two γ-rays on each side for the $2\pi^o$ case only have opening angles less than a maximum value $= \Omega$ eliminated most of the background due to the $n\pi^o$ ($n \geq 3$) final states. Another effective means of eliminating background was to require that the projected γ-ray angles be consistent when transformed back into the $\bar{p}p$ cm system with the $2\pi^o$

hypothesis. Namely, the sum of the cm angles of the upstream γ-ray on each side had to be greater than 170° and the sum of the cm angles of the downstream γ-ray on each side had to be $\leq 180^{\circ}$, i.e. the two π°'s had to be traveling in opposite directions in the $\bar{p}p$ cm system. The $3\pi^{\circ}$ final state was studied by looking for events which didn't satisfy these cm requirements. For the $\pi^{\circ}\gamma$ final state only the opening angle requirement was used.

The analysis program which carried out the above operations is described in Appendix IV, Section b.

To determine the $3\pi^{\circ}$, $2\pi^{\circ}$, $\pi^{\circ}\gamma$, and $\gamma\gamma$ detection efficiencies several Monte Carlo computer programs were written which generated random events subject only to the conservation laws and the requirements of phase space. The programs punched fake data cards which were analyzed by the analysis program with the number of successful events for a given number of trials giving directly the detection efficiency. These programs were described in Appendix III, Sections b and c.

The detailed requirements placed on each of the final states are discussed in the Appendix or Section of an Appendix dealing with the particular final state.

a. Experimental Method and Analysis

During several short runs the Pb plate spark chambers used in detecting the $e^{+} + e^{-}$ final state were triggered and photographed if an antiproton disappeared, there were no charged particles passing through any of the hodoscope counters, and the pulse height from each of the Čerenkov counters was greater than 1/2 the minimum value used during

the runs looking for the $e^+ + e^-$ final state. The incident antiproton momenta for these runs was varied from 1.0 GeV/c to 2.50 GeV/c.

The Pb chamber film from these runs was scanned for events with two converting γ-rays in each Pb chamber. The angles of each of the four γ-rays which were the projected angles onto the $\phi = 0$ plane were measured with respect to the beam direction and were punched on a data card along with the event number.

The data cards for the measured events were analyzed using the computer program described in Section b. of Appendix IV.

In this program the π^o directions were assumed to be given by the means of the γ-ray angles on each side of the target. The experimental opening angle for the two assumed π^o directions was compared with the two expected opening angles assuming each π^o direction to be correct. This opening angle error histogram ($=\Delta\theta_{op}$-histogram) was compared to a theoretical one obtained by analyzing fake data cards generated by a Monte Carlo program described in Appendix III, Section b. to test the

correctness of the $2\pi^o$ hypothesis. The Monte Carlo program assumed a flat center of mass angular distribution for the $2\pi^o$'s.

The background due to the $3\pi^o$ final state was determined by comparing the $\Delta\theta_{op}$-histograms for the experimental events which didn't satisfy the criteria placed on the angles γ_i* of the γ-rays in the center of mass in the analysis program to the $\Delta\theta_{op}$-histogram obtained by analyzing the same class of events in the set of fake data events generated by the Monte Carlo program for the $3\pi^o$ final state where only four of the π^o decay γ-rays were detected.

No attempt was made to analyze the background contributions due to the $n\pi^o$ final states where $n > 3$. Since the total center of mass energy will be roughly divided equally between the π^o's it was difficult to see how the Čerenkov pulse height spectra from such events could exhibit the form shown by the experimental ones which agreed with the ones expected for the $2\pi^o$ final state. In addition it was difficult to see how the ≥ 4 extra γ-rays could all escape detection in either the lead chambers or the veto counters.

b. Results

Figure V.1 shows two typical Pb chamber photographs of two four γ-ray events for an incident antiproton momentum of 1.50 GeV/c. The uncertainty in measuring the γ-ray angles in such photographs was obtained from an event by event comparison of the measurements of two scanners who measured the same film. Figure V.2 shows this uncertainty.

The results of submitting the 1.50 GeV/c data to the analysis program described in Appendix IV are shown in Figures V.3 thru V.5.

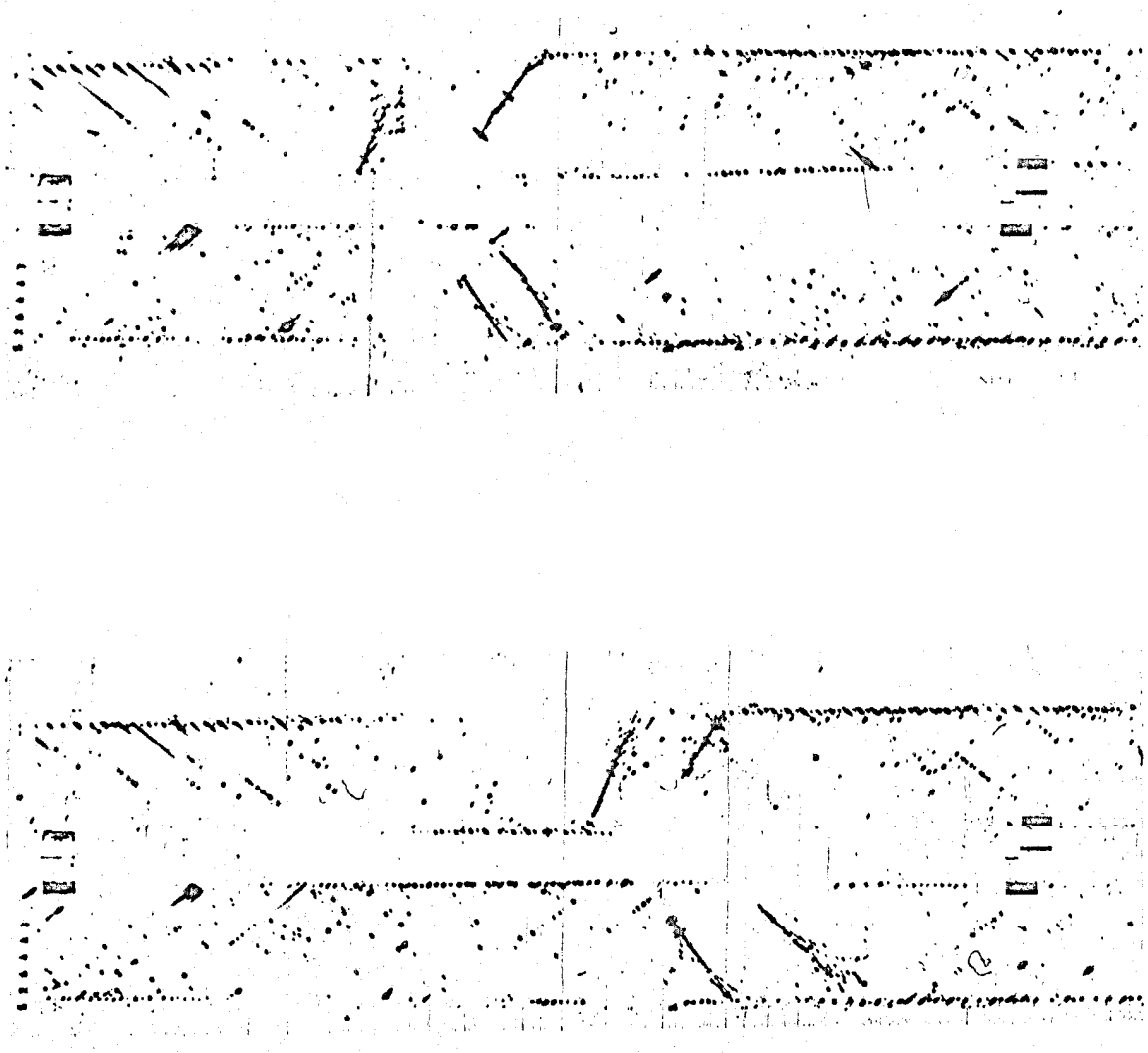

Figure V.1 Typical Four γ-ray Events From 1.50 GeV/c Data

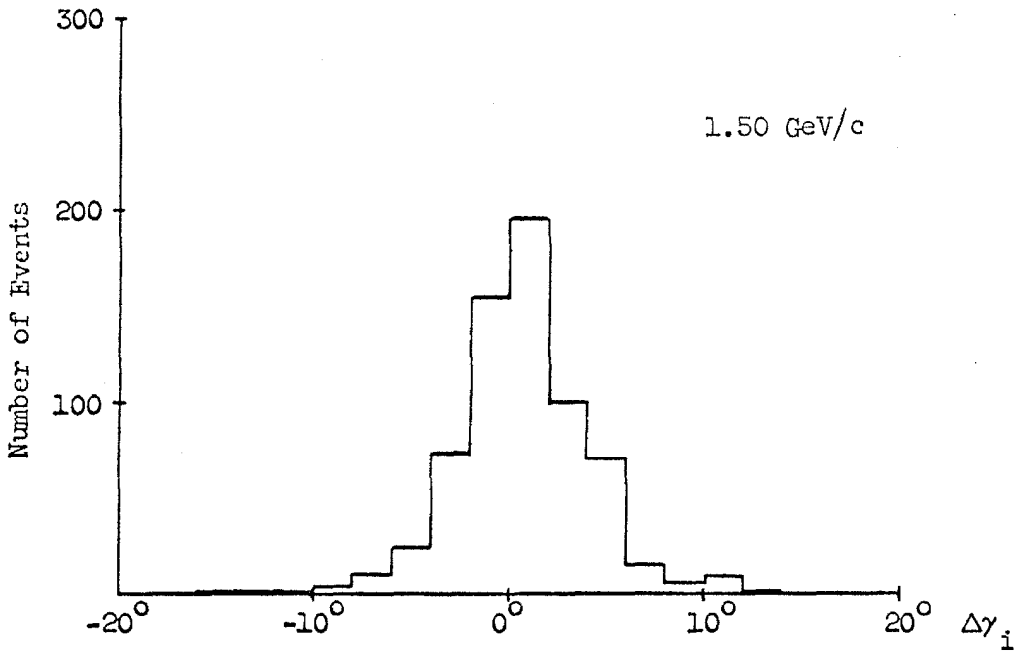

Figure V.2 Error in Measurement of γ-ray Angles in Pb Chambers

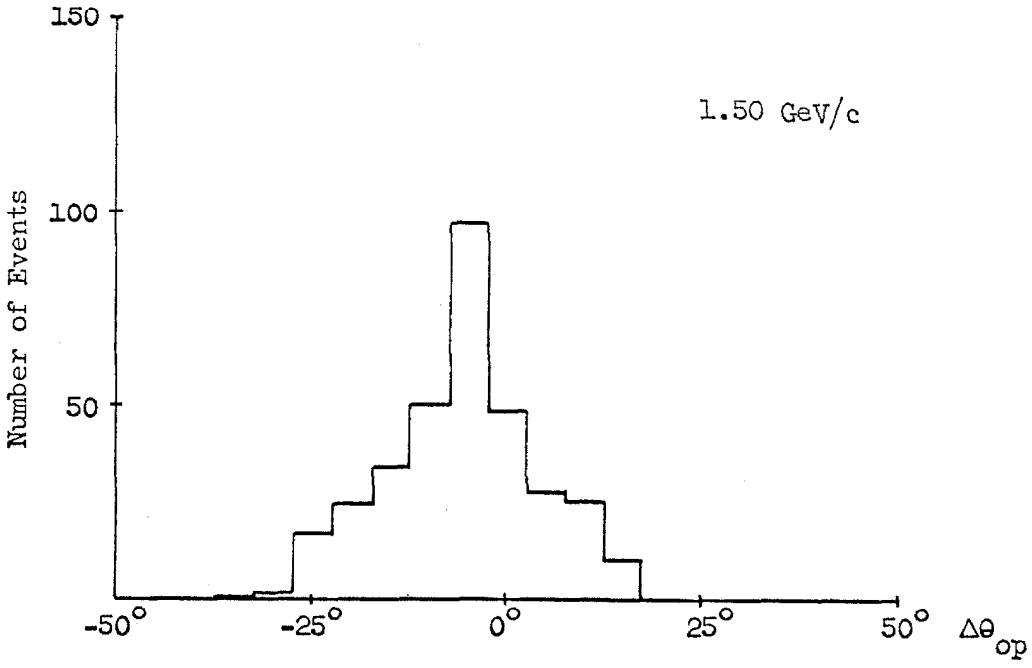

Figure V.3 $\Delta\theta_{op}$-Histogram for all Four γ-ray Events

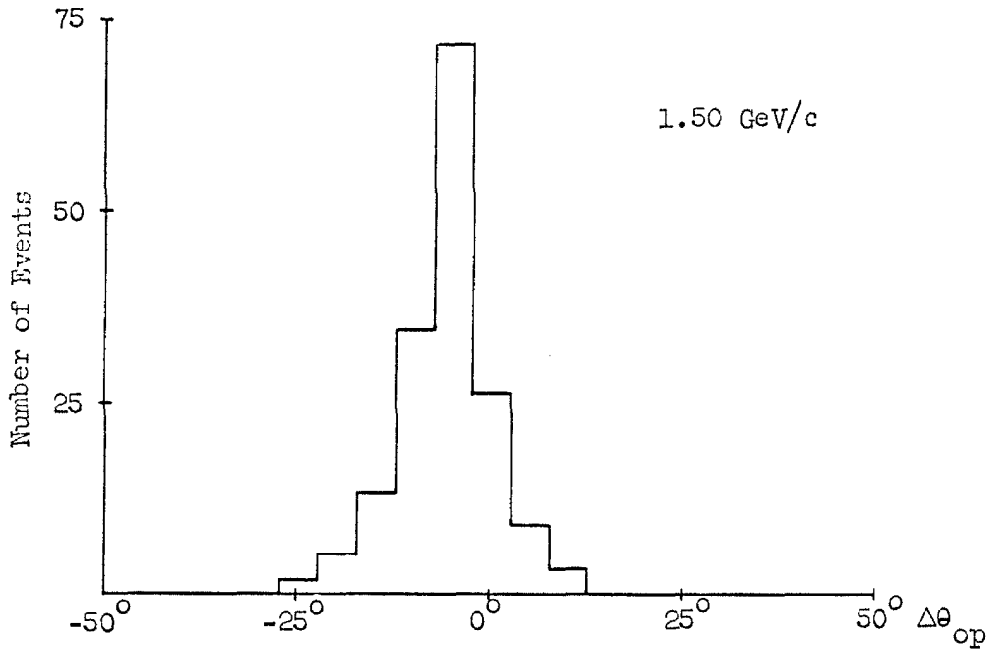

Figure V.4 $\Delta\theta_{op}$-Histogram for all Four γ-ray Events Satisfying $\alpha_{1,2} \leq 18^{\circ}$ and cm Projection Test

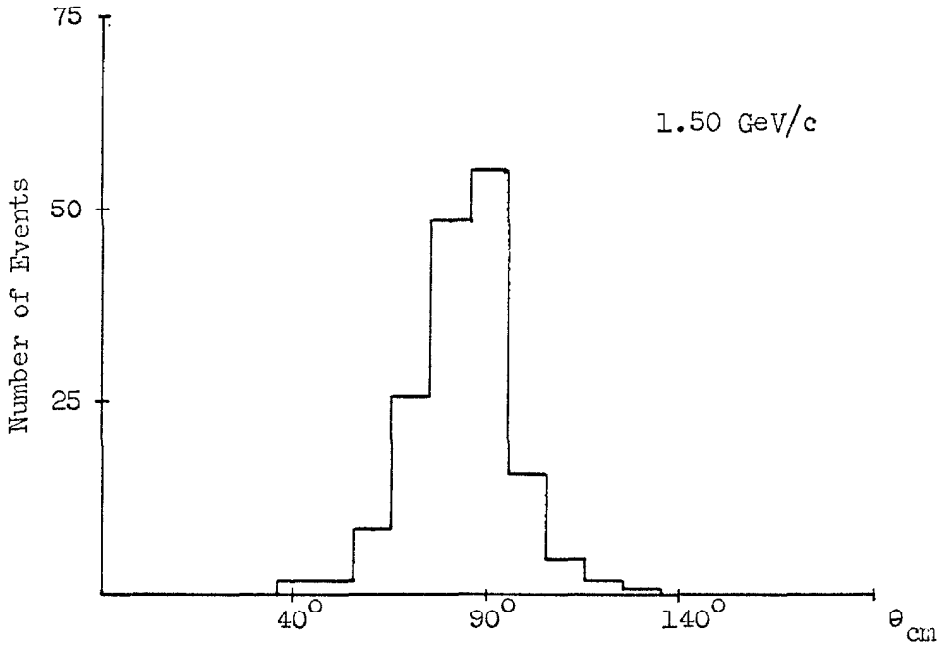

Figure V.5 $\theta\ (\pi^{\circ})_{cm}$ Distribution for all Four γ-ray Events Satisfying $\alpha_{1,2} \leq 18^{\circ}$ and cm Projection Test

Figures V.6 thru V.9 illustrate the results obtained by submitting the fake data cards generated by the $2\pi^o$ Monte Carlo program to the analysis program. Figure V.10 shows the $\Delta\theta_{op}$ histogram for a sample of the fake data cards generated by the $3\pi^o$ Monte Carlo program. This sample has been corrected for the veto counter γ-ray detection efficiencies (= 65%) by including in the sample 35% of the events in which one γ-ray struck a veto counter and 12% of the events in which two γ-rays struck the veto counters.

By comparing the number of events in the data which when the four γ-rays angles are transformed into the center of mass system are not consistent with the $2\pi^o$ hypothesis to the number of similar events from the $3\pi^o$ Monte Carlo generated data an upper limit on the $3\pi^o$ cross section can be obtained. Using all of the events in the interval from -7.5^o to -62.5^o in the $\Delta\theta_{op}$ histograms shown in Figures V.11 and V.12 and using the directly determined detection efficiency from the Monte Carlo program gives

$$\sigma(3\pi^o) \leq (89 \pm 14) \times 10^{-30} cm^2$$

for 1.50 GeV/c antiprotons. This result assumes a flat angular distribution while the apparatus only covers roughly 10% of 4π centered around $\theta_{cm} = 90^o$ in the $\bar{p}p$ center of mass system. This should be compared to $\sigma(\pi^+\pi^-\pi^o) = 1.4 \times 10^{-27}$ cm^2 measured by Lynch,[11] etal. for 1.61 GeV/c antiprotons in a hydrogen bubble chamber. Checks on the Čerenkov counter pulse heights and the conversion points of the γ-rays in the Pb chamber for these events indicate no experimental bias against detecting this class of events. The error quoted is purely statistical.

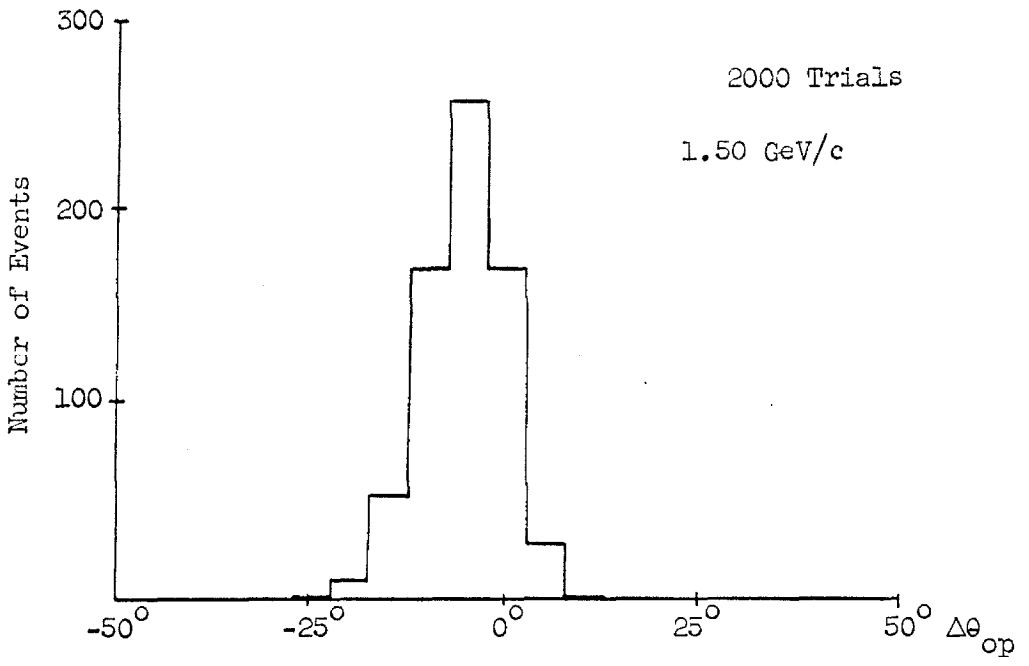

Figure V.6 $\Delta\theta_{op}$-Histogram for $2\pi^{o}$ Monte Carlo Events Satisfying $\alpha_{1,2} \leq 18^{o}$ and cm Projection Test

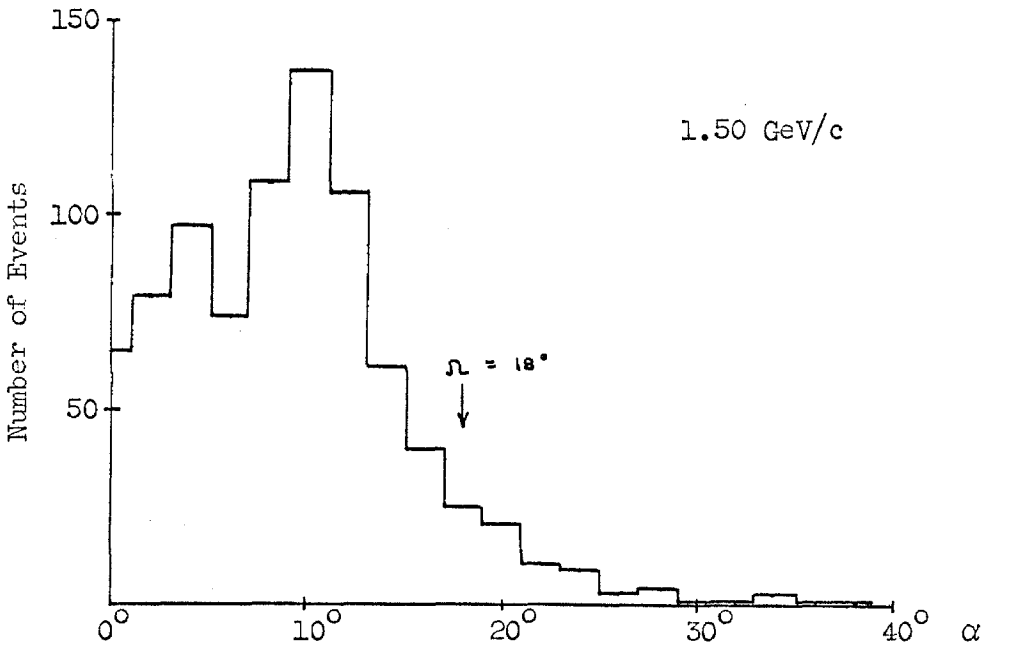

Figure V.7 Opening Angle, α_i, Distribution for $2\pi^{o}$ Monte Carlo Events

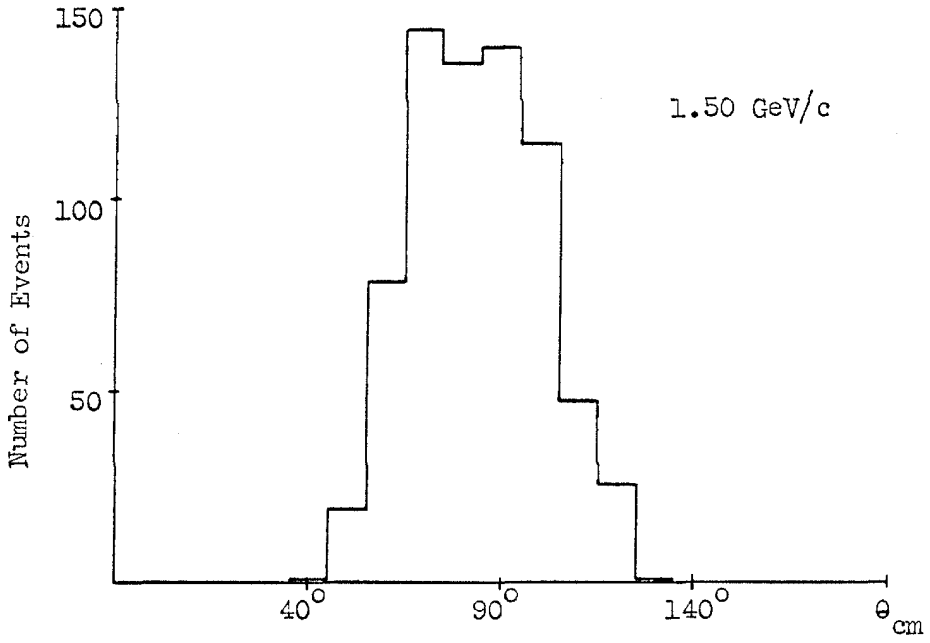

Figure V.8 $\theta\ (\pi^{o})$cm Distribution for $2\pi^{o}$ Monte Carlo Events Satisfying $\alpha_{1,2} \leq 18^{o}$ and cm Projection Test

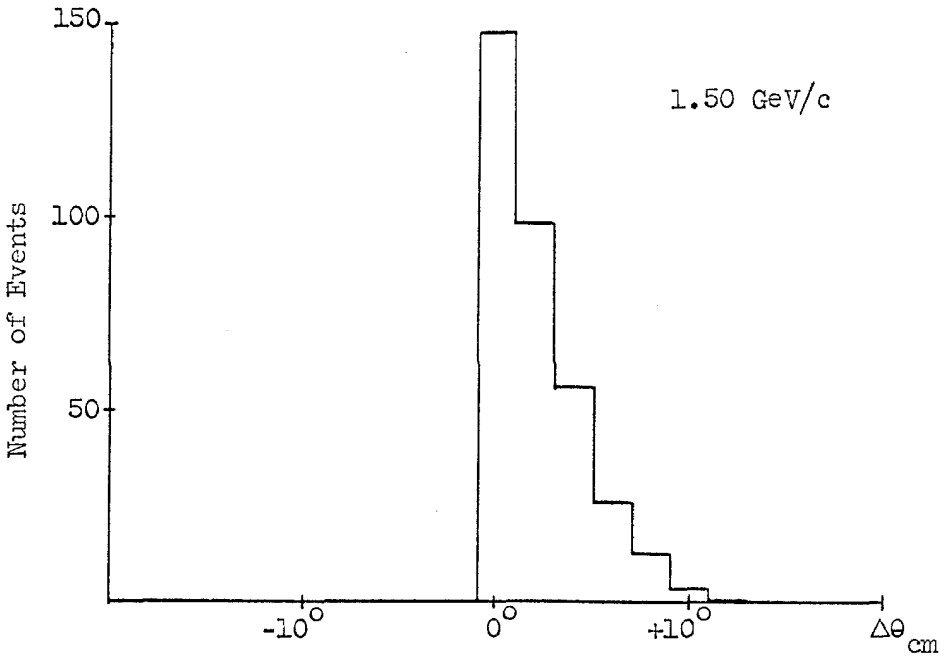

Figure V.9 Error in $\theta\ (\pi^{o})_{cm}$ Due to the Assumption That $\phi = 0$ for $2\pi^{o}$ Monte Carlo Events

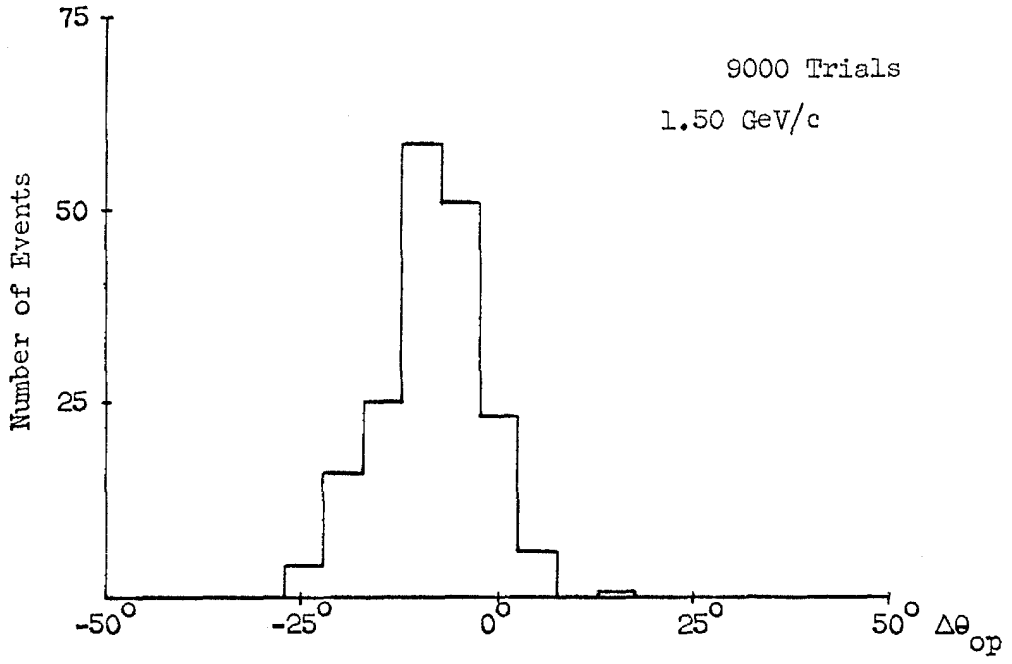

Figure V.10 $\Delta\theta_{op}$-Histogram for $3\pi^{\circ}$ Monte Carlo Events Satisfying $\alpha_{1,2} \leq 18^{\circ}$ and cm Projection Test

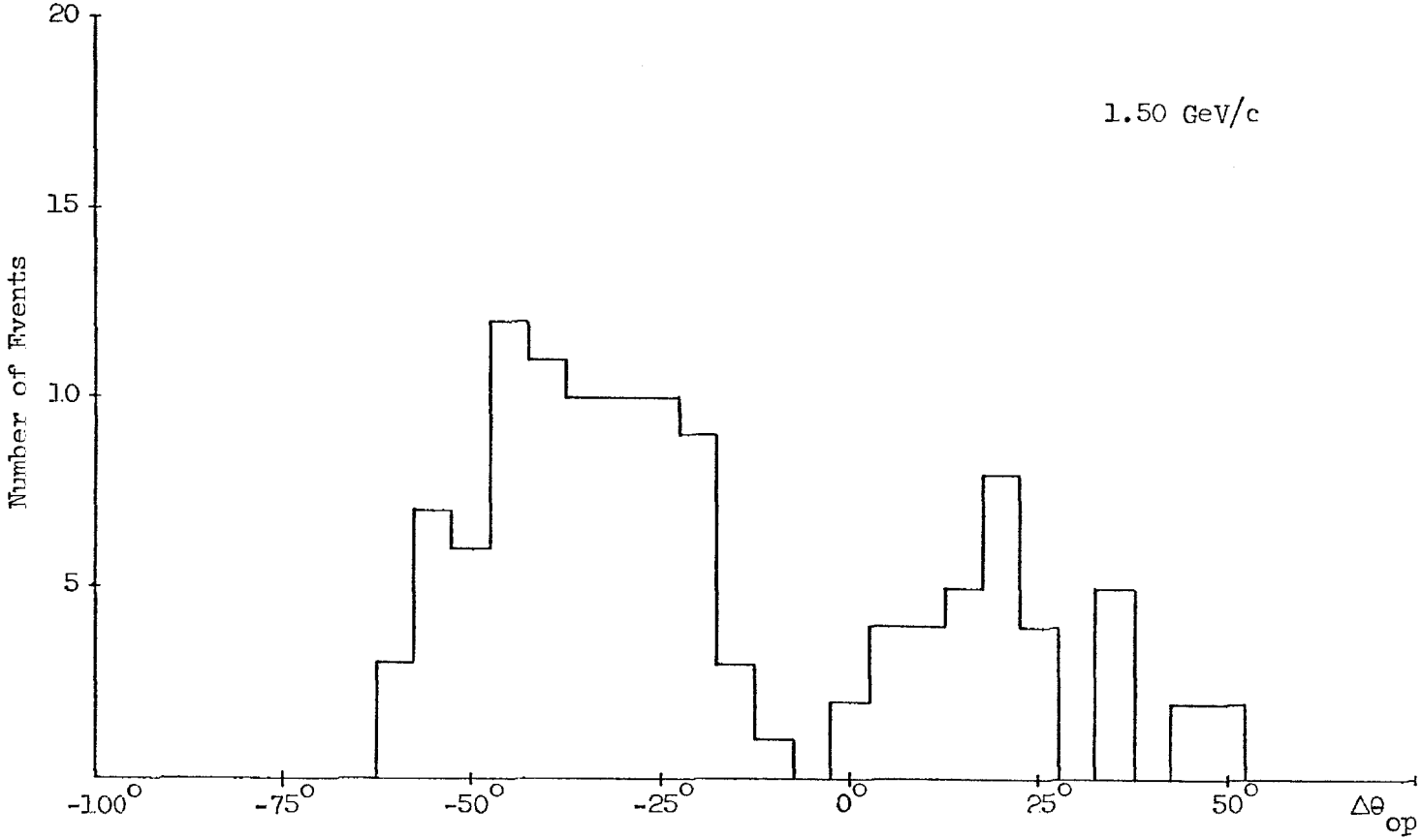

Figure V.11 $\Delta\theta_{op}$-Histogram for Four γ-ray Events not Satisfying cm Projection Test

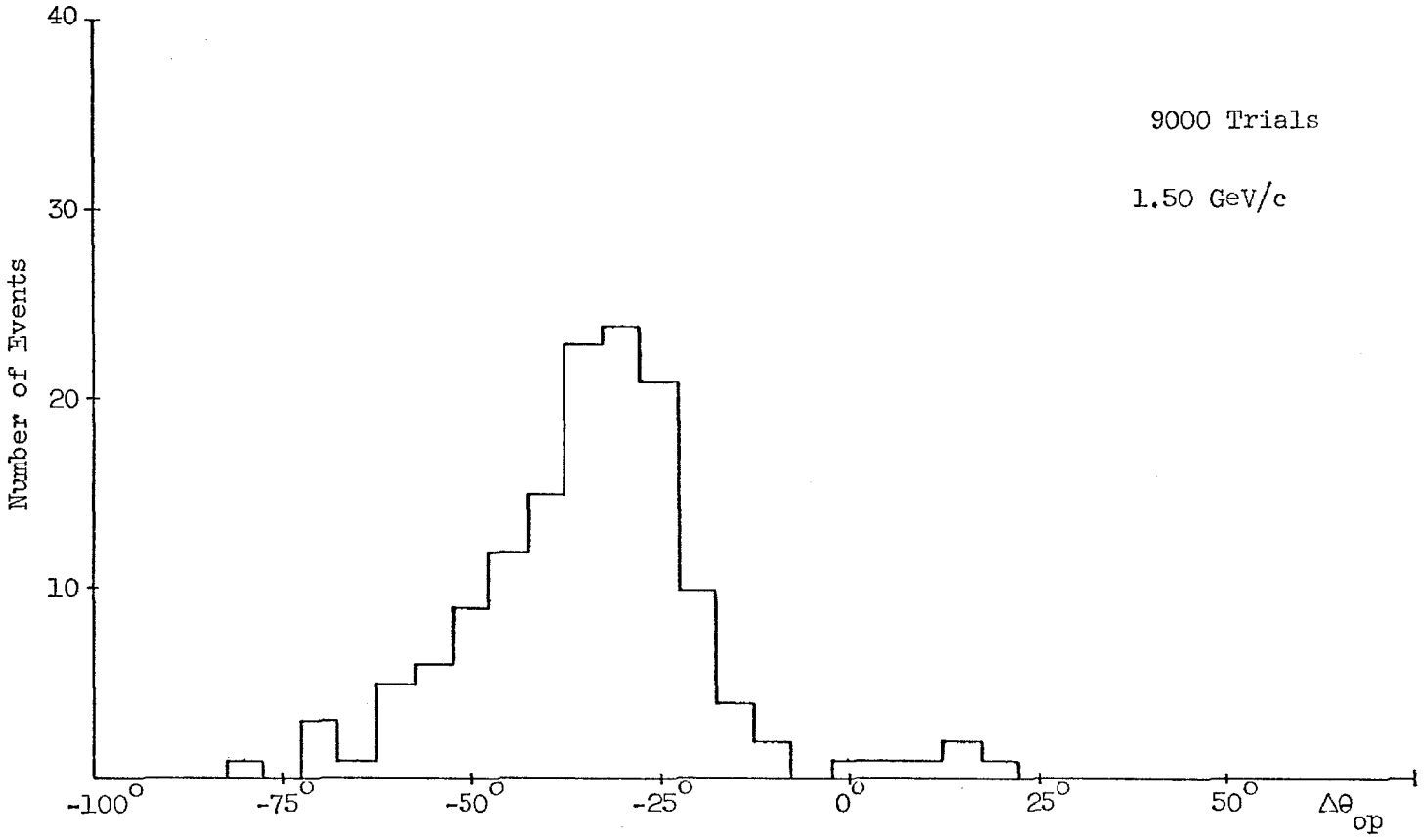

Figure V.12 $\Delta\theta_{op}$-Histogram for $3\pi^{o}$ Monte Carlo Events not Satisfying cm Projection Test

The results of similar analyses for the other incident momenta are given in Figure V.14. Figure V.13 shows the detection efficiencies used for calculation of the upper limits to the $3\pi^o$ cross section.

Comparison of the relative detection efficiencies obtained by analyzing the Monte Carlo generated events then implies that with the above limits on the $3\pi^o$ cross section less than one half of the events in the opening angle error histogram of the data satisfying the opening angle requirement for the γ-rays on each side and the consistency test for the $2\pi^o$ hypothesis can be due to the $3\pi^o$ final state. χ^2 tests on the $\Delta\theta_{op}$-histograms have equal probability ($\approx$15%) for all the events coming from the $2\pi^o$ final state or a 50% mixture of $2\pi^o$ and $3\pi^o$ final states. The χ^2 test using the $3\pi^o$ final state has a probability of $< 1\%$. Since in this thesis only upper limits on the $2\pi^o$ cross section are used all the events in the data satisfying the opening angle requirement and the consistency test will be assumed to come from the $2\pi^o$ final state.

Under this assumption Figures V.15 thru V.20 summarize the $2\pi^o$ differential cross section data for the incident momenta used for this series of runs. Figure V.21 shows the 90^o cross sections for the various momenta.

The differential cross-sections were obtained by comparing the experimental θ_{cm}-histogram to the θ_{cm}-histogram for successful Monte Carlo events. They have not been corrected for the Čerenkov counter detection efficiency (> 95%) or scanning efficiencies (> 95%).

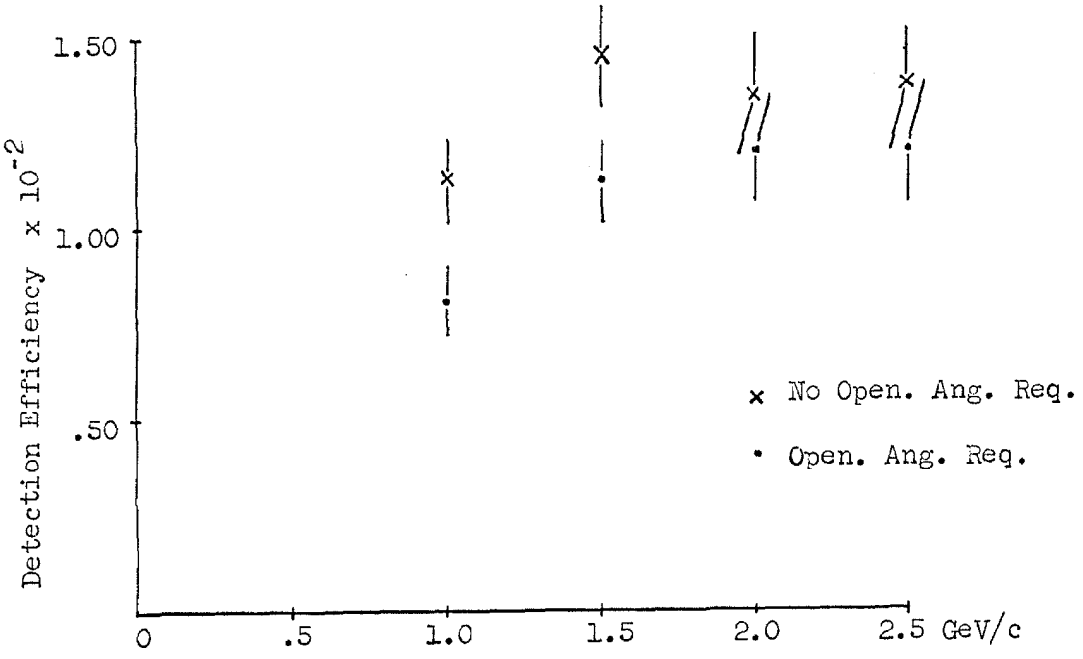

Figure V.13 $3\pi^0$ Detection Efficiency

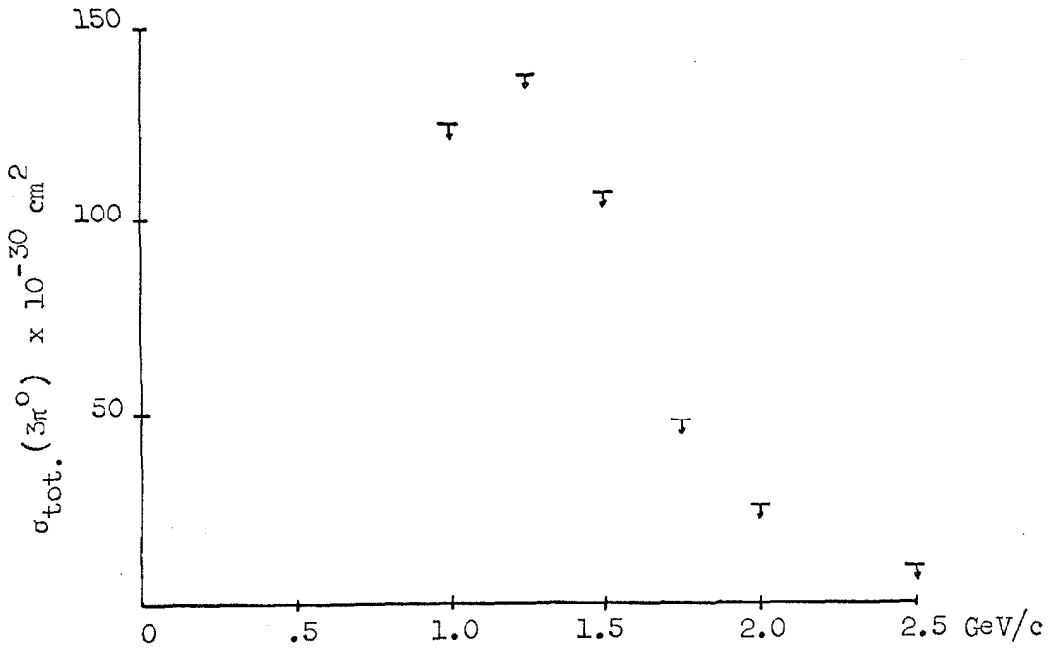

Figure V.14 Upper Limits to $\sigma_{tot.}(3\pi^0)$

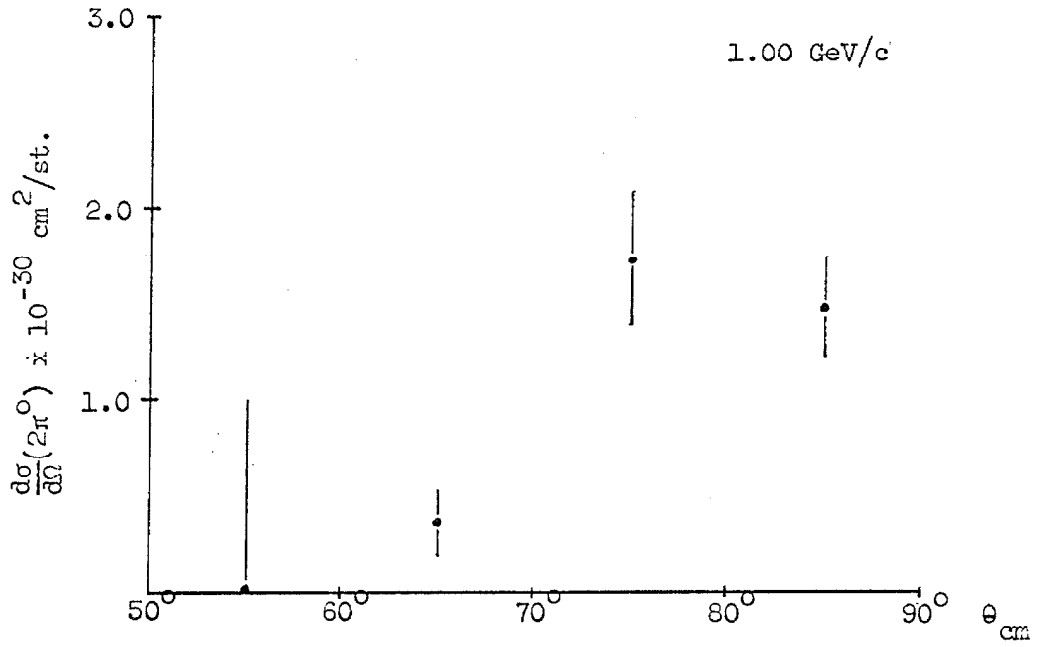

Figure V.15 $\bar{p}p \rightarrow 2\pi^o$ Differential Cross Section

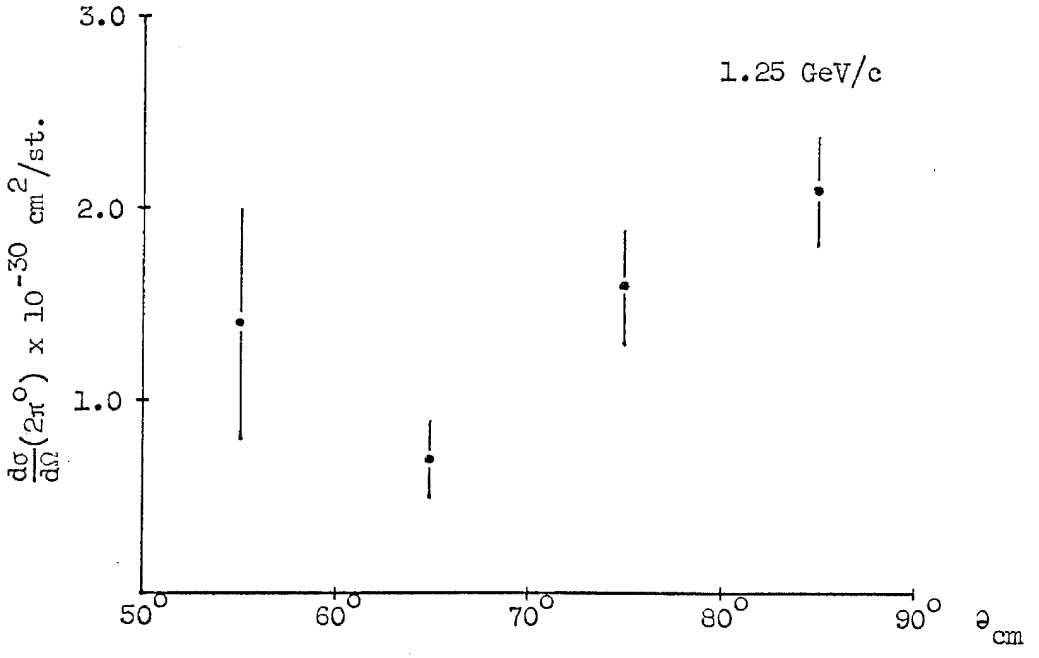

Figure V.16 $\bar{p}p \rightarrow 2\pi^o$ Differential Cross Section

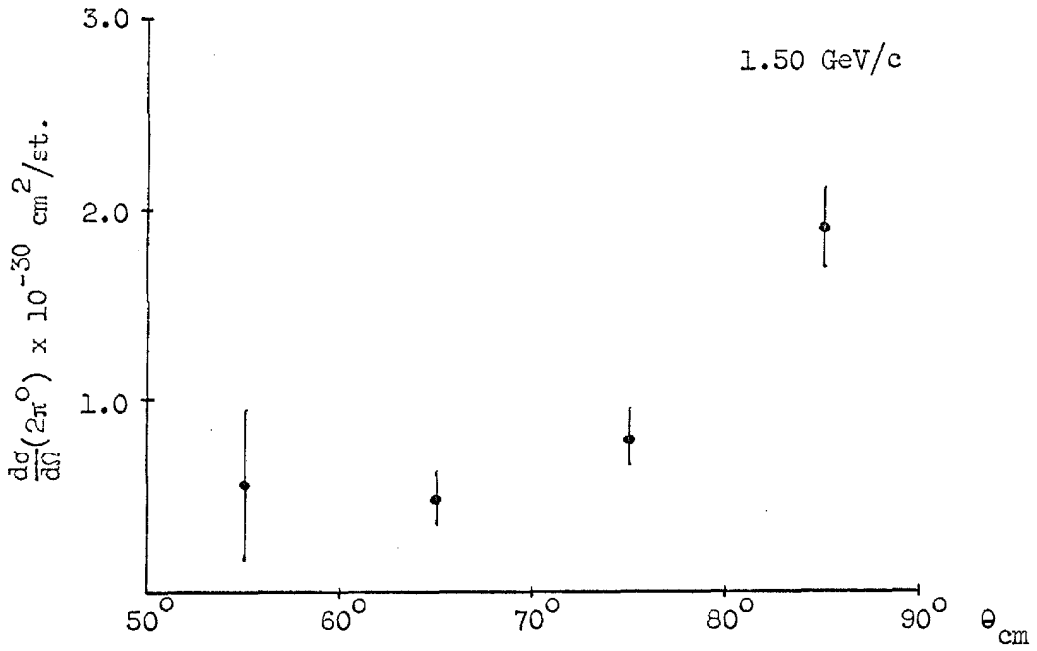

Figure V.17 $\bar{p}p \rightarrow 2\pi^o$ Differential Cross Section

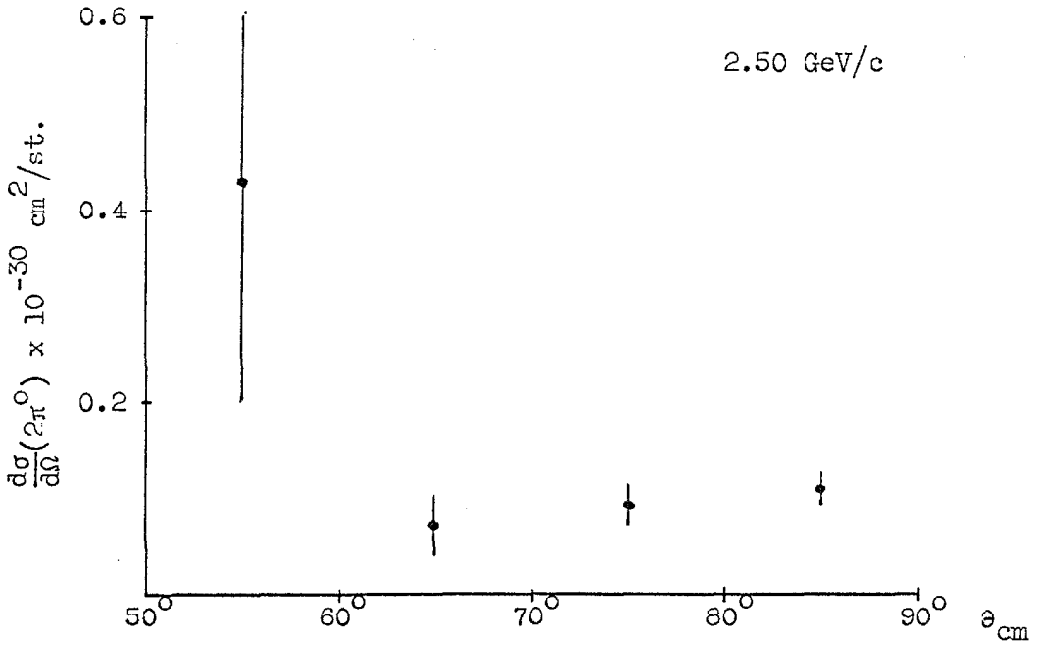

Figure V.18 $\bar{p}p \rightarrow 2\pi^o$ Differential Cross Section

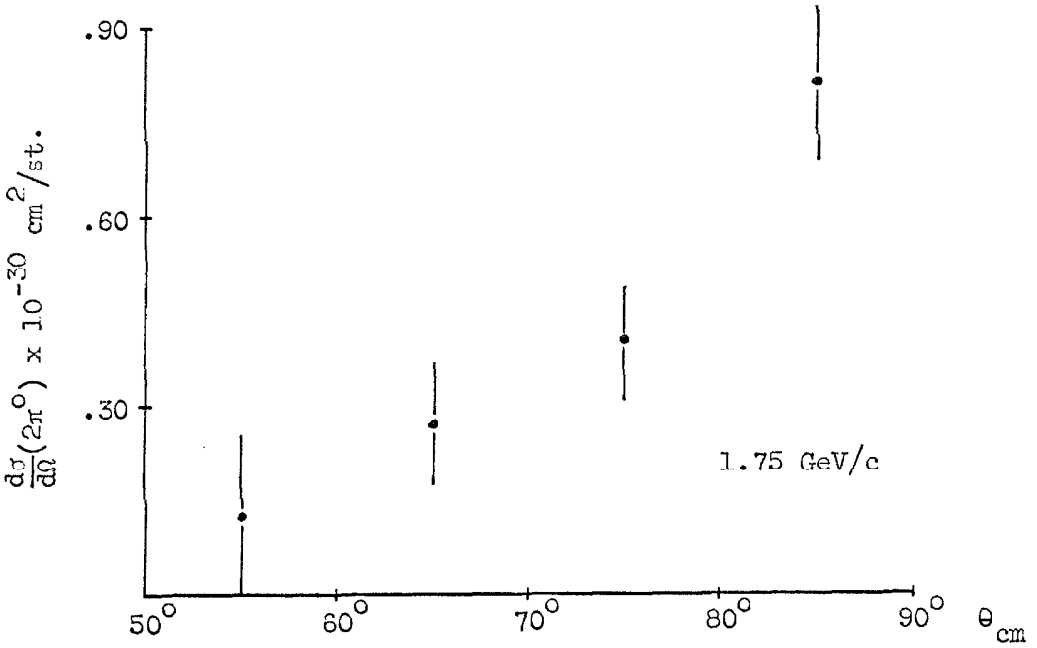

Figure V.19 $\bar{p}p \rightarrow 2\pi^o$ Differential Cross Section

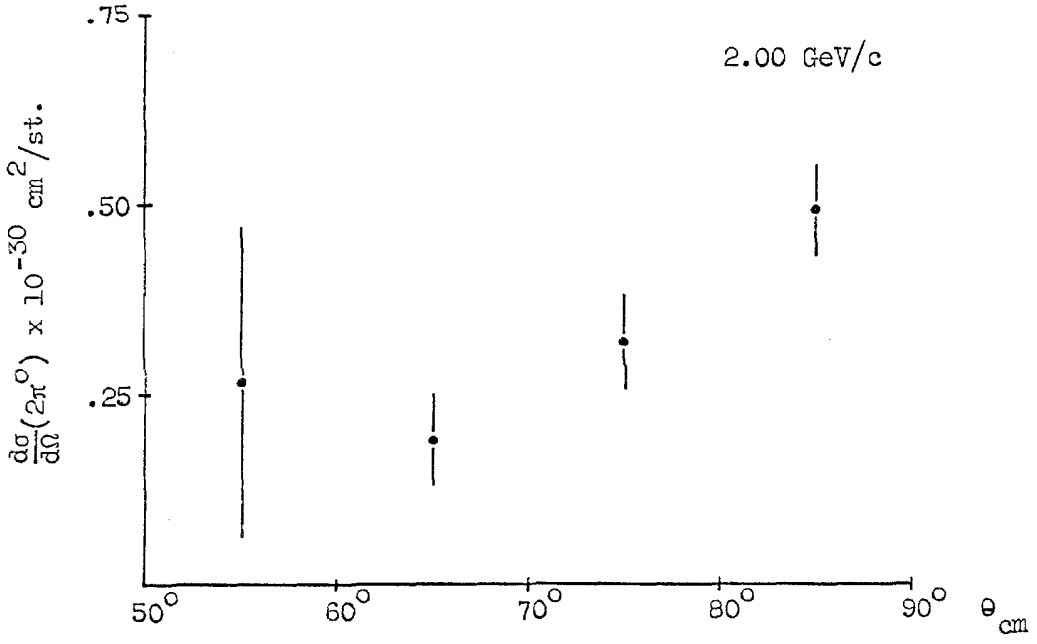

Figure V.20 $\bar{p}p \rightarrow 2\pi^o$ Differential Cross Section

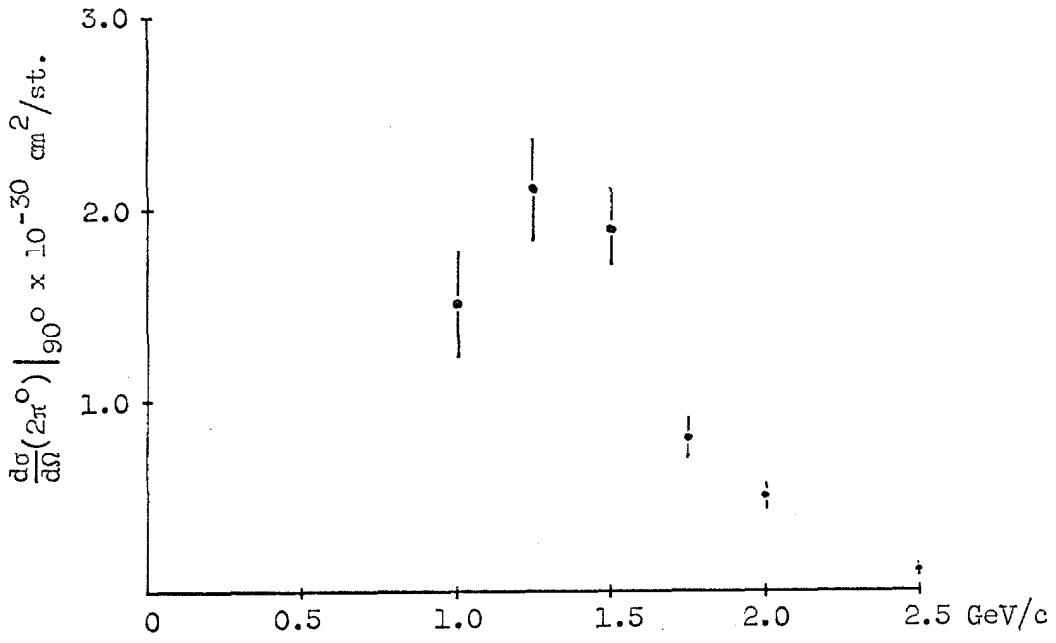

Figure V.21 $\bar{p}p \rightarrow 2\pi^o$ Differential Cross Section at $\theta_{cm} = 90^o$

Table V.1 Summary of $2\pi^o$ Cross Section Data

p mom. (GeV/c)	$\frac{d\sigma}{d\Omega}(\bar{p}p \to 2\pi^o)^*$ x 10^{-30} $cm^2/st.$				θ_{cm}
	55^o	65^o	75^o	85^o	
1.00	$0^{+1.8}_{-0}$	$0.37 \pm .16$	$1.74 \pm .33$	$1.50 \pm .23$	
1.25	$1.42 \pm .60$	$0.68 \pm .19$	$1.60 \pm .29$	$2.10 \pm .27$	
1.50	$0.56^{+1.1}_{-.3}$	0.47 ± 14	0.82 ± 14	$1.89 \pm .22$	
1.75	$0.13^{+.21}_{-.07}$	0.27 ± 10	0.40 ± 10	$0.81 \pm .12$	
2.00	$0.27^{+.40}_{-.15}$	$0.19 \pm .06$	$0.32 \pm .06$	$0.49 \pm .06$	
2.50	$0.43^{+.24}_{-.15}$	$0.07^{+.03}_{-.02}$	$0.09 \pm .02$	$0.11 \pm .02$	

* These cross sections are equal to 1/2 of the conventionally defined cross sections. See Page for further explanation.

APPENDIX VI

$$\bar{p} + p \rightarrow \pi^o + \gamma$$

a. Experimental Method and Analysis

The same Pb chamber film that was used in investigating the $2\pi^o$ final state for 1.50 GeV/c incident antiprotons was rescanned looking for events with two γ-rays in one chamber and one γ-ray in the other. Data cards were punched for these events with the same format as was used for the data cards for the $2\pi^o$ events. For the side with one γ-ray its projected angle was taken for both the projected angles of the two γ-rays for the corresponding side in the $2\pi^o$ investigation.

The data cards were then analyzed with the analysis program used for the $2\pi^o$ case. The experimental opening angle error histograms were then compared to the expected ones due to the $\pi^o\gamma$ and the $2\pi^o$ final states obtained by using Monte Carlo generated data cards for the two cases. The sample from the Monte Carlo generated data cards for the $2\pi^o$ final state included the cards for events which should have been vetoed but were not because of the 35% veto inefficiency.

The comparison of the experimental $\Delta\theta_{op}$-histogram obtained by subtracting the $2\pi^o$ contribution using the $2\pi^o$ cross section data from Appendix V which assumes no background contribution and the Monte Carlo distribution for $\pi^o\gamma$ then yields an upper limit on the $\pi^o\gamma$ cross section in the angular acceptance of the detection apparatus.

b. Results

The $\Delta\theta_{op}$-histograms are given in Figures VI.1 thru VI.6. Taking

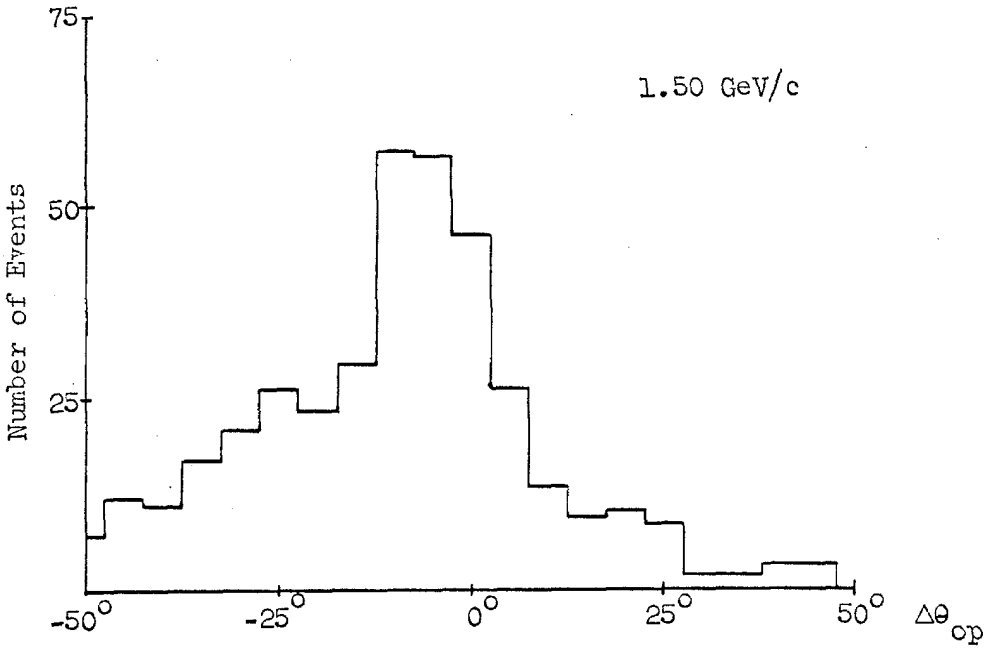

Figure VI.1 $\Delta\theta_{op}$-Histogram for all Three γ-ray Events

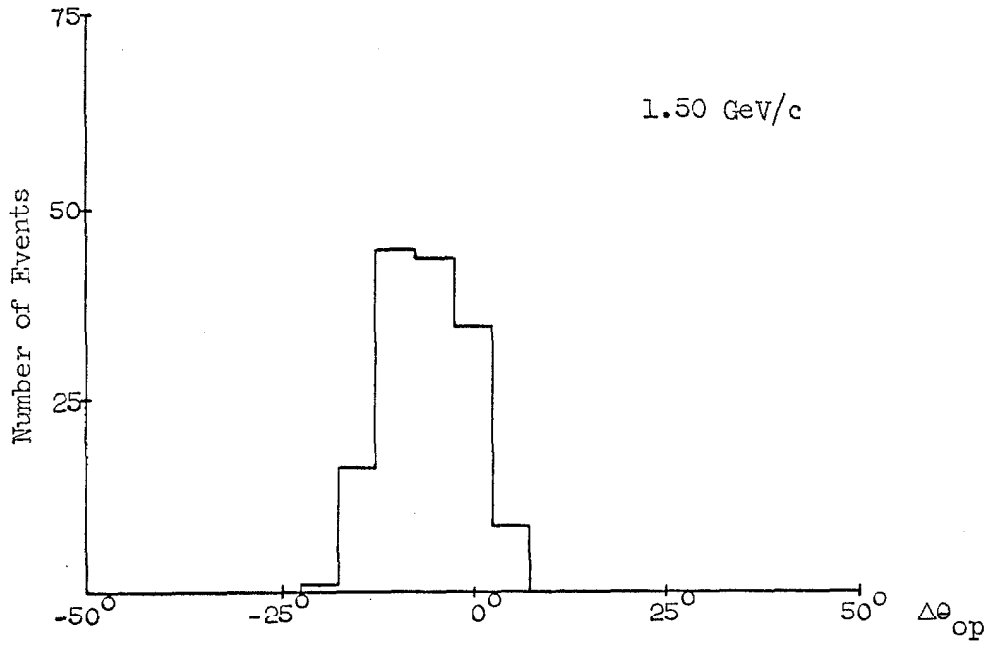

Figure VI.2 $\Delta\theta_{op}$-Histogram for all Three γ-ray Events Satisfying $\alpha_1 \leq 18^\circ$ and cm Projection Test

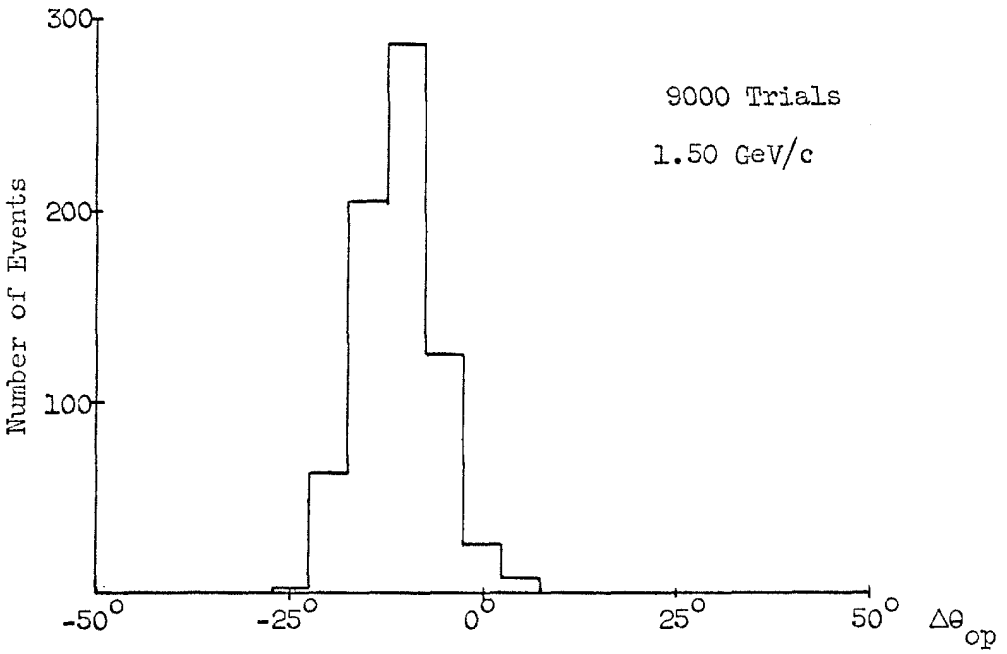

Figure VI.3 $\Delta\theta_{op}$-Histogram for $2\pi^{o} \rightarrow 3\gamma$ Monte Carlo Events Satisfying $\alpha_1 \leq 18^{o}$ and cm Projection Test

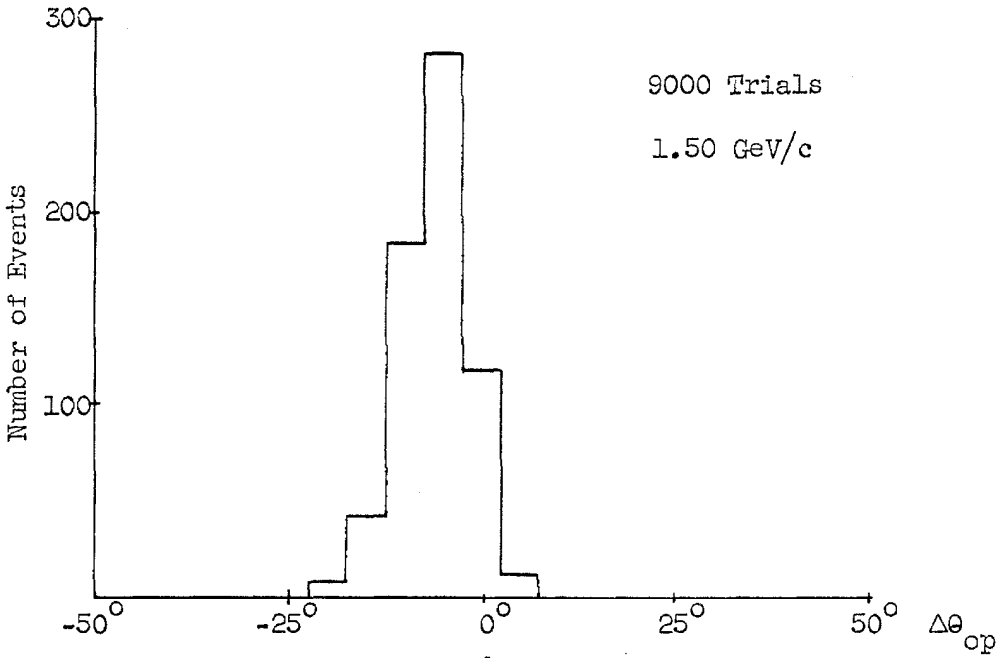

Figure VI.4 $\Delta\theta_{op}$-Histogram for $\pi^{o}\gamma$ Monte Carlo Events Satisfying $\alpha_1 \leq 18^{o}$ and cm Projection Test

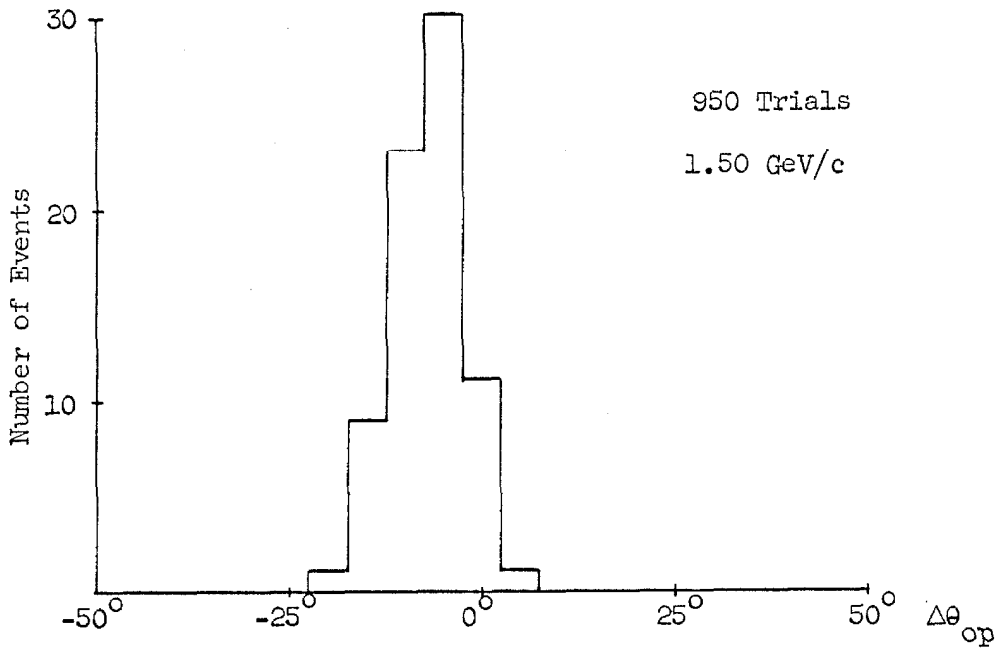

Figure VI.5 $\Delta\theta_{op}$-Histogram for $2\pi^o \rightarrow 3\gamma$ Monte Carlo Events Satisfying $\alpha_1 \leq 18^o$ and cm Projection Test

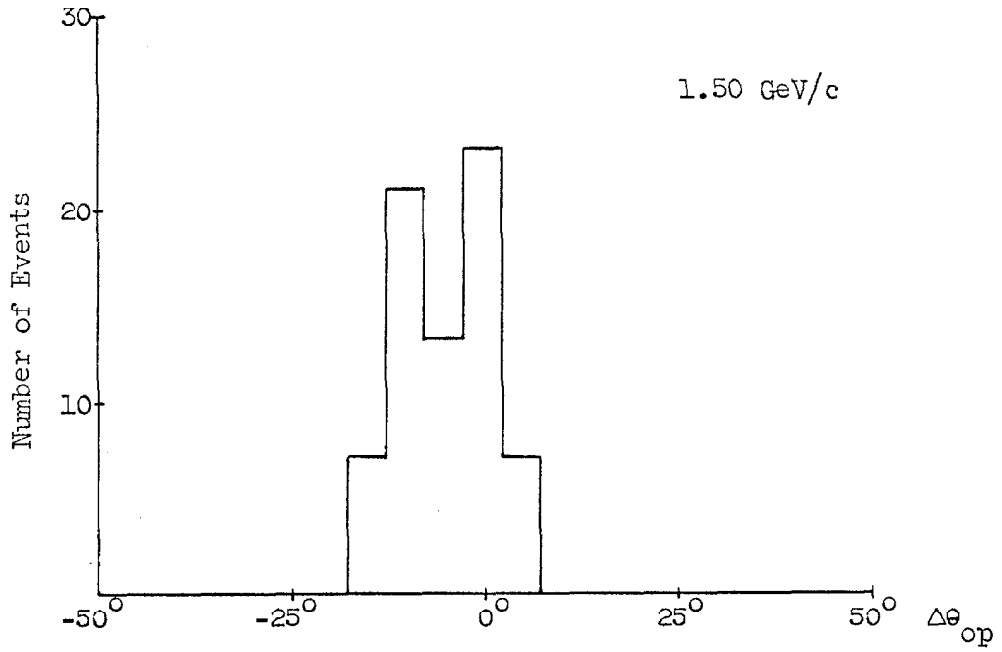

Figure VI.6 $\Delta\theta_{op}$-Histogram for all Three γ-ray Events with $2\pi^o$ Background Subtracted

all the events in Figure VI.6 then gives using the known detection efficiency from the Monte Carlo program and neglecting the scanning efficiency (> 95%) and the Čerenkov counter efficiency (> 95%) an upper limit of

$$\sigma(\pi^{o}\gamma) \leq (5.2 \pm 0.8) \times 10^{-30} \text{ cm}^2.$$

If no subtractions are made and all the events in Figure VI.2 are taken to be real the cross section limit is

$$\sigma(\pi^{o}\gamma) \leq (10.4 \pm .5) \times 10^{-30} \text{ cm}^2.$$

The errors included are statistical only however the systematic errors are estimated to be less than 20%. The Čerenkov counter pulse height spectra using all the unsubtracted events are the same as those expected from the $e^{+} + e^{-}$ final state for 1.50 GeV/c incident anti-protons.

APPENDIX VII

$\bar{p} + p \rightarrow 2\gamma$

a. Experimental Method and Analysis

To check the 2γ cross section results given in Section V the same Pb chamber film as used for investigating the $2\pi^o$ final state for 1.50 GeV/c incident antiprotons was rescanned to look for events with only one γ-ray converting in each chamber. Data cards were punched for these events using the same format as was used for the data cards for the $2\pi^o$ events with the projected angle of the γ-ray on each side punched twice.

As in the $2\pi^o$ case and the $\pi^o\gamma$ case the $\Delta\theta_{op}$-histograms obtained from the events were compared to those obtained from the fake data cards from the appropriate Monte Carlo program. The backgrounds due to the $2\pi^o$ and $\pi^o\gamma$ final states were subtracted from the experimental data by subtracting the appropriately scaled $\Delta\theta_{op}$-histograms obtained from the $2\pi^o \rightarrow 2\gamma$ and the $\pi^o\gamma \rightarrow 2\gamma$ fake data cards generated by the appropriate Monte Carlo program. The sample used included the events which should have been vetoed but were not because of the veto counter detection efficiency (= 65%). To set the scale of the $\Delta\theta_{op}$-histograms the upper limits to the $2\pi^o$ and $\pi^o\gamma$ cross sections given in Appendices V and VI were taken to be the cross sections for these processes.

b. Results

Figures VII.1 thru VII.4 summarize the expected backgrounds and the final results. Figure VII.5 shows the $\Delta\theta_{op}$-histogram for the 2γ final state Monte Carlo generated events.

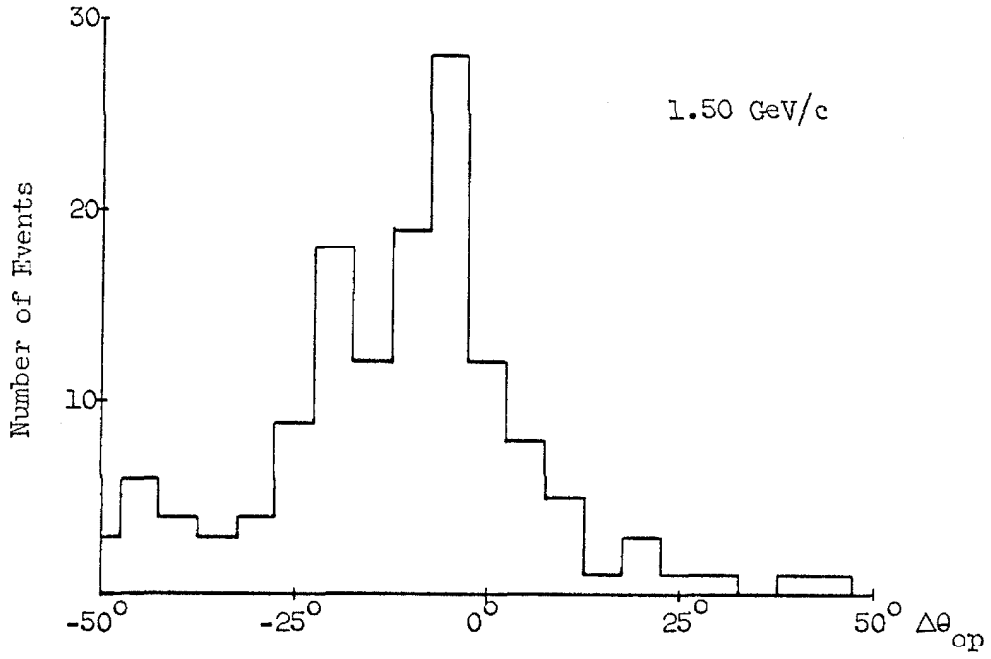

Figure VII.1 $\Delta\theta_{op}$-Histogram for all Two γ-ray Events

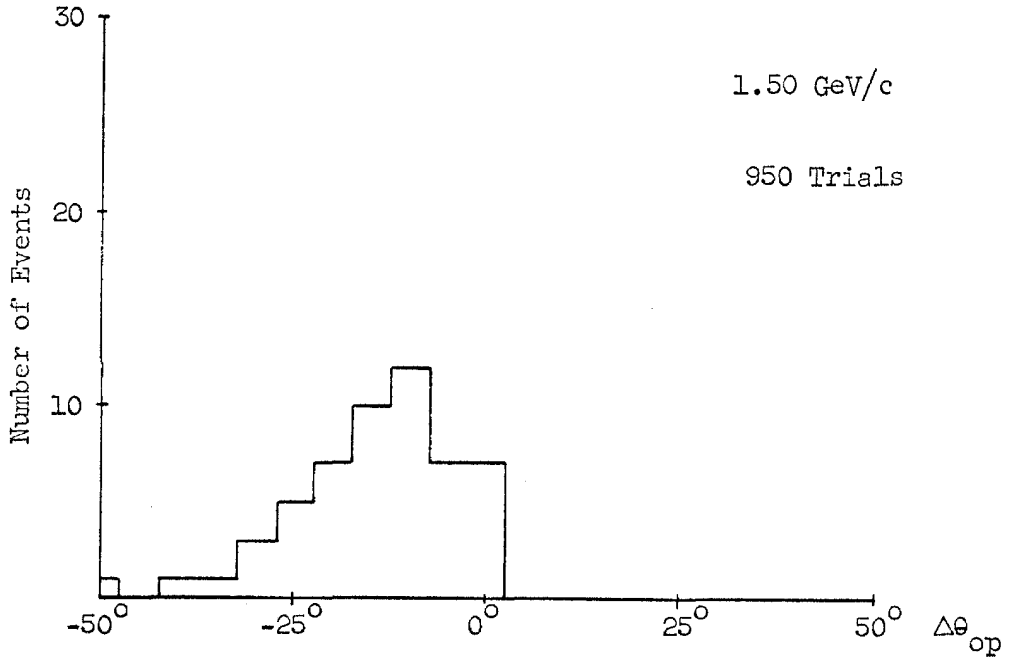

Figure VII.2 $\Delta\theta_{op}$-Histogram for $2\pi^{o} \rightarrow 2\gamma$ Monte Carlo Events

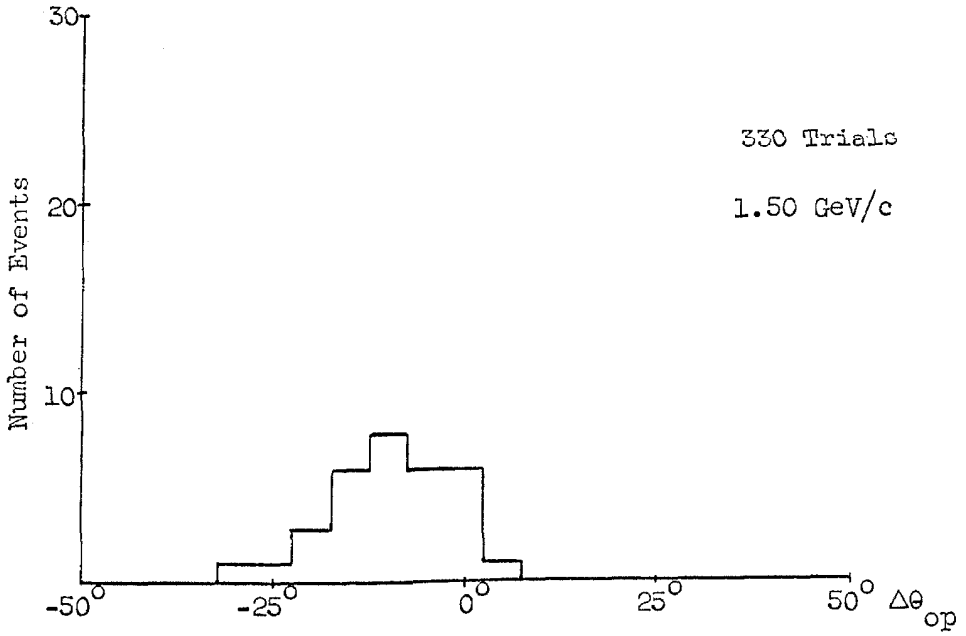

Figure VII.3 $\Delta\theta_{op}$-Histogram for $\pi^{o}\gamma \rightarrow 2\gamma$ Monte Carlo Events

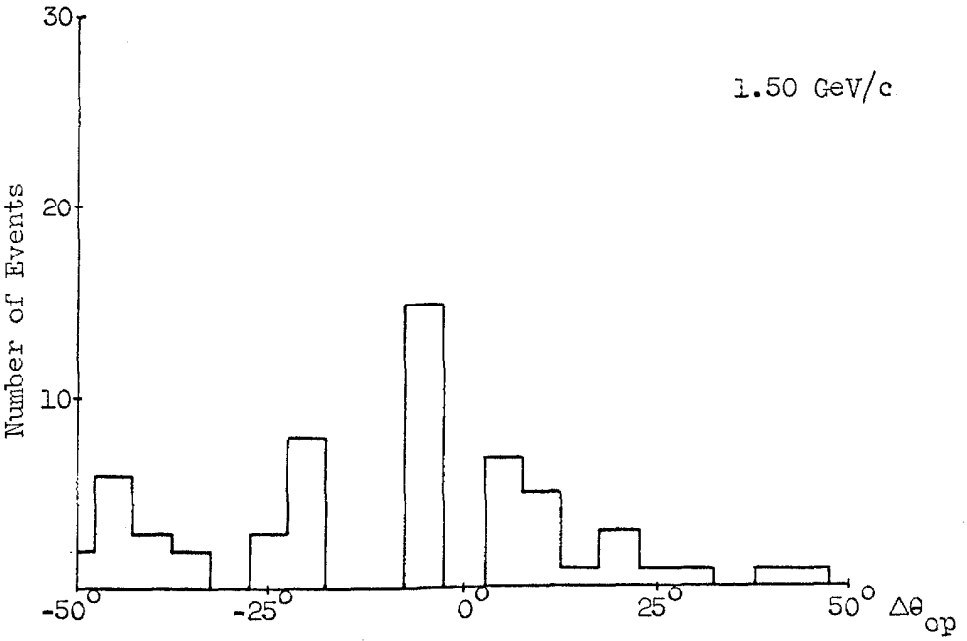

Figure VII.4 $\Delta\theta_{op}$-Histogram for all Two γ-ray Events with $2\pi^{o}$ and $\pi^{o}\gamma$ Background Subtracted

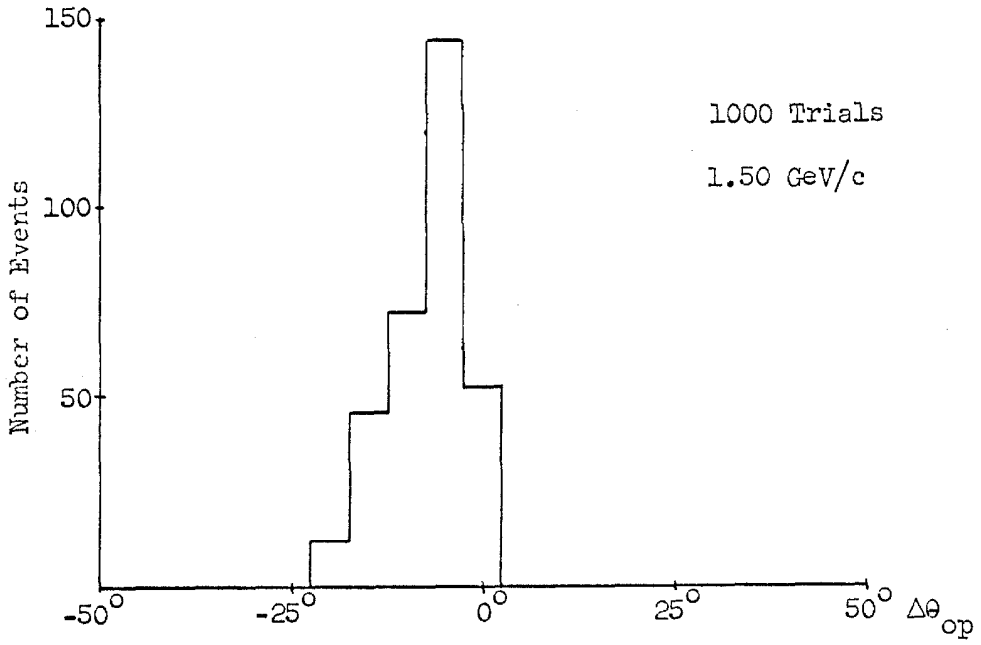

Figure VII.5 $\Delta\theta_{op}$-Histogram for 2γ Monte Carlo Events

Assuming that all the events in Figure VII.4 between -2.5^{o} and -17.5^{o} come from the 2γ final state gives the following upper limit on the 2γ cross section.

$$\sigma(2\gamma) \leq (1.0 \pm 0.3) \times 10^{-30} \text{ cm}^2$$

This limit should be used with caution, however, because of the large and uncertain background subtractions made in obtaining it.

APPENDIX VIII

Antiproton Beam

The antiproton beam used in this experiment was obtained using the partially separated beam transport system at the AGS known as Beam Number 5. The G-10 internal target was the source for the beam. This system was designed by one of the members of our group, Barry Barish, and has been written up in detail by him. His report will appear in the form of an unpublished AGS internal report. For details such as ray traces, layout of the beam elements, magnifications, etc. the reader is referred to this report.

The general properties of the beam are summarized in the following table.

Table VIII.1

Acceptance:	Horizontal = $\pm$ 15 mrad
	Vertical = $\pm$ 10 mrad
Momentum Acceptance:	$\pm$ 2% with 100% transmission
	+ 3% or -3% with 50% transmission
	$\div$ 4% or -4% with 0% transmission
Number of Spectrometers:	two, one before the separators
	and one following the mass slit.

$\pi^-/\bar{p}$ at liquid hydrogen target: 1/1

$\bar{p}$ Yield/10^{12} protons: 70,000 at 2.50 GeV/c

30,000 at 1.50 GeV/c

Figures VIII.1 and VIII.2 show the x and the y distributions of the beam at the center of the target. They were obtained from the positions of the vertices in a sample of 1500 events analyzed by Douglas Fong from the runs looking for the $\pi^+ + \pi^-$ final state for 1.50 GeV/c antiprotons.

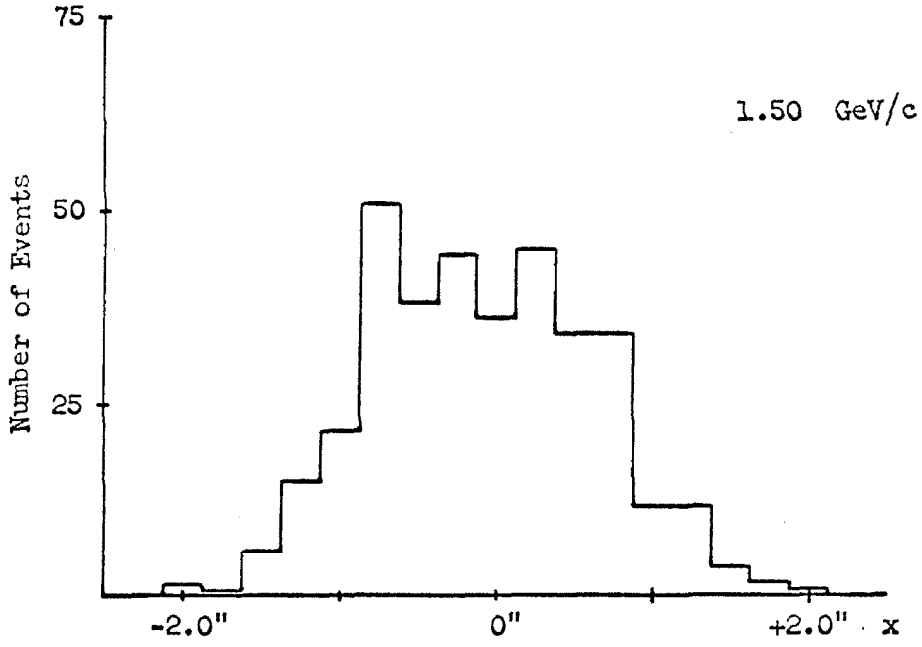

Figure VIII.1 x Distribution of Antiproton Beam at the Center of the Liquid Hydrogen Target

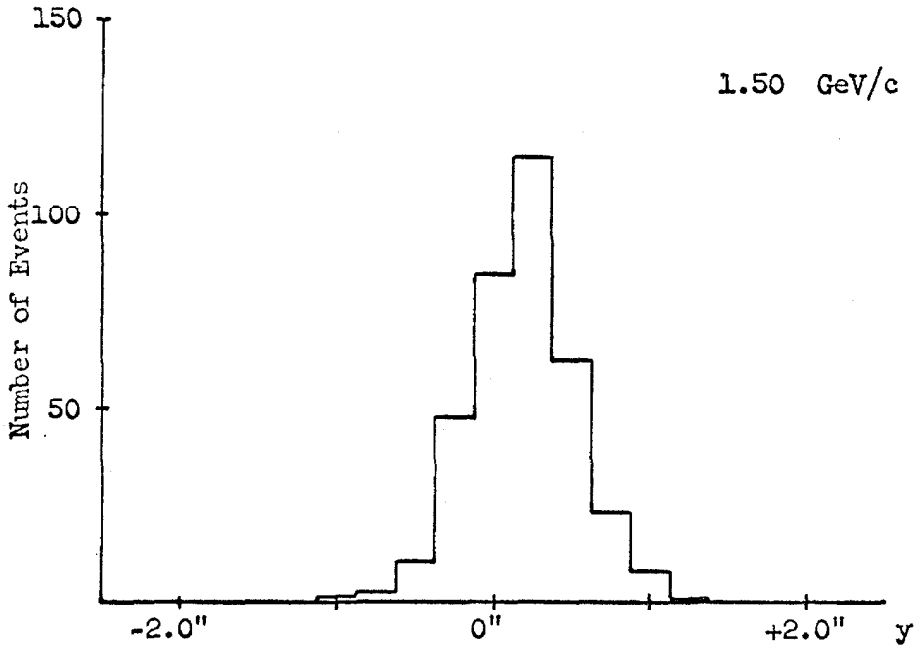

Figure VIII.2 y Distribution of Antiproton Beam at the Center of the Liquid Hydrogen Target

APPENDIX IX

Beam Electronics

The electronic identification of the $\bar{p}$'s in the beam was made by time of flight between two scintillation counters in the beam. The first counter was located at the triple focus behind the mass slit in the beam and the second counter was just in front of the hydrogen target with the path length between them such that 2.50 GeV/c $\bar{p}$'s required 9 nsecs. longer than π^-'s to reach the second counter. At 1.50 GeV/c this difference was 22 nsecs. Since the $\pi^-/\bar{p}$ ratio was ≈ 1 in the beam after the mass slit a single coincidence circuit with 5 nsec. resolving time reduced this ratio to < 0.01 in the electronic identification.

The block diagram of the beam associated electronics is shown in Figure IX.1.

All veto signals to the coincidence cirucits were generated by circuits which have zero dead time. Also a dead time veto was generated so that two compute signals had to be spearated by more than the computation time of the fast computers. The compute pulse which was sent to the fast computer then was made up by the following combination of signals.

$$\text{Compute} = S_2 \cdot S_4 \cdot \bar{V}_{\text{Rear}} \cdot \bar{V}_{\text{Top}} \cdot \bar{V}_{\text{Bottom}} \cdot \bar{V}_{\text{Front}} \cdot \overline{\text{Dead Time}}$$

with S_2 delayed for the $\bar{p}$ time of flight.

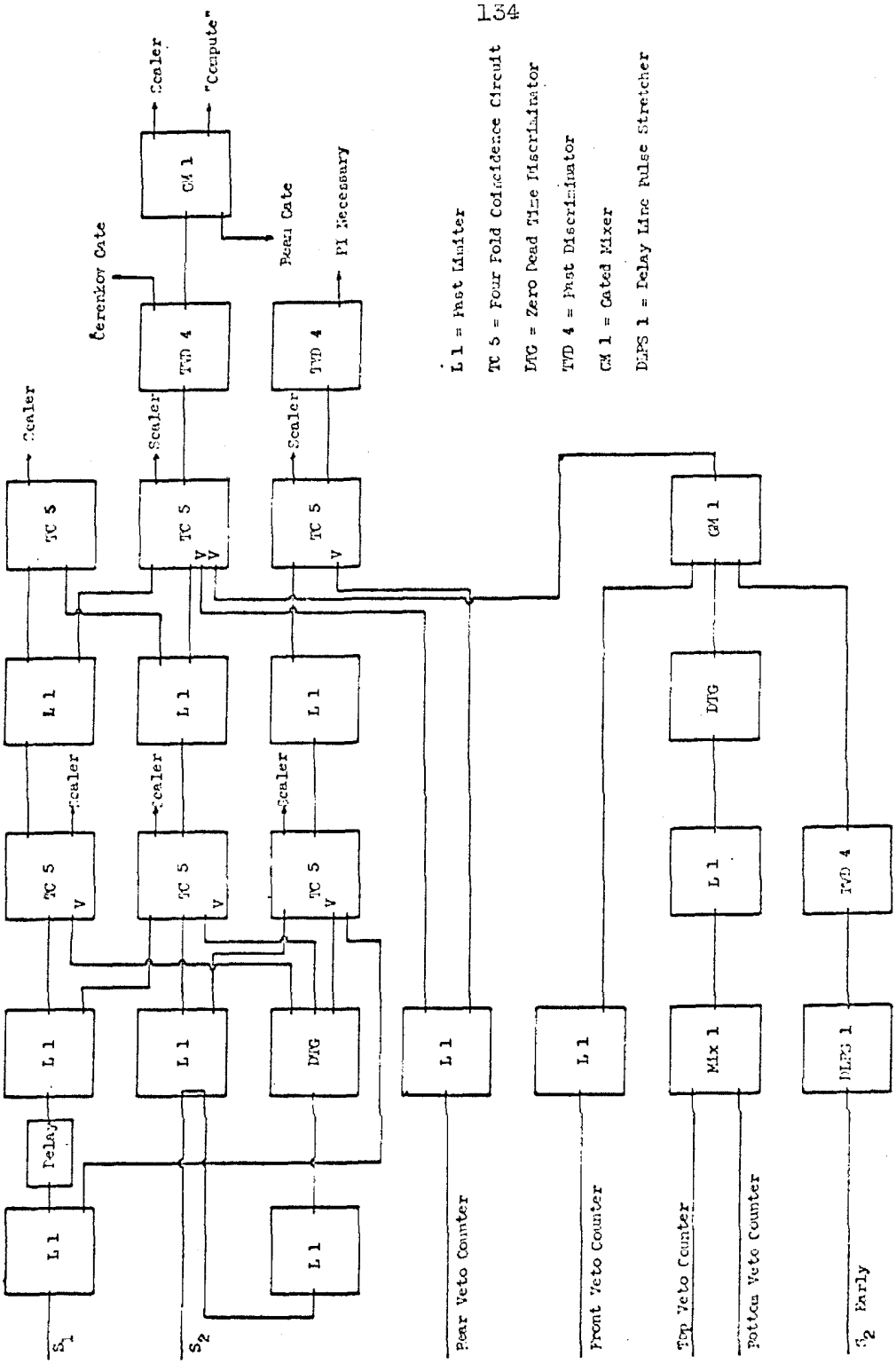

Figure IX.1 Block Diagram of Beam Electronics

APPENDIX X

Liquid Hydrogen Target

The hydrogen target was designed, constructed and operated by the Hydrogen Target Group in the Accelerator Division at Brookhaven. The main design criterion was to keep the amount of material between the liquid hydrogen and the detection apparatus at a minimum to limit backgrounds due to conversion of γ-rays from the annihilation products.

The liquid hydrogen was contained in a cylindrical Mylar flask 82.5" long and 4" in diameter with a wall thickness of 0.014." This was wrapped with thirty layers of Super Insulation (crinkled 1/4 mil aluminized Mylar). This assembly was supported from the target frame by small diameter stainless steel wire hangers spaced at 1 foot intervals along the flask. A brass collar 2" wide and 1/8" thick to which the 1/2" I.D. vent pipe and the 1/2" I.D. fill pipe were attached was bonded to the Mylar flask at its upstream end. The level indicators were placed inside this collar. The flask and its reservoir were contained in an evacuated region enclosed by the aluminum target frame and a 0.014" Mylar window for the reaction products. Thus the total material in the path of the reaction products was 0.036" of Mylar after leaving the liquid hydrogen until their entry into the inner hodoscope counters.

The target and reservoir boiled off approximately 40 liters of liquid hydrogen during eight hours. This boil off rate implied that 0.05 liters of nydrogen gas was produced per second in the liquid.

Assuming the very conservative exit time of 10 seconds for the gas to leave the flask there was 0.5 liters of gas in the target liquid and since the flask held 17 liters this implied that the apparent density of the liquid was $\rho = .95\ \rho_{liquid}$ at the operating pressure of the target.

The pressure in the reservoir and flask was controlled by a mechanical flapper valve which opened into the exhaust line out of the building when the pressure inside the reservoir and flask exceeded 5 p.s.i. above atmospheric pressure. This implied that $P_{abs.} = 19$ p.s.i. and that the temperature of the liquid was $T = 21.31^{\circ}K$ and hence the density was $\rho = 0.0690\ gm/cm^3$.[12]

In all cross section calculations $\rho_{LH_2} = 0.069\ gm/cm^3$ will be used since in the vapor density calculation above a 1 to 2 second exit time would be a more realistic estimate. This would give $\rho_{apparent} \geq .99\ \rho_{LH_2}$ or $\rho_{apparent} = \rho_{LH_2}$.

APPENDIX XI

Kinematics Spark Chambers

The angle measurements of the charged particles from the annihilation in the hydrogen target were carried out by means of two eight gap thin foil spark chambers placed between the inner and outer θ hodoscope trays on each side of the target. The optical system and the fiducial system were designed to give better than 1 mm. resolution in real space. The chambers were photographed to give a 90° stereo view. The top view of each chamber was photographed by separate cameras 16' above the top of the chambers while the end view of the chambers was photographed with a single camera located 32' from the downstream end of the chambers and centered on the beam line. Sections of a spherical lens with a 32' focal length were used as the field lens for the end view while prisms machined in a lucite plate which had a focal length of 16' were used for the field lenses for the top views.

The fiducial plates which were viewed through the field lenses were made from 1/4" lucite selected so that the maximum rate of variation in thickness was less than 0.001" per inch. The fiducial marks were scribed at 6" intervals perpendicular to the spark chamber plates using gauge blocks. The fiducial plates were edge lite by incandescent lamps which were pulsed on for 0.5 seconds for each event.

The chambers were made from plates made from 3" wide x 3/8" thick aluminum frames 38" x 96" over which a 0.001" thick tempered aluminum

foil was stretched and bonded with Eastman 910. Nine of these plates were then placed in a gas tight box made of aluminum with .014" Mylar windows for the particles and spaced apart by 0.340" thick lucite spacers at their four corners. Edge sparking was prevented by ≈ 5 layers of Mylar tape covering the outer 3" boundary of the plates. The high voltage pulse was applied to opposing plates by a parallel plate transmission line from a condenser bank - spark gap unit placed below the gas box. The capacitance ratio was 1 to 1 and the chambers were operated at 15 KV with a 30 volt sweep field. The risetime of the high voltage pulse was ≈ 40 nsec. at the plates of the chamber. Its width which was 400 nanoseconds was controlled by means of a termination resistor across the plates of the chamber.

A 10% He - 90% Ne gas mixture was used with no poisoning gas. The chambers had a continuous flow of ≈ 0.1 cu. ft. of the mixture through them per hour and were kept at a positive pressure of 0.05" of H_2O by a sensitive pressure switch and solenoid gas valve. With this gas mixture and sweep field the chambers had a sensitive time of 2.5 μsec. after which their efficiency dropped rapidly to zero.

APPENDIX XII

Pb Spark Chambers

The final discrimination between electrons and pions was made by requiring that an electron shower be present in a spark chamber made with 0.11 radiation length thick lead plates. Two of these chambers were used with one on each side of the liquid hydrogen target. They were $\approx$ 4 radiation lengths thick for particles at typical angles from the target and they acted as the initial radiators for the Čerenkov counters described in Appendix XVI.

a. Design, Construction, and Operation

The size and layout of the chambers used in the detection apparatus is shown in Figures 3 and 4.

The herring bone layout of the plates in the chambers was chosen so that the trajectory of a typical particle from an annihilation was as nearly perpendicular as possible to the plates of the chamber. Each chamber was made up of eighteen ten gap modules. Each of these modules was a complete spark chamber except for a gas container. The lead plates used were actually a 0.010" Al - 0.022" Pb - 0.010" Al sandwich which was bonded together with Biggs 823 Epoxy.[15] Because of the construction method used for the modules the outer 1.25" of the Pb sheet was replaced with aluminum to minimize the amount of material traversed by the particles before reaching the usable region of the spark chamber. The size of the finished plates was 17" wide x 72" long and they were flat to $\approx$ 0.002" when they were hanging and not supporting their own weight. Ten of these plates plus a 0.010 Al - 0.010 Al

sandwich plate to complete the ten gaps were cast into a Lucite base plate using a polyester potting compound to form the module. This base plate held the 0.340" Lucite spacers between the plates and contained the parallel plate transmission line to which the condenser bank-spark gap unit was attached and the electrical connections between the transmission line and the plates. The plate spacing at the top end of the module was maintained by epoxying 0.340" x 1" Lucite spacers between the plates. Since the chambers were photographed through this end these spacers had both edges carefully polished. The plate spacing along the long edges of the module was maintained by epoxying in 0.340" x 0.250" x 12" Lucite spacers every other foot. The exposed edges of the plates on these long edges of the module were covered with an extruded polyethylene u-channel to prevent edge sparking and corona. There were no internal spacers used between the plates with the edge spacers alone controlling the gap spacing to better than $\pm$ 0.005." The completed module formed a rigid unit which weighed $\approx$ 130 pounds and which could be handled conveniently by two people.

The modules were placed in a gas tight box with the two leads of the parallel plate transmission line extending through a hole in the aluminum base plate of the box. The sides of the box were 0.016" aluminum with .028" of Mylar bonded to the inside of the aluminum sheet. A base frame mounted on casters contained the spark chamber trigger unit, the master trigger spark gap, and the eighteen condenser bank-spark gap units which produced the high voltage pulse to drive the modules in an aluminum box and supported the box containing the modules. The top of

the gas box was covered with a 1/2" thick Lucite plate through which the chamber was photographed. To focus the parallel light from the spark chamber on the camera lens 500" away an oil filled field lens was mounted above the Lucite plate on supports from the base frame.

With the chambers assembled in this manner particles with $\theta = 50^{\circ}$, $\phi = 0$ passed through 0.05 radiation lengths of material in the chamber before reaching the sensitive volume of the chamber.

Originally each module was driven by a separate condenser bank-spark gap unit with

$$\frac{\text{Capacitance of Condenser Bank}}{\text{Capacitance of Chamber}} = \frac{4}{1}.$$

However, because of jitter in the firing time of the eighteen spark gaps it was necessary to connect all the high voltage leads and all the ground leads of the parallel plate transmission lines together by means of two 2" x 1/8" aluminum bus bars. The high voltage pulse applied to the modules had approximately a 50 nsec. risetime with a peak amplitude of 13 kilovolts and a width of 300 nsec. The pulse width was set by using a shorting gap in series with a 2.0 Ω resistor between the bus bars at each end of the bus bars. The shorting gaps were triggered at the same time as the main gaps however they didn't fire until the high voltage pulse had reached $\approx 80\%$ of its maximum amplitude.

The chambers were filled with a 10% He - 90% Ne gas mixture obtained from Linde Co. and from the Air Reduction Corporation. A purifier using an activated charcoal filter maintained at liquid nitrogen temperature was connected to both chambers. The system was

maintained at a positive pressure of 0.2" of H_2O by means of two sensitive pressure switches and several solenoid valves. The gas in the chambers passed through the purifier every six hours and the charcoal filter was warmed to room temperature and evacuated once a day during the experiment.

b. Response for Electrons

To test the response of the chambers to electrons one of the chambers was placed in an electron beam at the AGS. This electron beam was the same beam used to test the Čerenkov counters described in Appendix XVI and was made by placing a differential gas Čerenkov counter tuned for electrons in the antiproton beam described in Appendix VIII with the electrostatic separators tuned for pions. Typical fluxes were a few hundred electrons/accelerator pulse with the contamination of pions in the electron trigger being essentially zero at 1.0 GeV/c and reaching $\simeq$ 10 - 20% at 2.5 GeV/c. Pictures were taken of the chamber placed in this beam and triggered on electrons. The angle of incidence of the beam was varied by rotating the chamber and the beam momentum was set equal to the momentum expected at that particular angle of incidence from the kinematics for $\bar{p} + p \rightarrow e^{+} + e^{-}$ for the two incident antiproton momenta studied in the experiment.

Figure XII.1 is a print of one of the photographs for an electron with $\theta = 50^{\circ}$, $\phi = 0$, and a momentum of 1.50 GeV/c. A convenient way of representing showers like this is to count the total number of sparks contained in a 40° opening angle cone centered on the initial particle direction with the apex of the cone placed at the beginning of the track

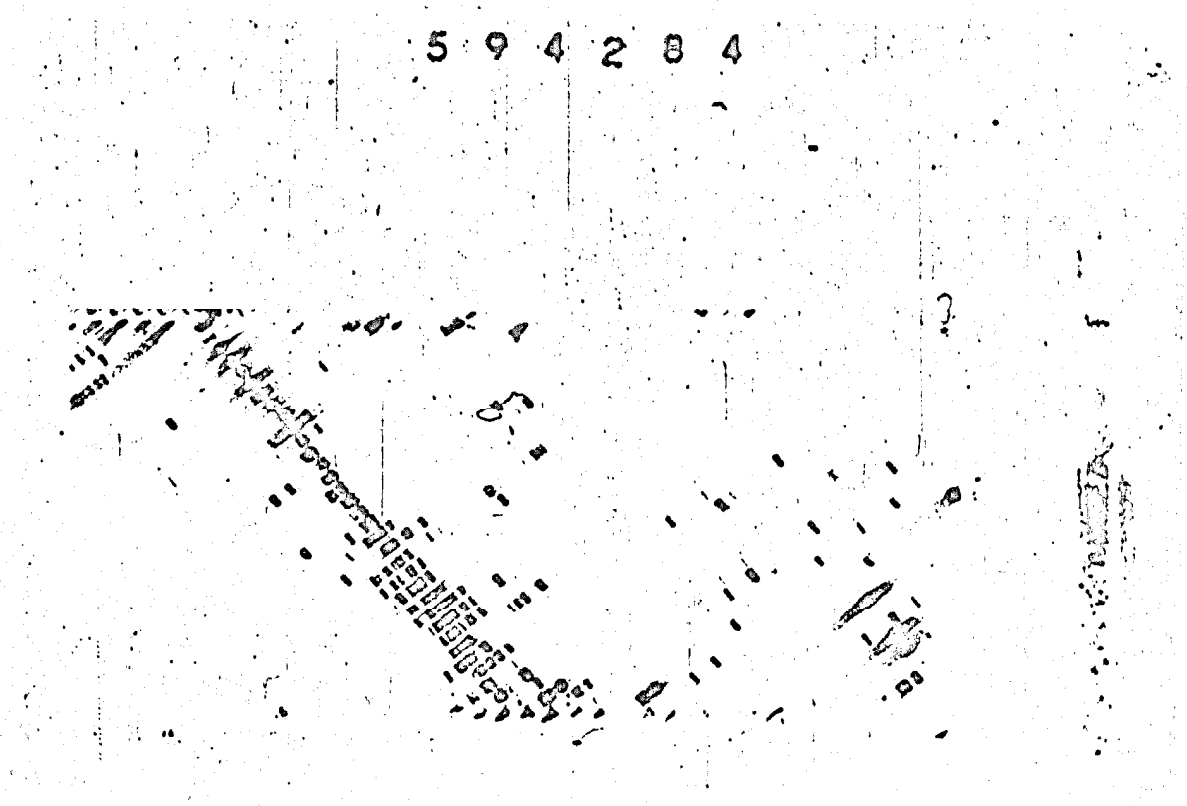

Figure XII.1 1.50 GeV/c Electron Shower in Pb Spark Chamber

in the chamber. Figures XII.2 and XII.3 are histograms of the total number of sparks in the showers produced by electrons for $\theta = 50^{\circ}$ and $\theta = 60^{\circ}$ respectively. In both cases the incident momentum was 1.50 GeV/c. This choice of angles and momentum corresponded roughly to the symmetric annihilation for incident antiproton momenta of 2.50 GeV/c and 1.50 GeV/c respectively.

During these runs one of the Čerenkov counters was placed behind the spark chamber and the pulse height was recorded for each event using the same system as was used during the experiment.

Figure XII.4 shows the pulse height distribution for events from the run with $\theta = 60^{\circ}$. Figures XII.5 thru XII.7 illustrate the lack of correlation between the number of sparks, N_s, in a particular shower and the pulse height in the Čerenkov counter for this run.

An important feature of electron showers in these chambers which was used to discriminate against backgrounds due to narrow angle pairs was where the shower began.

Figure XII.8 is a histogram of the first gap number in which there were two sparks for 1.30 GeV/c positrons incident on the Pb chamber used in the γ-ray studies at Caltech described in Appendix II. Figure XII.9 illustrates the same histogram for the events used in the spark number histogram for $\theta = 50^{\circ}$.

c. Response for Charged Pions

To check the response of the chambers to pions which was averaged over the solid angle acceptance of the apparatus the spark chambers

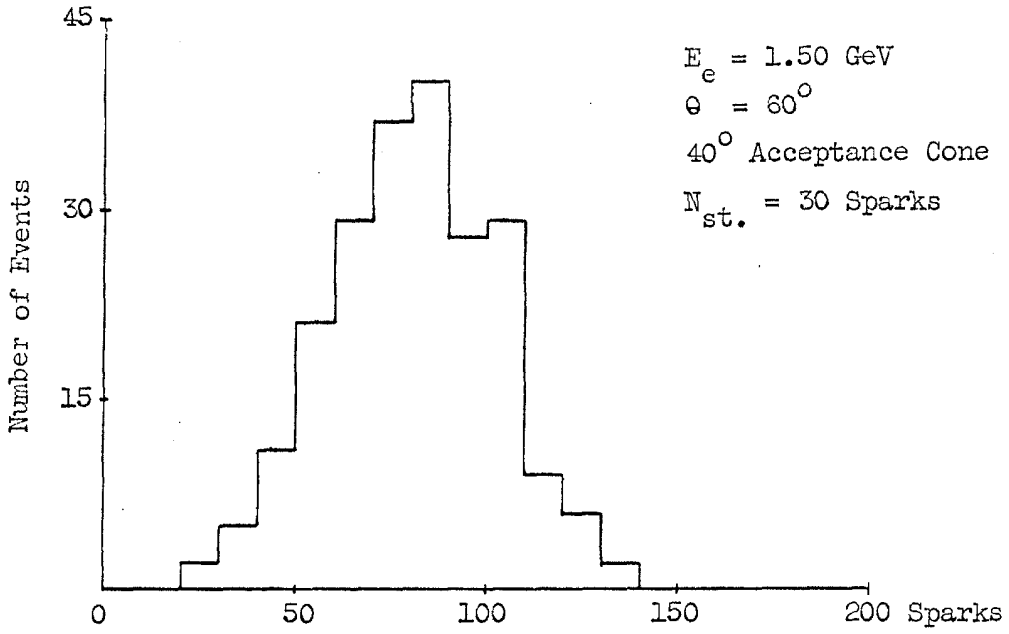

Figure XII.2 Distribution of the Total Number of Sparks Inside a 40° Cone

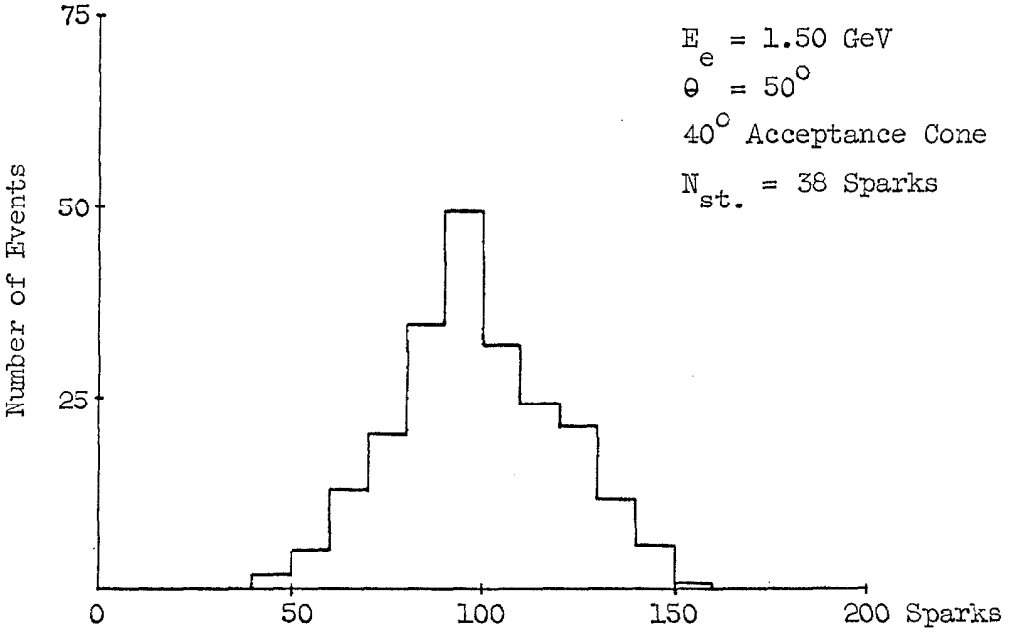

Figure XII.3 Distribution of the Total Number of Sparks Inside a 40° Cone

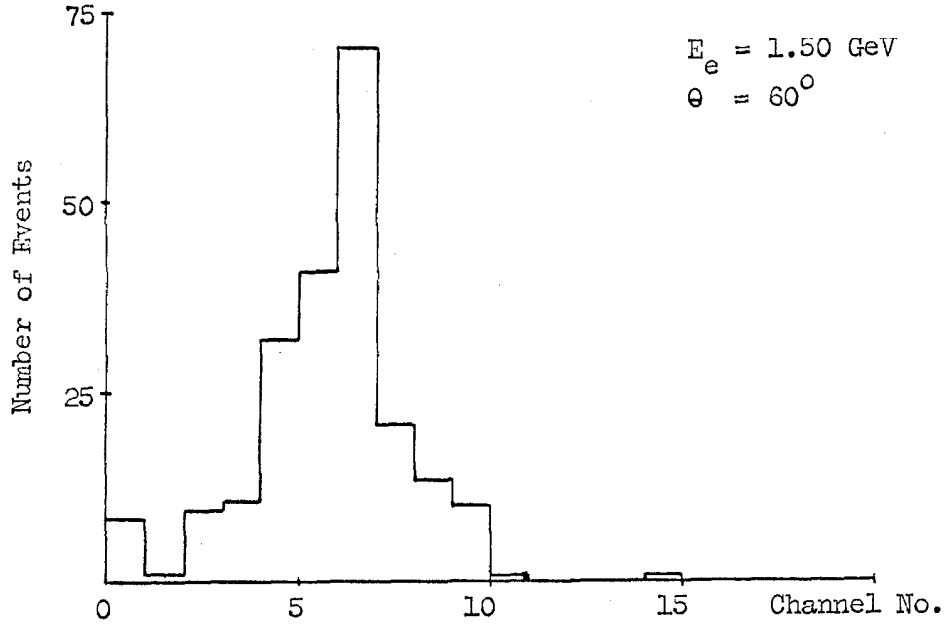

Figure XII.4 Pulse Height Distribution for 1.50 GeV/c Electrons with $\theta = 60^{\circ}$, $\phi = 0^{\circ}$

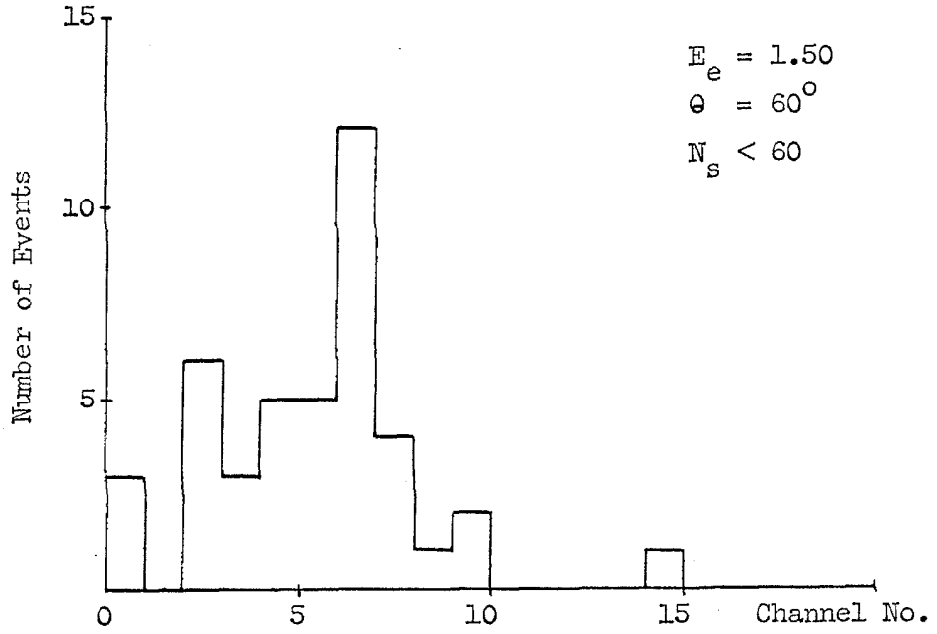

Figure XII.5 Pulse Height Distribution for 1.50 GeV/c Electrons with $\theta = 60^{\circ}$, $\phi = 0^{\circ}$ for Events with $N_s < 60$

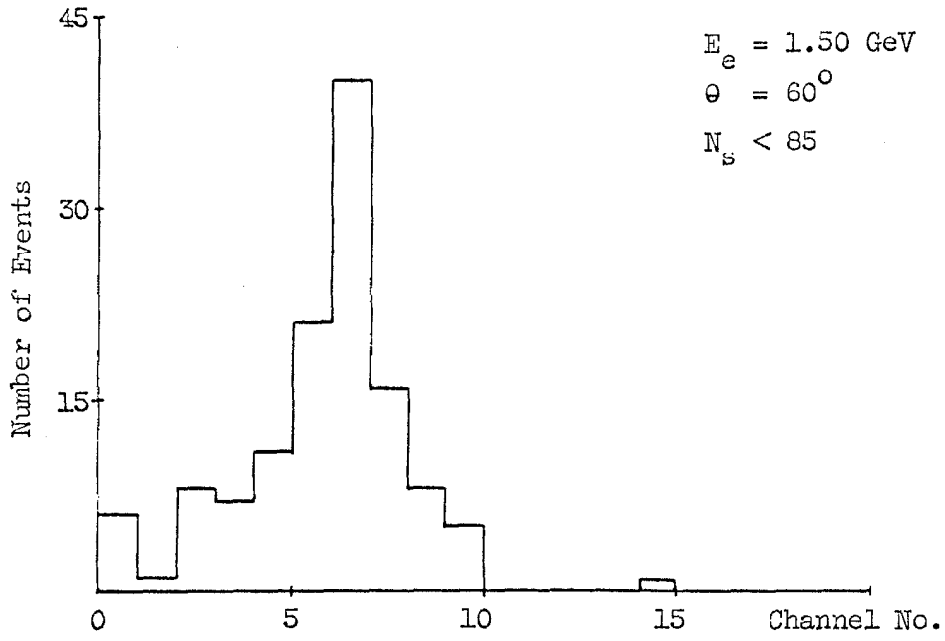

Figure XII.6 Pulse Height Distribution for 1.50 GeV/c Electrons with $\theta = 60^{\circ}$, $\phi = 0^{\circ}$ for Events with $N_s < 85$

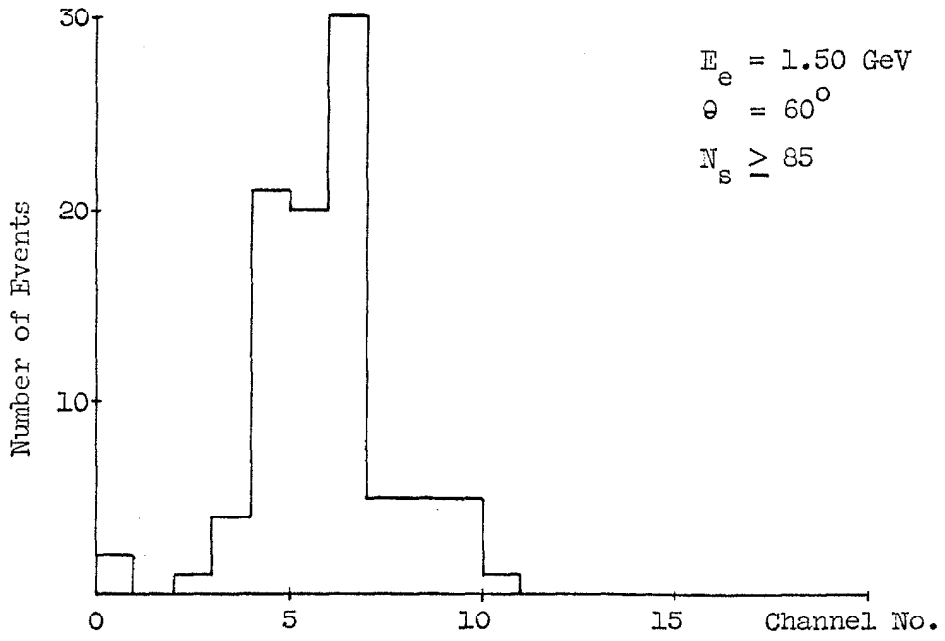

Figure XII.7 Pulse Height Distribution for 1.50 GeV/c Electrons with $\theta = 60^{\circ}$, $\phi = 0^{\circ}$ for Events with $N_s \geq 85$

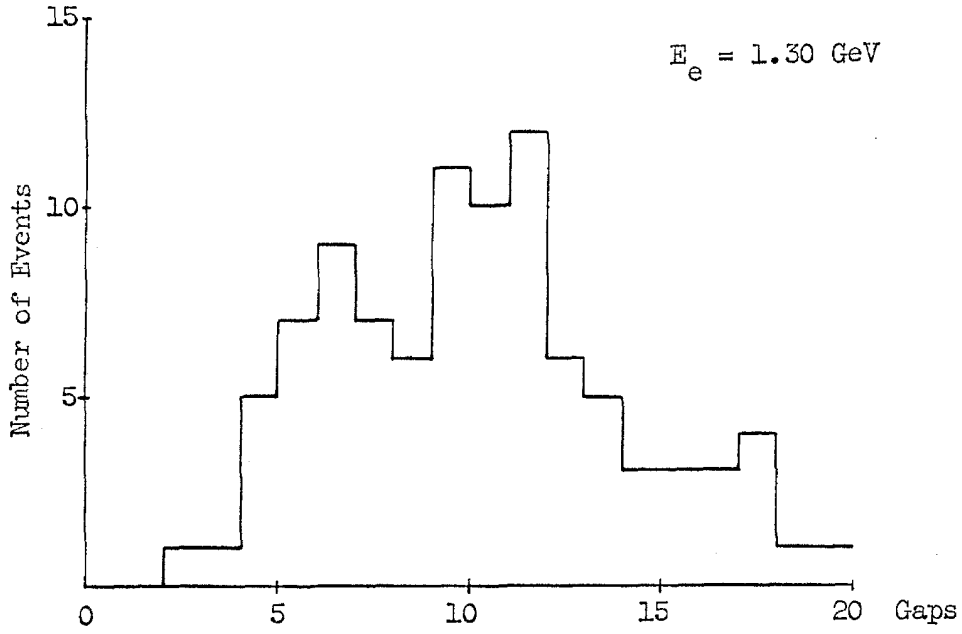

Figure XII.8 Distribution of Starting Point of the Showers Produced by 1.30 GeV/c Positrons

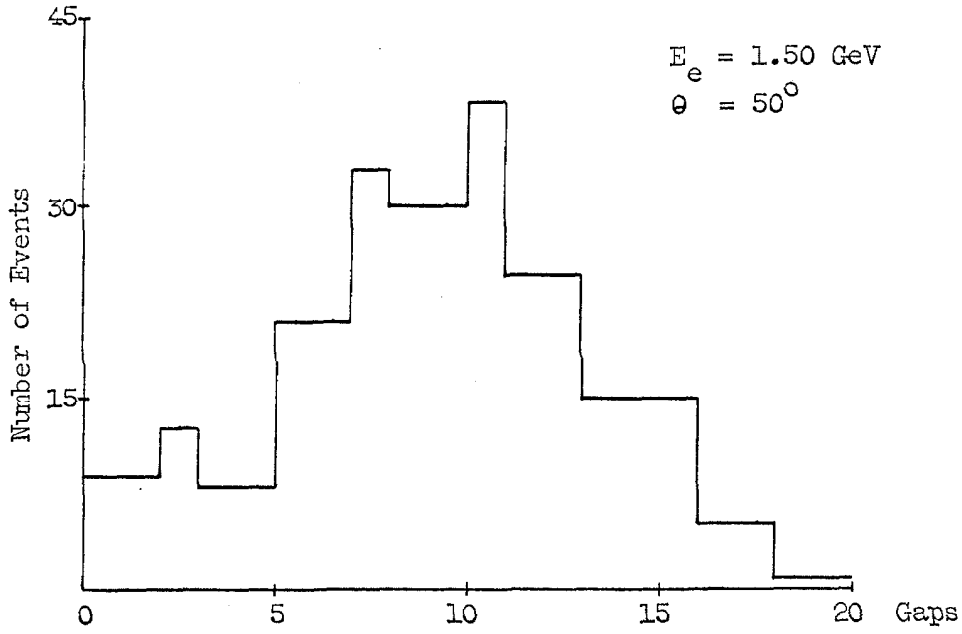

Figure XII.9 Distribution of Starting Point of the Showers Produced by 1.50 GeV/c Electrons with $\theta = 50^{\circ}$, $\phi = 0^{\circ}$

were triggered on events satisfying the requirements for the $\pi^+ + \pi^-$ final state for 1.50 GeV/c antiprotons. There were 3830 events in this sample and measurement of the angles of the particles in the kinematics chambers for the first 200 events in this sample indicated that 50% of the events represented the $\pi^+ + \pi^-$ final state.

The Pb chamber film was scanned for events which had one track which satisfied the following criteria.

1.) The "shower" was not asymmetric, i.e. the shower wasn't completely contained on one side of incident particle direction.

2.) The "shower" had no tracks ($\geq$ 3 correlated sparks) making an angle $\geq 45^{\circ}$ to the incident particle direction.

3.) The "shower" had no breaks with no sparks in $\geq$ four consecutive gaps.

4.) The total number of sparks in the "shower" contained within a 40° opening angle cone centered on the incident particle direction was $\geq$ the number of sparks for a straight track, $N_{st.}$, plus ten sparks.

5.) The "shower" had no definite vertex, i.e. a straight track coming in with two or more straight tracks coming out. The track in the left chamber (upper) of Figure XII.10 is an example of a definite vertex.

6.) The "shower" didn't have a straight track as its core characteristic of a γ-ray superimposed on a straight track.

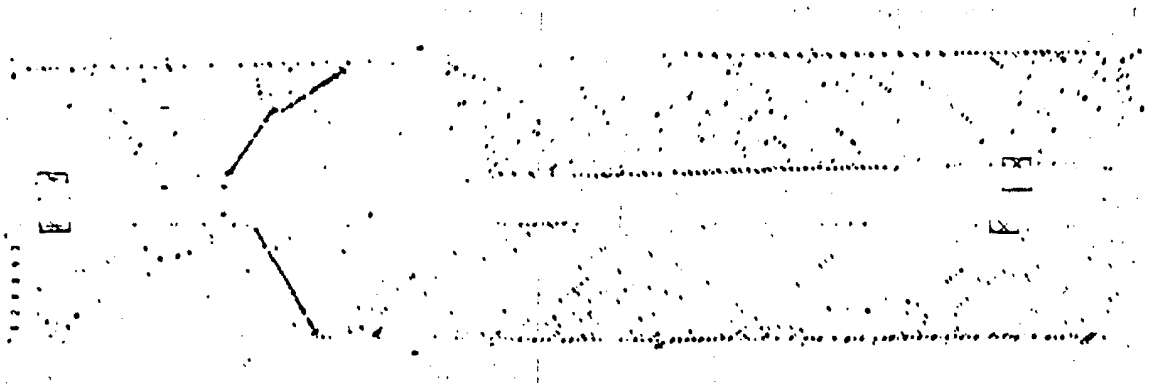

Figure XII.10 Example of a Definite Vertex Event

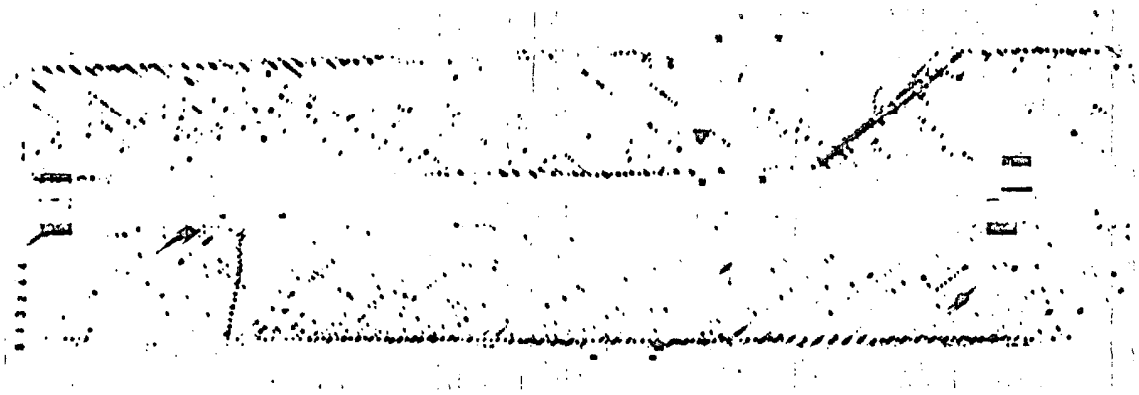

Figure XII.11 Final Candidate for a π Faking an Electron

The scanning was carried out in two steps with the first step, a rough scan, yielding thirty-two candidates which were measured. Ten of these candidates satisfied the 95% kinematics cuts for the $\pi^+ + \pi^-$ final state.

Of these ten candidates the one shown in Figure XII.11 comes closest to satisfying all the above shower criteria, however, there is some question as to whether or not it satisfies the second criterion. Taking this event as satisfying the above criteria then gives for the π detection efficiency of each chamber averaged over the solid angle of the apparatus

$$\epsilon_\pi = \frac{1}{3830}\left(1 \begin{smallmatrix} + 1.6 \\ - 0.6 \end{smallmatrix}\right) = \left(2.6 \begin{smallmatrix} + 4.2 \\ - 1.6 \end{smallmatrix}\right) \times 10^{-4}$$

d. Final Electron Detection Efficiency

Applying these same criteria to the showers in the known sample of 220 electrons with $\theta = 50^\circ$ and momentum = 1.50 GeV/c gave the following results. There were sixteen showers which had definite vertices and there were two showers which had tracks making an angle of $\geq 45^\circ$ with respect to the incident particle direction. In addition there were two showers which did not satisfy the symmetry requirement.

Combining these results then gives for the electron detection efficiency in the Pb chambers

$$\epsilon_e = \frac{200 \pm 5}{220} = 0.91 \pm .03$$

for this angle and momentum. The detection efficiencies for electrons at the other angles and momenta encountered in the experiment as determined by similar analyses agree within their uncertainties with the above efficiency.

Checks on γ-rays converting in the chambers during the course of the experiment indicated no detectable change in the multispark efficiency of the chambers.

APPENDIX XIII

PDP-5 and BS-2 System

In order to have a continuous monitor on nearly all the electronic elements of the apparatus and to have a flexible device to investigate the properties of the apparatus a PDP-5 digital computer was connected on-line to the experiment. The PDP-5 is a 12-bit word digital computer with a 4K word memory and a memory cycle time of $\approx 4\mu$sec. It was connected to an input buffer consisting of eight 12-bit words. These words stored the encoder answer for each tray of counters in the hodoscope, the fast adder result for each angle computer, and the pulse heights in the two Čerenkov counters as measured by the two fast 15 - channel pulse height analyzers connected to them. This information was stored in the computer in one and two dimensional matrices where each element of the matrix was a word in memory corresponding to a possible answer from the experiment and the value of that word was equal to the number of times in a given run that this answer occurred in an event. The actual format consisted of three 16 x 16 matrices of $\cot \theta_R$ vs. $\cot \theta_L$, with upper limits variable from 15 → 63 on either axis, a 16 x 16 matrix which could plot anything vs. anything and with variable upper limits from 15 → 63, one 1 x 64 matrix for the ϕ computer answer, and six 1 x 32 matrices for the encoder answer for each tray.

Upon a typed command from the teletype unit connected to the computer the computer printed out using the teletype unit the contents of these matrices. In addition to the teletype output a live scope

display with a 16 x 16 dot grid gave a visual display of a matrix which was selected by the main program. If the number of counts in a certain position in the matrix was greater than a value selected by the switch register on the console of the PDP-5 the dot for this position was intensified giving a rough three dimensional picture of the matrix.

A trigger from the fast electronics initiated the following steps in order to store the event in the PDP-5. All the flip-flops in the 8 words were set to 0 after which the information from the fast electronics was gated into the flip-flops. This gate signal also set a flag in the PDP-5 telling it that an event was ready to be read in. The program then initiated the sending of a pulse train to the buffer which then read the word corresponding to this pulse train into the accumulator register of the PDP-5. This code also set a gate inhibit flip-flop so that no more events could be read into the buffer. The program then deposited the contents of the accumulator into the appropriate memory cell and sent out the pulse code for the next word continuing until all eight words were read in. After the last word was read in the 8 words were processed and these memory locations were cleared. When they were cleared the gate inhibit flip-flop was reset and the buffer was ready to accept the next event. About thirty events could be processed by the PDP-5 during the 400 msec. beam spill.

APPENDIX XIV

BS-1 System

For every event that was photographed in the spark chambers an IBM card was punched which recorded the event number, which counters in each tray had been hit by the particles, the fast angle computer answers for cot θ_R, cot θ_L, and ϕ and the pulse heights in the right and left Čerenkov counters as measured by the two 15 - channel fast analyzers. This information was then used as a check for scanning and measuring errors. Also this system lit numbered lights arranged along the edges of the spark chambers corresponding to the counter position in the hodoscope to aid in scanning when more than one interaction occurred during the sensitive time of the spark chambers. A data panel indicating all the information on the IBM card was also photographed in the end view of the kinematics chambers.

The storage and display of this information was accomplished in the following manner. In a typical channel the -1 volt 50 nsec. pulse from the discriminator connected to the counter was gated into a flip-flop by the compute signal. The flip-flop was clamped while the spark chambers were firing. The clamp was removed and the output of the flip-flop was used to generate a 17 volt, 0.76 msec. long pulse which was applied to a small 3 volt incandescent lamp. The light pulse from the lamp fired an LASCR which acted as a switch for the display lamps and caused the proper column and row to be punched on the card punch.

The reason for using the lamp - LASCR stage was to eliminate any

ground connection to the long unshielded wires on the display lamps attached to the spark chambers. The noise from the spark chambers was never observed to set any of the storage flip-flops during the course of the experiment even though it was ≈ 20 volts in amplitude on some of the display lamp wires. All flip-flops were reset at the end of the punch cycle.

A block diagram of the storage and display system is shown in Figure XIV.1.

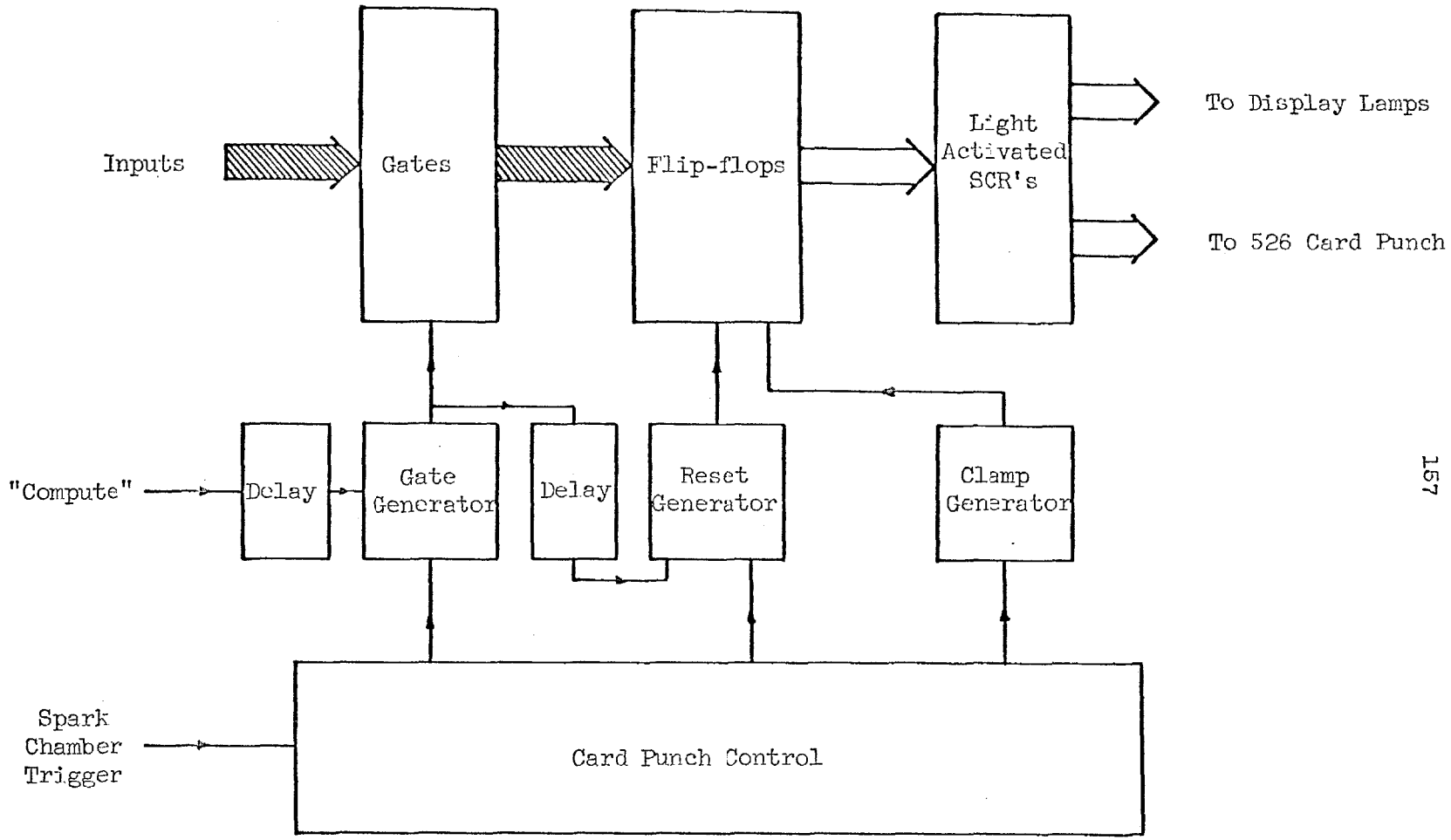

Figure XIV.1 Block Diagram of Storage and Display Electronics

APPENDIX XV

Hodoscope System

The general properties of the system were that it required that one and only one changed particle come from the target on each side, that the two particles together with the incident beam direction be coplanar to within $\approx 15^{\circ}$ and that the θ angles of both of the particles be correct to within $\approx 5^{\circ}$ of that for $\bar{p} + p \rightarrow e^{+} + e^{-}$ or $\pi^{+} + \pi^{-}$. The computation of the angles required $\approx$ 100 nsec. The overall delay time between the particles passing through the spark chambers and the peak of the high voltage pulse applied to the chambers was $\approx$ 450 nsec.

The overall layout of the scintillation counter hodoscope which was used to selectively trigger on only those events with kinematics appropriate for $\bar{p} + p \rightarrow e^{+} + e^{-}$, $\pi^{+} + \pi^{-}$ or $K^{+} + K^{-}$ was shown in Figures 3 and 4 of Chapter I.

The θ trays were made up of fifteen 1/4" thick 7.5" wide counters and two 1/4" x 5" counters which overlapped giving 33 2.5" wide channels by taking the single counters and coincidences between overlapping counters. The inner tray located 6.5" from the $\mathfrak{C}$ of the target used straight counters 13.5" long and the outer tray located at 22.2" from the $\mathfrak{C}$ of the target used counters which had a radius of curvature = 34" so that the distance between the inner tray and outer tray was a constant independent of ϕ for an annihilation taking place at the center of the target.

Both the inner and outer counters had a single 6655A photo-

multiplier attached to their bottom ends by a PVT plastic light pipe.

The ϕ trays were made up of nine 1/4" thick x 6.6" wide counters and two 1/4" x 4.4" wide counters which were overlapping giving twenty-one 2.2" wide channels. The counters were 80" long and a 6655A photomultiplier was attached to each end of the counter by means of a PVT plastic light pipe. The anode currents of both tubes were added by using a 180 Ω cable from the anode of each tube to a BNC tee which was attached to the 90 Ω cable to the discriminator. The counters were located in a vertical plane at 24.0" from the $\mathfrak{C}$ of the target. These counters gave a mean pulse amplitude of $\approx$ 1/2 volt into 90 Ω 's with a distribution corresponding to $\approx$ 8 photoelectrons for a minimum ionizing particle passing through the center of the counter at 90°. For minimum ionizing particles going through the end farthest from the photomultiplier and perpendicular to the counter the outer θ counters gave typically a distribution in pulse height corresponding to 10 photoelectrons with a mean amplitude of $\approx$ 1/2 volt into 90 Ω 's.

As an example of how the fast angle computer operated a calculation of one of the θ angles will be described in detail, the other two computers operated in a similar manner. The circuits in the fast computer were dc coupled. Each of the counters of a tray was connected to a fast discriminator by 100' long 90 Ω cables. The fast discriminator which was dc coupled gave a 0 $\rightarrow$ -1 volt 50 nsec. long square pulse labelled (-) and a -3/4 $\rightarrow$ +1/4 volt square pulse 50 nsec. long labelled (+) for each pulse $\geq$ the discriminator threshold from the counter.

Both the positive and negative outputs of the discriminator were connected to a gated multiple coincidence circuit with 17 gates (channels) which took coincidences between all adjacent counters and added these on a coincidence sum bus, used the signal from counter N-1 to veto the gate channel output for counter N, summed all the gate channels on a bus, and gave a -1 volt 50 nsec. pulse from the surviving gate channels. Two fast discriminators were connected to the coincidence sum bus, one with its threshold set to detect single coincidences (Coinc. > 0) and the other set to detect two or more coincidences (Coinc. > 1). Similarly two fast discriminators were connected to the channel sum bus with one set for single channels (Ch > 0) and one set for greater than one channel (Ch > 1). The 17 channels were connected to the even numbers of a five bit binary encoder with the 1's bit attached to the output of the (Coinc. > 0) discriminator. Thus the counter tray was divided into 32 channels with even numbers corresponding to a single counter and the odd numbers corresponding to a coincidence between overlapping counters.

From Figures 3 and 4 it is seen that the inner trays were labelled so that channel numbers increase in a direction opposite to the direction of travel of the $\bar{p}$ beam and the outer trays were labelled so that channel numbers increase in the direction of travel of the $\bar{p}$ beam. The five bits of the inner encoder and the five bits of the outer encoder were connected to the inputs of a 6 bit fast adder. The output of the adder was then a binary number from 0 to 63 with the answer 32 corresponding to $\theta = 45^{o}$. Actually the answer was proportional to

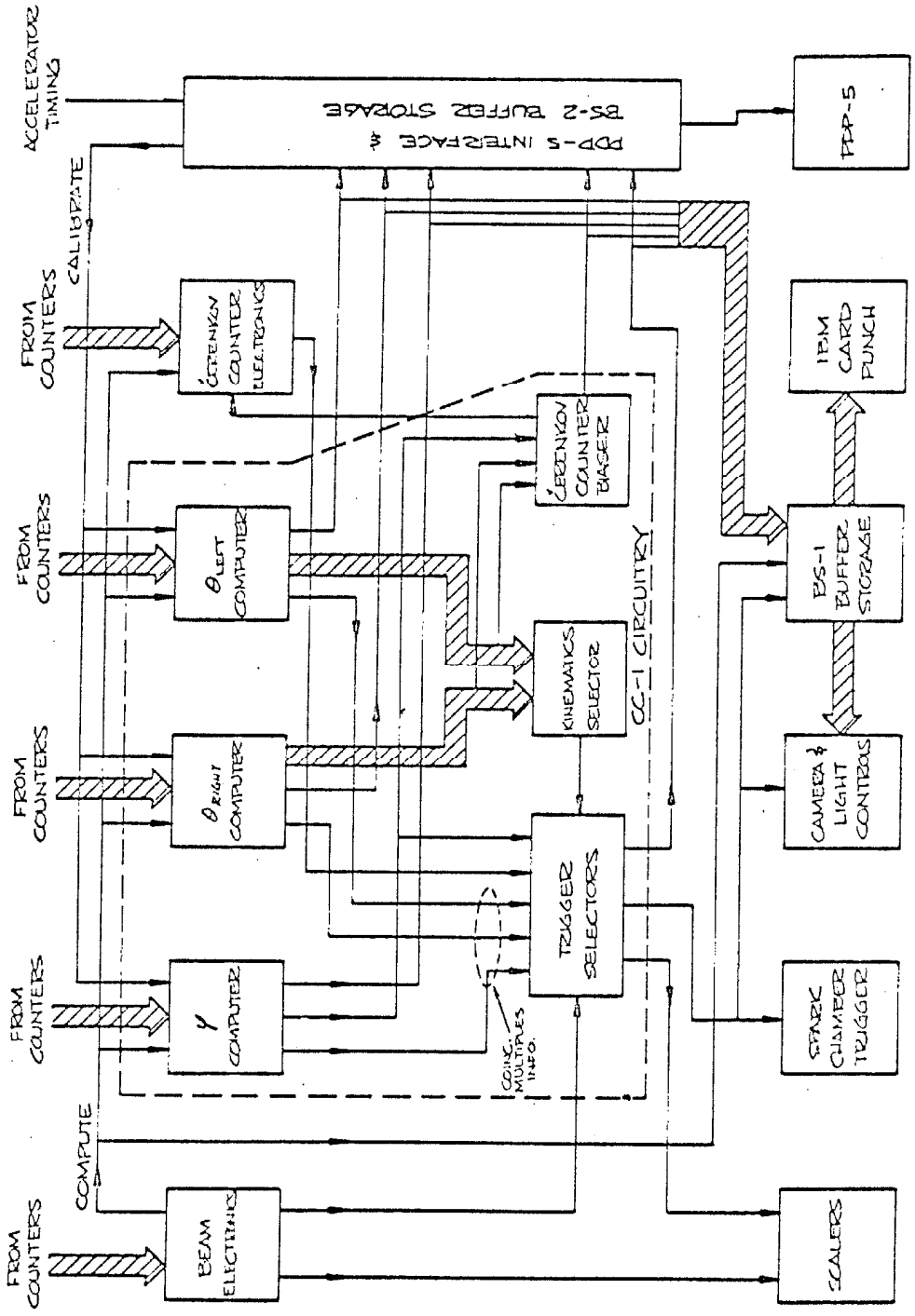

Figure XV.1 Block Diagram of the Electronic Logic

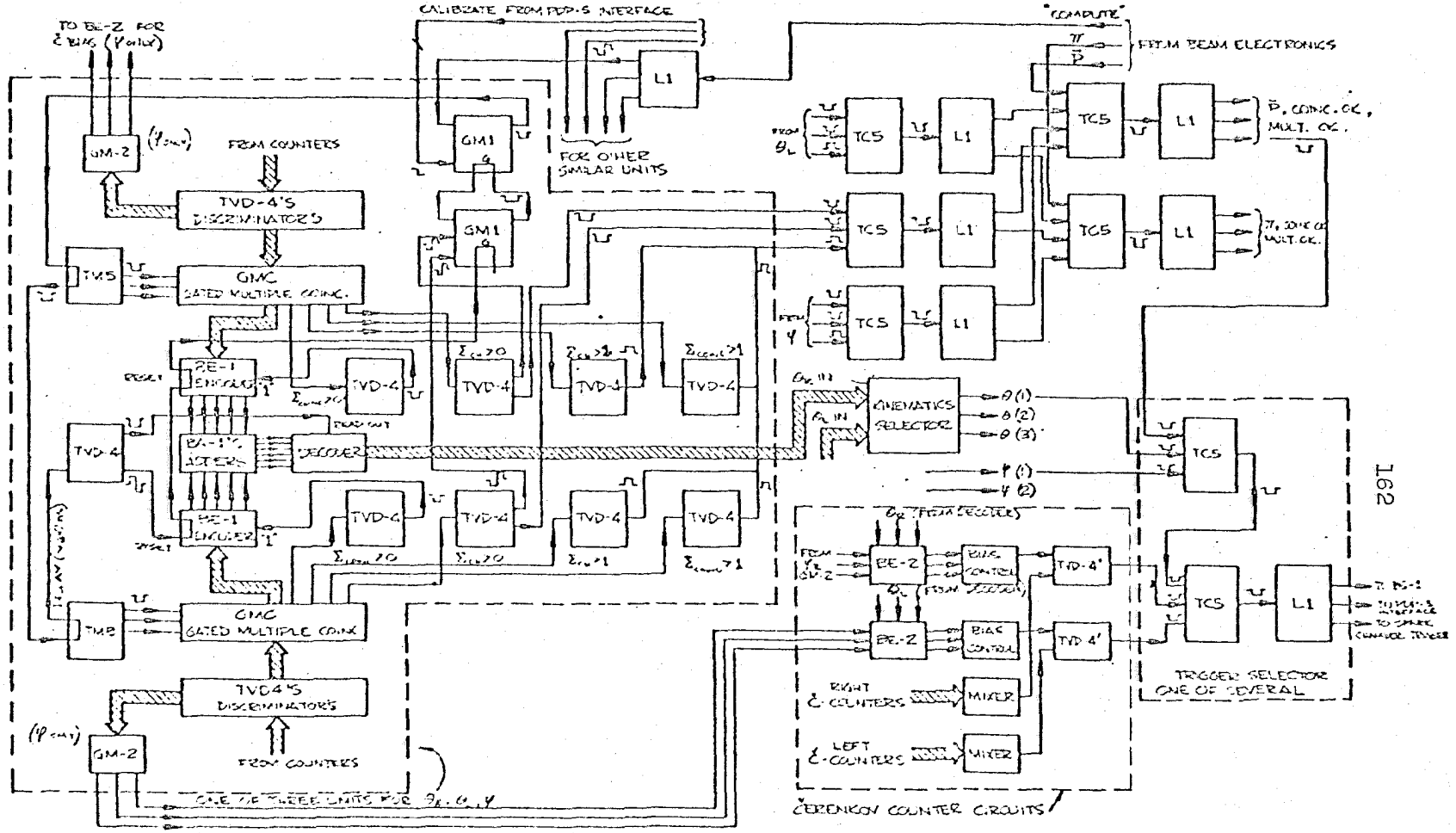

Figure XV.2 Block Diagram of One of the Fast Computers and Details of the Trigger Selector

cot θ because of the layout of the θ trays. The answers 23 to 38 were decoded onto 16 gated flip-flops (which were gated by the reset pulse to the encoders 85 nsec. after the compute pulse from the beam electronics) whose outputs were used to drive one side of a 16 x 16 coincidence matrix with the other side being driven by the other θ computer. The kinematics region occupied by $\bar{p} + p \rightarrow e^+ + e^-$, $\pi^+ + \pi^-$, and $K^+ + K^-$ was then selected on this matrix.

The ϕ computer fast added the ϕ_L channel to the ϕ_R channel with the answer 32 representing coplanar events. The answers 31, 32, and 33 were decoded onto 3 flip-flops whose outputs were connected to an or circuit which gave the ϕ OK signal.

The final kinematics OK signal required that the following (all computers were gated by the $\bar{p}$ OK signal (compute) from the beam time of flight electronics described above) combination of signals be present simultaneously.

$$K = \theta_{IR}\,(Ch > 0) \cdot \overline{\theta_{IR}\,(Ch > 1)} \cdot \theta_{OR}\,(Ch > 0) \cdot \overline{\theta_{OR}(Ch > 1)} \cdot$$

$$\theta_{IL}\,(Ch > 0) \cdot \overline{\theta_{IL}\,(Ch > 1)} \cdot \theta_{CL}\,(Ch > 0) \cdot \overline{\theta_{CL}\,(Ch > 1)} \cdot$$

$$\phi_L\,(Ch > 0) \cdot \overline{\phi_L\,(Ch > 1)} \cdot \phi_R\,(Ch > 0) \cdot \overline{\phi_R\,(Ch > 1)} \cdot$$

$$\overline{\theta_{IR}\,(Coinc. > 1)} \cdot \overline{\theta_{OR}\,(Coinc. > 1)} \cdot \overline{\theta_{IL}\,(Coinc. > 1)} \cdot$$

$$\overline{\theta_{OL}\,(Coinc. > 1)} \cdot \overline{\phi_L\,(Coinc. > 1)} \cdot \overline{\phi_R\,(Coinc. > 1)} \cdot$$

$$(K - matrix)$$

$$= N \cdot (K - matrix)$$

and $\phi = \phi\,(31, 32, 33)$.

Figure XV.3 is a print out of one of the cot θ_R vs. cot θ_L matrices stored in the PDP-5 computer. The interface, buffer storage, and program for the PDP-5 is described in Appendix XIII. The matrix shown was obtained by triggering the PDP-5 on $N \cdot \phi$ for 1.50 GeV/c incident p's. The numbers are the number of events falling in that particular bin for that particular run. The kinematics region covered by this print out is identical to the kinematics matrix (namely fast computer answers 23 → 38 for both cot θ_R and cot θ_L). The region bounded by the black lines is the region which was selected by the K - matrix requirement. The three curves represent the ideal kinematics for $\bar{p} + p \rightarrow \pi^+ + \pi^-$, $K^+ + K^-$, and $\bar{p} + p$ respectively. From the Figure it is seen that the outlined region has zero efficiency for $\bar{p}p$ elastic scattering and 100% efficiency for $\pi^+ + \pi^-$, $K^+ + K^-$, and $e^+ + e^-$ (which has the same kinematics as $\pi^+ + \pi^-$).

The corresponding matrix for 2.50 GeV/c antiprotons is shown in Figure XV.4. The $\pi^+ + \pi^-$ cross section for this momentum is smaller than it is for 1.50 GeV/c and the $\pi^+ + \pi^-$ kinematics curve moves closer to the $\bar{p}p$ kinematics curve so that the separation in the matrix is not as clear. The selected region however has 100% efficiency for $\pi^+ + \pi^-$ and $K^+ + K^-$ and zero efficiency for $\bar{p}p$ elastic scattering based on the spark chamber analysis of the $\pi^+ + \pi^-$ and $K^+ + K^-$ final states being carried out by Douglas Fong.

The average detection efficiency for minimum ionizing particles for each tray of counters was determined from a detailed comparison of counters which gave pulses to trigger the event as recorded on the IBM

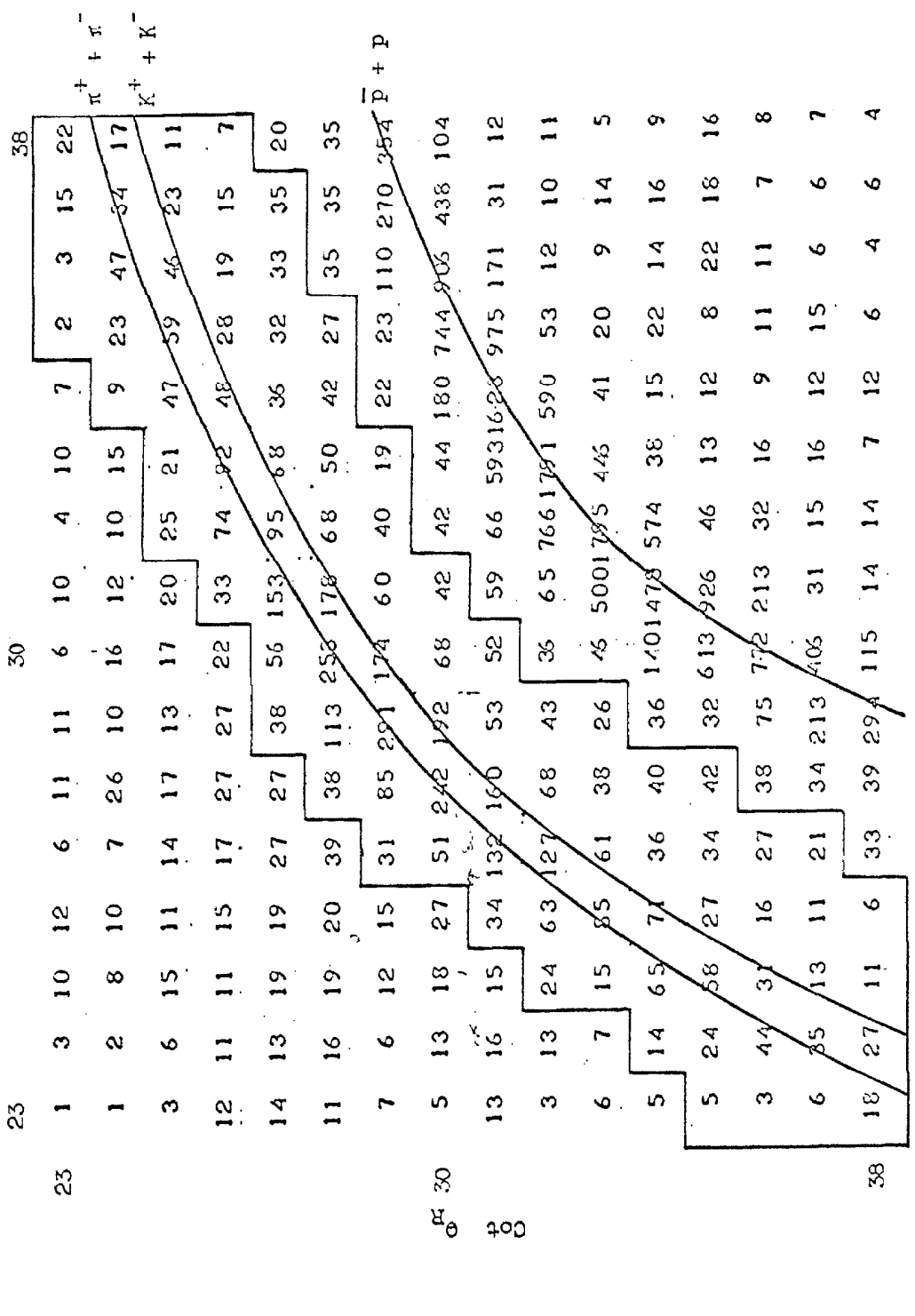

Figure XV.3 Cot θ_R vs. Cot θ_L Matrix from PDP-5 Triggered on N·ϕ for 1.50 GeV/c Antiprotons

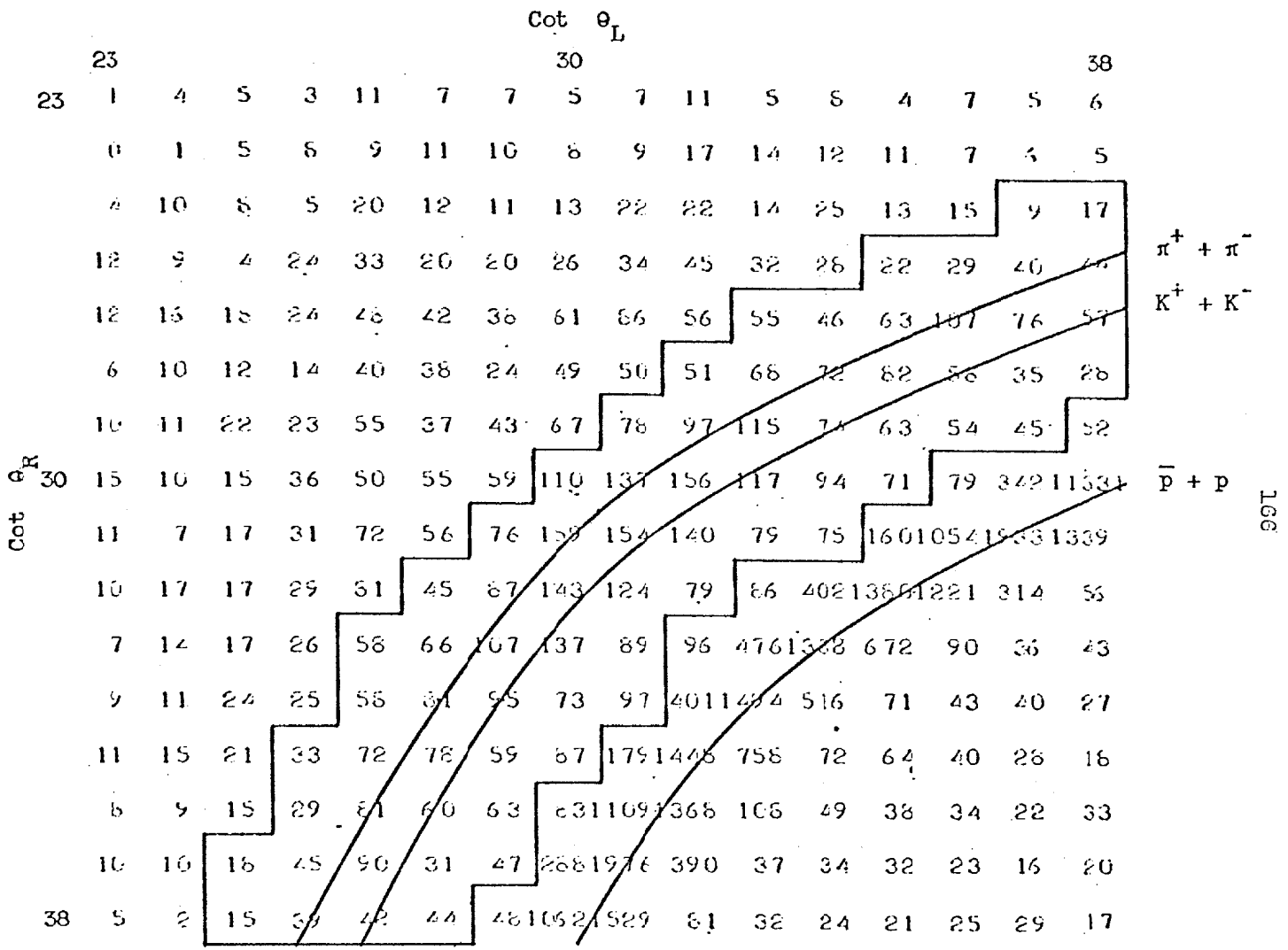

Figure XV.4 Cot θ_R vs. Cot θ_L Matrix from PDP-5 Triggered on N·$\emptyset$ for 2.50 GeV/c Antiprotons

card punched when the event was photographed to the ones which should have given pulses according to the spark chamber film measurements.

The comparisons of four thousand events from Douglas Fong's analysis give the following average efficiencies for each counter in each tray.

Tray	Average Efficiency
θ_{IL}	$= .993 \pm .002$
θ_{IR}	$= .994 \pm .001$
θ_{OL}	$= .985 \pm .002$
θ_{OR}	$= .982 \pm .002$
ϕ_{L}	$= .984 \pm .002$
ϕ_{R}	$= .975 \pm .003$

Combining these efficiencies and taking into account the effect of the ϕ counter inefficiencies on the ϕ answer the overall hodoscope efficiency is given by

$$\epsilon_{hodo} = \epsilon_{\phi} \times (\epsilon_{\theta})^2$$
$$= .95 \pm .01.$$

APPENDIX XVI

Čerenkov Counters

The electronic discrimination between electrons and pions was accomplished by means of lead - Lucite Čerenkov counters.[12] There was one such counter array in each side of the apparatus each having a sensitive area of 92" long by 80" high.

Each counter array was made up of ten counters consisting of three 1" thick UVT Lucite plates 9" wide x 100" long separated by 1/2" thick UVT spacers 9" x 10" long at each end. This assembly was then bonded together with PS-18 and each end was tapered to a 4 1/2" diameter to match the face of a RCA 7046 5" photomultiplier. Each of the Lucite plates was carefully polished and wrapped with 1/4 mil Aluminized Mylar. A 1/4" x 9" x 80" lead plate was inserted into each of the gaps between the three Lucite plates and held away from the Lucite plates by means of slots in the thin (0.020") light-tight stainless steel box which enclosed the unit. The 7046 photomultipliers were attached to each end of the unit by two bolts which passed through a bakelite ring glued to the phototube with RTV-602 and through two Lucite "ears" glued to the light pipe of the unit. The optical joint between the light pipe and the photomultiplier was made using a Dow Corning Silicone Compound Number C-20057. The ten units were then mounted on a steel frame supported on four casters. The complete assembly weighed approximately 3 tons.

A block diagram of the Čerenkov counter electronics is shown in

Figure XVI.1.

The anode pulses from each of the 7046's were added in two linear 12 channel mixers and the summed outputs of the two mixers were added in a two channel linear mixer. The signal from this mixer was delayed by 40 nanoseconds and amplified. The amplified pulse was passed through a linear gate which was opened by the compute pulse from the beam time of flight electronics described above.

The gated pulse was attenuated by 10db and stretched by a delay line pulse stretcher giving a 50 ns long output pulse. The stretched pulse was amplified and divided by a distributor network to give the proper signal levels to drive the Čerenkov OK fast discriminator, the TMC 1024 channel multichannel analyzer, and the 15 channel fast analyzer which recorded the Čerenkov counter pulse height for each spark chamber trigger.

The linearity and gain of the entire system was checked by means of a critically damped pulse with the same shape as the anode pulse from the 7046's from an SKL mercury relay pulser. This pulse was split and one side was fed into one of the unused inputs of one of the 12 channel mixers. The other side was used to generate the necessary gate pulses for the linear gate and the TMC analyzer. This procedure permitted a cross correlation between TMC channel numbers, fast analyzer channel numbers and the Čerenkov OK discriminator setting in terms of the voltage applied to the SKL mercury relay pulser. As a result all gain curves, pulse height analyzer calibrations and Čerenkov counter response curves were in terms of SKL volts.

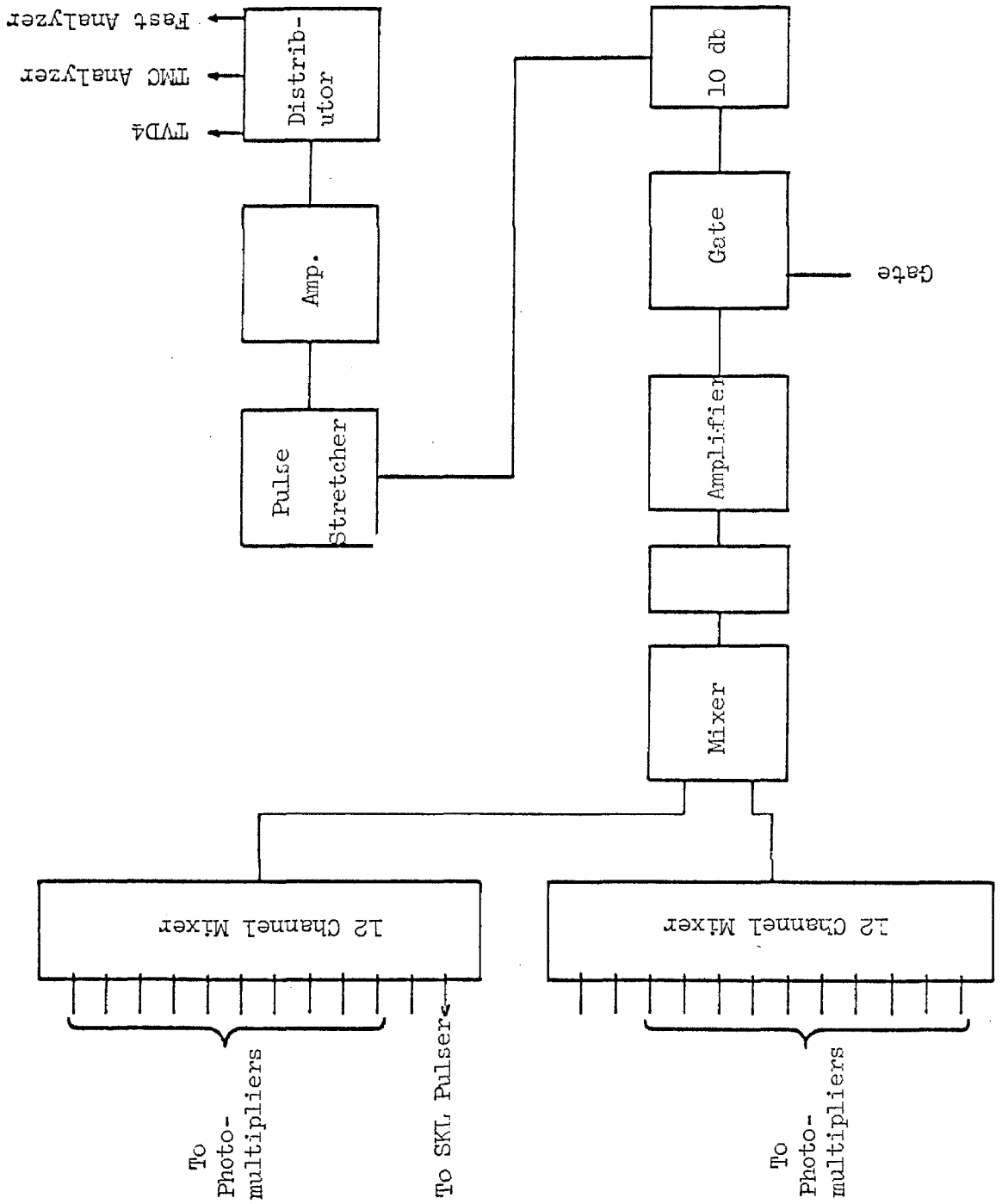

Figure XVI.1 Block Diagram of Cerenkov Counter Electronics

The photocathode efficiency of each of the forty 7046 photomultiplier tubes used on the two trays of counters was measured and the tubes were paired so that the average photocathode efficiency for each counter was as uniform as possible. The gain of each one of the phototubes was adjusted so that the peak of the pulse height distribution resulting from 1.25 GeV/c electrons normally incident on the counter under study with two radiation lengths of lead in front of it was equal to 22.0 $\pm$ 0.5 volts (SKL) with all other tubes off.

The overall gain of each phototube was monitored by means of a 1" x 1" x 1/16" piece of NE102 plastic scintillator bonded to the light pipe portion of the counter near the phototube. This scintillator was exposed to the 2.2 MeV electrons from a Sr^{90} source mounted on a solenoid so that it could be moved behind a shutter during the experiment. This source-scintillator combination gave a pulse height distribution in the TMC of which Figure XVI.2 is a typical example. The SKL voltage corresponding to the peak due to the 2.2 MeV electrons passing through the scintillator in the pulse height distribution was recorded after the gain of the tube was set as described above. The peak was typically 25 volts. This gave a standard gain for the tube. During the run the gain of each tube was checked once each week. The maximum variation in gain was less than 4% for the course of the experiment. The high voltage applied to the photomultipliers was checked daily with a digital voltmeter.

The overall response of each counter array to electrons is given in Figure XVI.3. The energy, angle and point of impact of the electron beam

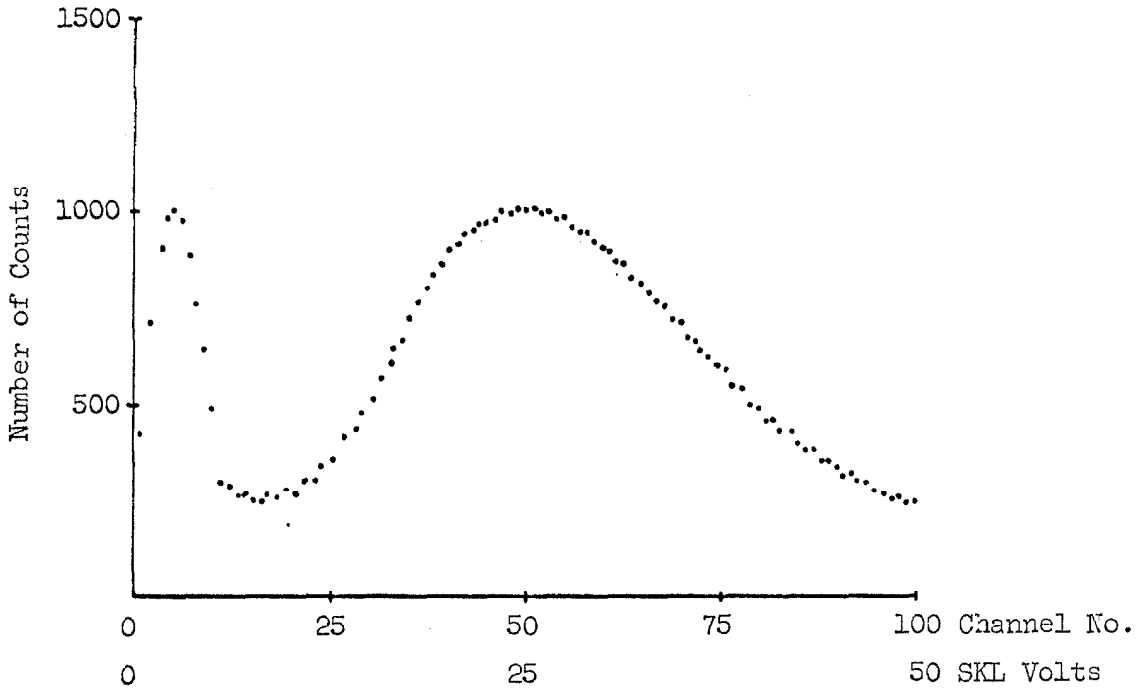

Figure XVI.2 Pulse Height Distribution of One of the Sr^{90} Calibration Sources

on the counter array was matched to the kinematics of a typical annihilation $\bar{p} + p \rightarrow e^+ + e^-$ for 2.50 GeV/c antiprotons. The curves in Figure XVI.4 are smooth hand fits to the experimental points. Only the point at $\phi = 0$, $\theta = 48^\circ$ was obtained using the actual Pb plate spark chamber as the initial radiator, the other points being obtained using an equivalent thickness of the Al-Pb-Al sandwich material which was used for the plates in the chamber.

An analytic-graphical theory of the response of the counter array was developed from the data for the 2.5 GeV/c kinematics. The results of shower development studies of Heusch[9] etal. were combined with a geometrical factor due to the changes in the radiator and the detector thickness and an experimentally determined correction factor to give the final theory.

Figure XVI.3 is the calculated Cerenkov counter response for 1.50 GeV/c incident $\bar{p}$'s on hydrogen giving $e^{\mp} + e^-$. The points are data obtained in a short check run at the end of the experiment and are seen to agree with the theoretical curves.

The average efficiency for detecting a pion from $\bar{p} + p \rightarrow \pi^+ + \pi^-$ at 1.50 GeV/c for one counter array was ≈ 0.25 for the discriminator bais used during the experiment. For the bias used for the part of the experiment using 2.50 GeV/c incident $\bar{p}$'s, the average efficiency for detecting a pion from $\bar{p} + p \rightarrow \pi^+ + \pi^-$ was ≈ 0.14.

The average electron efficiency was obtained by means of a Monte Carlo computer program described in Appendix III, Section a. For all angular distribution considered the efficiency for detecting both

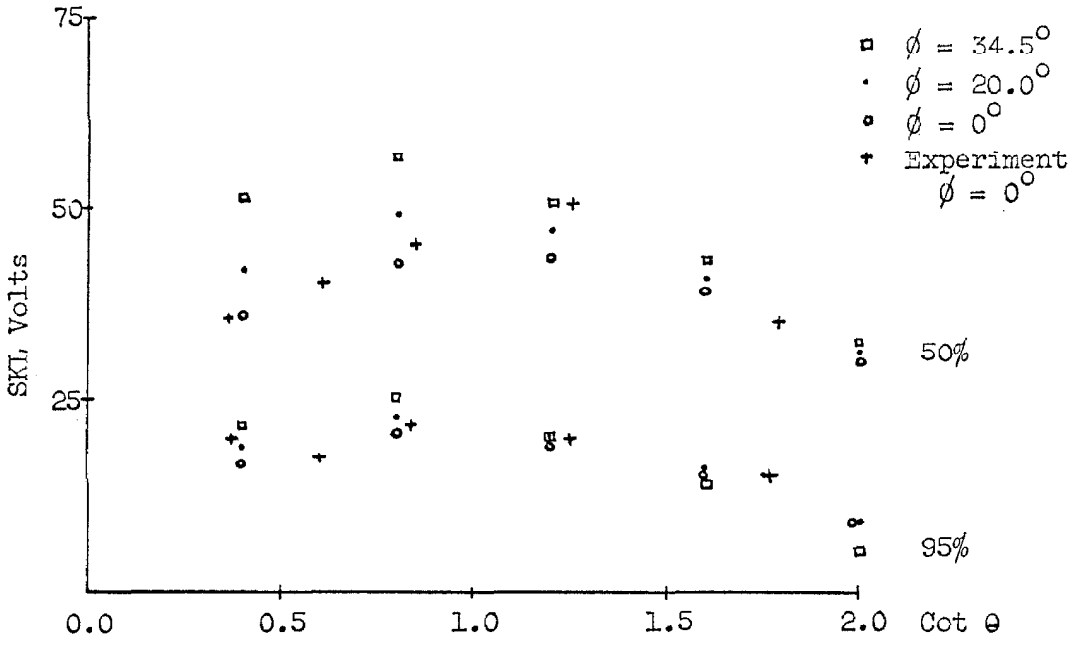

Figure XVI.3 Čerenkov Counter Detection Efficiency for Electrons from $\bar{p}p \rightarrow e^+e^-$ at 1.50 GeV/c

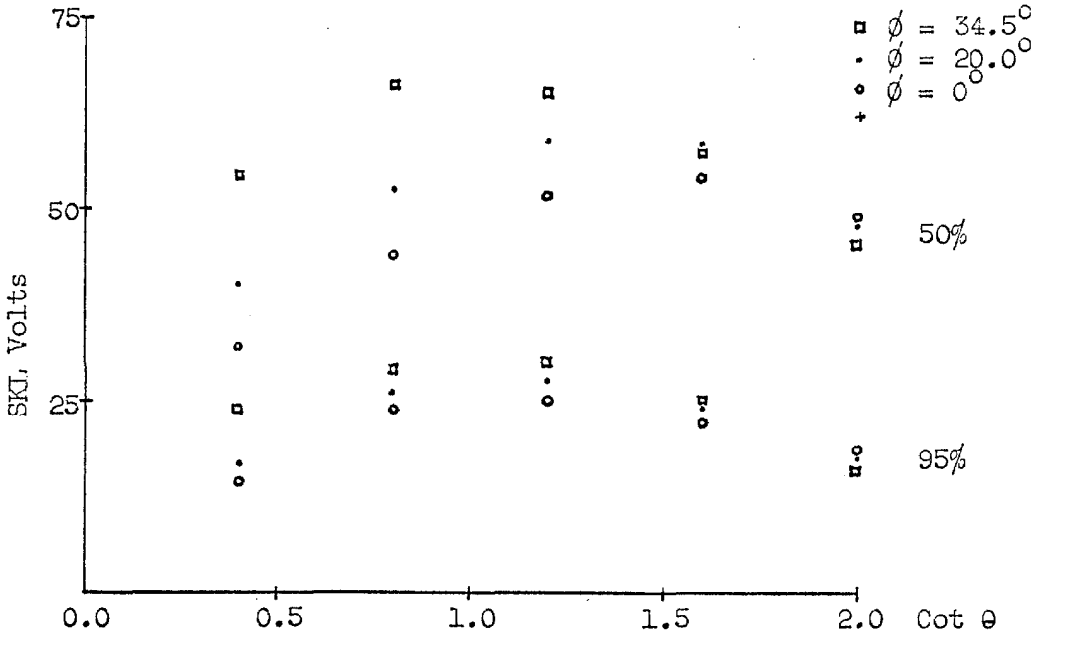

Figure XVI.4 Čerenkov Counter Detection Efficiency for Electrons from $\bar{p}p \rightarrow e^+e^-$ at 2.50 GeV/c

electrons was greater than .02.

A more detailed description of these Čerenkov counters will be available in a CTSL Internal Report by R. Gomez when it is completed.

APPENDIX XVII

Analysis of the Background Contribution of $\pi^+\pi^-n\pi^o$ to the e^+e^- Final State

The contribution of the $\pi^o\pi^-n\pi^o$ n = 1, 2,... final states to the background of the e^+e^- final state was determined by scanning two samples of the data for the e^+e^- final state. The sample taken from the 2.50 GeV/c data was scanned for events which had one charged particle and one distinguishable converting γ-ray (>10 sparks) in each Pb chamber. The separations parallel to the beam direction of the charged particles and the converted γ-rays were then measured for each of these events. In the sample taken from the 1.50 GeV/c data events which had one charged particle plus one converting γ-ray (>10 sparks) were accepted along with events with this configuration plus one extra converting γ-ray which was within 1.5" of the charged particle. This later class was accepted because of radiative correction γ-rays for the e^+e^- final state. The separations parallel to the beam direction of the charged particles and the γ-ray were then measured for these events.

Figure XVII.1 shows a histogram of this separation for 311 events (each event has two separations) obtained from a sample of the 2.50 GeV/c data. This sample of data represents 1.9×10^9 $\bar{p}$'s incident on the liquid hydrogen target. Figure XVII.2 shows this same histogram for 117 events from the 1.50 GeV/c sample for 6.9×10^7 $\bar{p}$'s incident on the target. In Figure XVII.3 the expanded scale histogram for the separations from $0 \rightarrow 1$" in Figure XVII.1 is shown. From this figure it

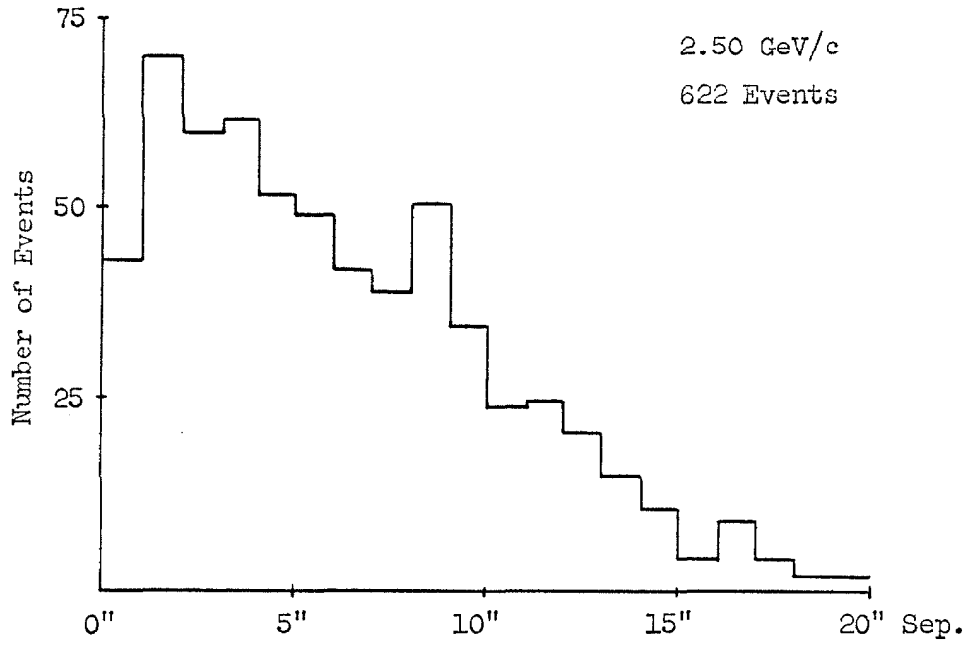

Figure XVII.1 Histogram of the Separation of the Charged Particle and the γ-ray in the Pb Chamber

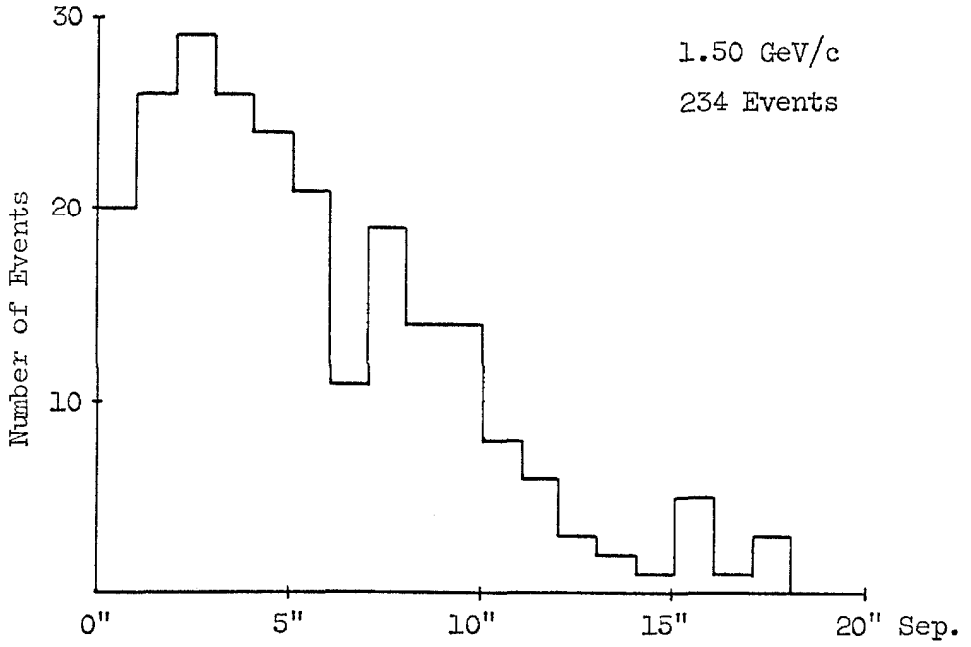

Figure XVII.2 Histogram of the Separation of the Charged Particle and the γ-ray in the Pb Chamber

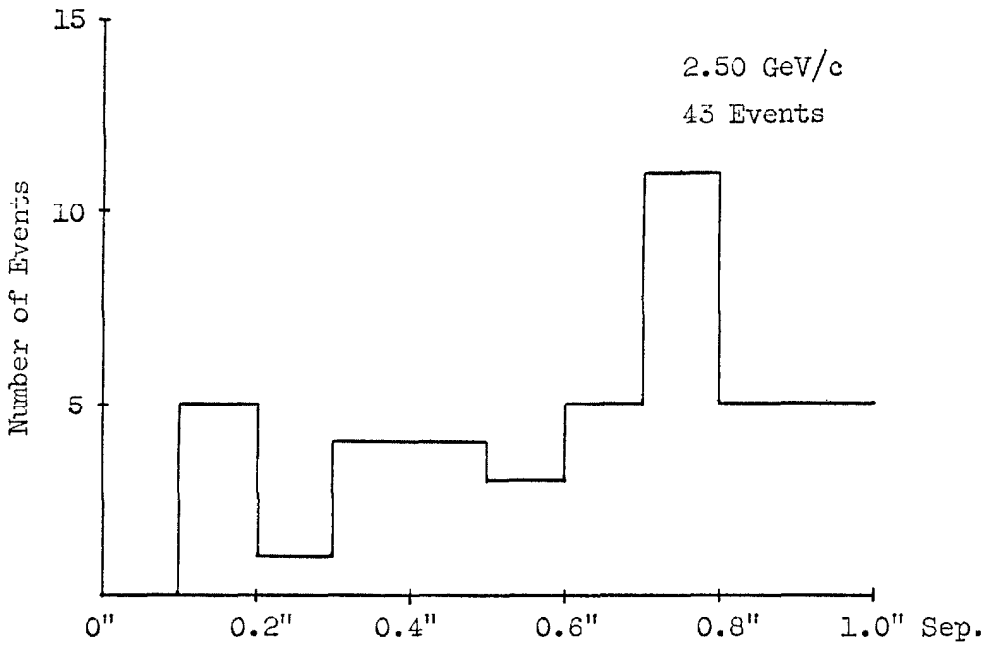

Figure XVII.3 Histogram of the Separation of the Charged Particle and the γ-ray in the Pb Chamber

is seen that the minimum separation that can be resolved is 0.1" and that the histogram is essentially flat up to that point.

In calculating the background to the e^+e^- final state from this source the probability that both γ-rays are within 0.1" of the charged particles has been taken to be

$$P_{0.1} = \left(\frac{0.1 \times \text{Number of Events in } 0'' \rightarrow 1''}{\text{Total No. of Events}}\right)^2$$

$$= (8.1 \pm 1.2) \times 10^{-5} \text{ for 2.50 GeV/c}$$

$$= (7.4 \pm 1.7) \times 10^{-5} \text{ for 1.50 GeV/c.}$$

$P_{0.1}$ for 2.50 GeV/c contains a correction factor = $(1.3)^2$ determined from the 1.50 GeV/c sample to account for not including extra γ-rays in the original scan. One hundred of the events used for Figure XVII.2 were measured with seven of the events having kinematics within the 95% acceptance range for the e^+e^- final state. Combining this with the above probability gives the overall probability that an event of this type will fake the e^+e^- final state.

The results are

$$P_{\pi^+\pi^-n\pi^0} = (5.7 \, {}^{+\,3.1}_{-\,2.0}) \times 10^{-6} \text{ for 2.50 GeV/c}$$

and

$$P_{\pi^+\pi^-n\pi^0} = (5.2 \, {}^{+\,2.8}_{-\,1.8}) \times 10^{-6} \text{ for 1.50 GeV/c.}$$

The Čerenkov counter pulse height distributions for the events from the 1.50 GeV/c sample are essentially the same as are expected for the e^+e^- final state. As a result no correction due to the Čerenkov counter pulse heights has been made in these probabilities.

Using these probabilities, the total numbers of these events, and

the total numbers of $\bar{p}$'s give the effective background cross sections

$$\frac{d\sigma}{d\Omega}|_{90^\circ} \text{ (Fake } e^+e^-) = (7.8 \,^{+\,4.2}_{-\,2.7}) \times 10^{-38} \text{ cm}^2/\text{st.} \quad (2.50 \text{ GeV/c})$$

$$\frac{d\sigma}{d\Omega}|_{90^\circ} \text{ (Fake } e^+e^-) = (8.8 \,^{+\,4.7}_{-\,3.0}) \times 10^{-37} \text{ cm}^2/\text{st.} \quad (1.50 \text{ GeV/c})$$

for the e^+e^- final state.

VII. REFERENCES

1) A. Zichichi, et. al., Nuovo Cimento 24, 170, (1962).

2) L. Hand, et. al., RMP 35, 335, (1963).

3) R. Hofstadter, et. al., PRL 6, 293, (1961).

4) R. Wilson, et. al., PR 141, 1298, (1966).

5) H. Behrend, et. al., Paper Submitted to 1966 Berkeley Conference on High Energy Physics.

6) W. Albrecht, et. al., Paper Submitted to 1966 Berkeley Conference on High Energy Physics.

7) A. Zichichi, et. al., Paper Presented at the Fifth International Conference on High-Energy Accelerators, Frascati, Italy, 9-16 September, 1965.

8) A. Rosenfeld, et. al., UCRL - 8030 Rev. (1967).

9) C. A. Heusch, et. al., PR 135, B772, (1964).

10) D. Crawford and H. Messel, Private Communication.

11) G. Lynch, et. al., PR 131, 1276, (1963).

12) J. Dean, NBS Technical Note No. 120.

13) C. A. Heusch, et. al., Nuclear Inst. and Methods 29, 205, (1964).

14) K. Chen, et. al., PR 141, 1267, (1966).

15) Carl H. Biggs Co., Inc., Santa Monica, California

16) C. Baltay, et. al., PRL 15, 532, (1965).

17) B. Barish, et. al., PRL 17, 720, (1966).

18) T. Ferbel, et. al., PR 143, 1096, (1966).

19) O. Czyżewski, et. al., Paper submitted to the 1963 Sienna International Conference on Elementary Particles.

20) K. Böckmann, et. al., Nuovo Cimento 42 (10), 954, (1966).

21) T. Ferbel, et. al., Nuovo Cimento 38 (10), 12, (1965).

22) A. Pais, Ann. Phys. 9, 548, (1960).

23) Y. S. Tsai, Paper presented at the International Symposium on Electron and Photon Interactions at High Energies, DESY, June 1965.

24) T. T. Wu and C. N. Yang, PR 137B, 708, (1965).

25) E. C. Molina, "Poisson's Exponential Binomial Limit", D. Van Nostrand Co. Inc. (1942).

26) Y. S. Tsai, Private Communication.